

# Rare Earth Element Distribution during Progressive Weathering of a Granodiorite, Boulder, Colorado

by

Jesse B. Dengate

*Submitted in partial fulfillment of the  
requirements for the degree of  
Master of Science in Geology*

New Mexico Institute of Mining and Technology  
Socorro, New Mexico  
May, 1994

## **Acknowledgments**

I would like to thank Dr. Kent Condie for creating this project and for guiding me carefully through it. I would also like extend thanks to my committee members Drs. George Austin and Peter Mozely. Finally, a very warm thanks goes to Greg Hill and Jim Chrichton for their efforts in helping me to collect samples and to Dan Detmer for reading a rough draft of this manuscript and providing many useful suggestions.

## ABSTRACT

A Pennsylvanian paleoweathering profile developed on the Boulder granodiorite was chosen to study the transfer of REE from the source material, through a weathering profile to derivative sediments. With distance from the parent granodiorite  $\text{SiO}_2$ ,  $\text{Na}_2\text{O}_3$ ,  $\text{CaO}$ ,  $\text{Cr/Th}$ ,  $\text{Zr/Y}$ ,  $\text{Co/Th}$ ,  $\text{La/Th}$ ,  $\text{Cr/Sc}$ , and  $\text{La/Sc}$  decrease.  $\text{Sr}$  decreases until 1 m beneath the Permian unconformity where values increase suddenly.  $\text{Al}_2\text{O}_3$ ,  $\text{Fe}_2\text{O}_3$ ,  $\text{TiO}_2$ ,  $\text{K}_2\text{O}$ ,  $\text{Rb}$ ,  $\text{Ba}$ ,  $\text{Co}$ ,  $\text{Th}$ ,  $\text{Zr}$ ,  $\text{Hf}$ ,  $\text{Ta}$ ,  $\text{Nb}$ ,  $\text{Sc}$ ,  $\text{Y}$ ,  $\text{REE}$ ,  $\text{Cr}$ , and  $\text{Ti/Nb}$  increase and reach maximums 1 to 10 m before the Permian unconformity. Across the grey-red contact there is a decrease in  $\text{SiO}_2$  and  $\text{K}_2\text{O}$  and an increase in  $\text{Al}_2\text{O}_3$ ,  $\text{Fe}_2\text{O}_3$ ,  $\text{TiO}_2$ ,  $\text{MgO}$ , and  $\text{P}_2\text{O}_5$ .  $\text{Zr/Cr}$  and  $\text{Th/Sc}$  remain unchanged from parent to weathered granodiorite.

Chondrite-normalized REE distributions show an increase in HREE during weathering and the development of a significant negative Eu anomaly. The Eu anomaly is formed as the result of the relative enrichment of other REE and only a very slight loss of Eu due to the breakdown of plagioclase. In the parent granodiorite the majority of the REE are housed in sphene. Approximately 10-20 % of the REE are contained in the apatite and biotite with lesser amounts housed in feldspar, allanite, and with exception of HREE, zircon. Feldspars contribute 8% to the fresh rock Eu. As sphene is altered during weathering, REE are released and transferred to clay minerals. In the uppermost meter of the weathering profile, more than 75% of the REE are contained in the clay minerals. The crossover in REE control occurs within less than a meter from the fresh rock.

Isocon and Brimhall plots show losses of  $\text{Ca}$ ,  $\text{Na}$ ,  $\text{Sr}$ , and some  $\text{Si}$  due to the breakdown of plagioclase. There is variable loss of  $\text{Eu}$ ,  $\text{Ta}$ ,  $\text{Nb}$ ,  $\text{P}$ , and  $\text{Ba}$  during weathering. The remainder of the elements show an increase in concentration that may be a relative increase due to the removal of plagioclase and other constituents during weathering.

$\text{Cr/Th}$ ,  $\text{Co/Th}$ ,  $\text{La/Th}$ ,  $\text{Eu/Eu}^*$ ,  $\text{Cr/Sc}$ ,  $\text{La/Sc}$ ,  $\text{Zr/Cr}$ , and  $\text{Th/Sc}$  were not transferred unchanged from the parent rock to the Fountain shales and caution should be exercised when using these ratios as provenance indicators.  $\text{Ti/Nb}$  may have been transferred relatively unchanged from the parent granodiorite to the Permian sediments. The majority of the element ratios and the REE distributions differ significantly in the weathering profile and the Permian shales implying that there may have been additional sources for the sediments.

## CONTENTS

Acknowledgments	ii
Abstract	iii
List of Figures	iv
List of Tables	x
Introduction	
Introduction	1
General Geology	5
Methods	8
Petrographic Results	10
Geochemical Results	
Major Element Distributions	14
Chemical Weathering Indices	24
Trace Element Distributions	26
REE Distributions	46
Discussion	
Element Losses and Gains During Weathering	54
Mass Balance Calculations	72
REE Mobility During Weathering	82
Provenance of the Shales from the Fountain Formation	84
Diagenesis	87
Conclusions	88
Appendices	
A    Selected Plots of Major Element and Trace Element Distributions	89
B    Precision and Accuracy Determined for INAA and XRF	102
C    Chemical Analyses of Boulder Granodiorite Weathering Profile and Fountain Formation Shales	109
D    Mass Balance Data for Parent Granodiorite	113
E    Sampling, Sample Preparation and Analytical Techniques	114
References	117

## List of Figures

Figure 1.	Index map showing location of the Boulder weathering profile, north-central, Colorado.	6
Figure 2.	Cross section of the Pennsylvanian paleoweathering profile on East flank of Flagstaff Mountain, west of Boulder, Colorado (after Wahlstrom, 1948).	7
Figure 3.	Plot of $\text{SiO}_2$ versus distance from the Fountain Formation sediments along Boulder granodiorite paleoweathering profile.	15
Figure 4.	Plot of $\text{Na}_2\text{O}$ versus distance from the Fountain Formation sediments along Boulder granodiorite paleoweathering profile.	16
Figure 5.	Plot of $\text{Al}_2\text{O}_3$ versus distance from the Fountain Formation sediments along Boulder granodiorite paleoweathering profile.	18
Figure 6.	Plot of $\text{TiO}_2$ versus distance from the Fountain Formation sediments along Boulder granodiorite paleoweathering profile.	19
Figure 7.	Plot of $\text{K}_2\text{O}$ versus distance from the Fountain Formation sediments along Boulder granodiorite paleoweathering profile.	20
Figure 8.	Plot of $\text{MgO}$ versus distance from the Fountain Formation sediments along Boulder granodiorite paleoweathering profile.	21
Figure 9.	Plot of $\text{P}_2\text{O}_5$ versus distance from the Fountain Formation sediments along Boulder granodiorite paleoweathering profile.	23
Figure 10.	Plot of CIA index versus distance from the Fountain Formation sediments along the Boulder Granodiorite paleoweathering profile.	25
Figure 11.	Plot of Rb versus distance from the Fountain Formation sediments along Boulder granodiorite paleoweathering profile.	27

Figure 12.	Plot of Sr versus distance from the Fountain Formation sediments along Boulder granodiorite paleoweathering profile.	28
Figure 13.	Plot of Ba versus distance from the Fountain Formation sediments along Boulder granodiorite paleoweathering profile.	29
Figure 14.	Plot of Zr versus distance from the Fountain Formation sediments along Boulder granodiorite paleoweathering profile.	31
Figure 15.	Plot of Ta versus distance from the Fountain Formation sediments along Boulder granodiorite paleoweathering profile.	33
Figure 16.	Plot of Sc versus distance from the Fountain Formation sediments along Boulder granodiorite paleoweathering profile.	34
Figure 17.	Plot of La versus distance from the Fountain Formation sediments along Boulder granodiorite paleoweathering profile.	36
Figure 18.	Plot of Eu versus distance from the Fountain Formation sediments along Boulder granodiorite paleoweathering profile.	37
Figure 19.	Plot of Yb versus distance from the Fountain Formation sediments along Boulder granodiorite paleoweathering profile.	38
Figure 20.	Plot of Cr/Th versus distance from the Fountain Formation sediments along Boulder granodiorite paleoweathering profile.	40
Figure 21.	Plot of Zr/Cr versus distance from the Fountain Formation sediments along Boulder granodiorite paleoweathering profile.	42

Figure 22.	Plot of Th/Sc versus distance from the Fountain Formation sediments along Boulder granodiorite paleoweathering profile.	43
Figure 23.	Plot of Ti/Nb versus distance from the Fountain Formation sediments along Boulder granodiorite paleoweathering profile.	44
Figure 24.	Plot of La/Sc versus distance from the Fountain Formation sediments along Boulder granodiorite paleoweathering profile.	45
Figure 25.	Chondrite-normalized REE distributions of parent granodiorite and weathered samples from Boulder granodiorite paleoweathering profile.	47
Figure 26.	Parent-normalized REE distributions of weathered samples from Boulder granodiorite paleoweathering profile.	48
Figure 27.	Chondrite-normalized REE distributions of parent granodiorite and Fountain Formation shales.	50
Figure 28.	Parent-normalized REE distributions of Fountain Formation shales.	51
Figure 29.	Plot of (La/Yb) <sub>n</sub> versus distance from the Fountain Formation sediments along Boulder granodiorite paleoweathering profile.	52
Figure 30.	Plot of Eu/Eu* versus distance from the Fountain Formation sediments along Boulder granodiorite paleoweathering profile.	53
Figure 31.	Isocon plot of the weathered rock element concentration versus fresh rock concentration at 25.6 m.	55
Figure 32.	Isocon plot of the weathered rock element concentration versus fresh rock concentration at 10.8 m.	56

Figure 33.	Isocon plot of the weathered rock element concentration versus fresh rock concentration at 10.6 m.	57
Figure 34.	Isocon plot of the weathered rock element concentration versus fresh rock concentration at 3.9 m.	58
Figure 35.	Isocon plot of the weathered rock element concentration versus fresh rock concentration at .4 m.	59
Figure 36.	Isocon plot of the weathered rock element concentration versus fresh rock concentration at .02 m.	60
Figure 37.	Brimhall plot of weathered rock - parent rock concentration ratio versus parent rock - weathered rock density ratio for SiO <sub>2</sub> , CaO, Na <sub>2</sub> O, K <sub>2</sub> O.	62
Figure 38.	Brimhall plot of weathered rock - parent rock concentration ratio versus parent rock - weathered rock density ratio for TiO <sub>2</sub> , Al <sub>2</sub> O <sub>3</sub> , Fe <sub>2</sub> O <sub>3</sub> , MgO, P <sub>2</sub> O <sub>5</sub> .	63
Figure 39.	Brimhall plot of weathered rock - parent rock concentration ratio versus parent rock - weathered rock density ratio for Zr, Th, Hf, Ta, Nb.	64
Figure 40.	Brimhall plot of weathered rock - parent rock concentration ratio versus parent rock - weathered rock density ratio for Y, Co, Sc, Sr, Cr, Rb, Ba.	65
Figure 41.	Brimhall plot of weathered rock - parent rock concentration ratio versus parent rock - weathered rock density ratio for La, Ce, Sm, Nd, Eu, Gd, Tb, Yb, Lu.	66



Figure 42.	Plot of the percent contribution of minerals to whole-rock REE content for parent rock from the Boulder granodiorite.	73
Figure 43.	Plot of the percent contribution of minerals to whole-rock REE content for weathered rock (25.6 m from sediment-granodiorite interface) from the Boulder granodiorite.	74
Figure 44.	Plot of the percent contribution of minerals to whole-rock REE content for weathered rock (6.7 m from sediment-granodiorite interface) from the Boulder granodiorite.	75
Figure 45.	Plot of the percent contribution of minerals to whole-rock REE content for weathered rock (.02 m from sediment-granodiorite interface) from the Boulder granodiorite.	76
Figure 46.	Plot of the percent contribution of minerals to the whole-rock La concentration versus distance from Fountain Formation sediments along the Boulder paleoweathering profile.	78
Figure 47.	Plot of the percent contribution of minerals to the whole-rock Yb concentration versus distance from Fountain Formation sediments along the Boulder paleoweathering profile.	79
Figure 48.	Plot of the percent contribution of minerals to the whole-rock Eu concentration versus distance from Fountain Formation sediments along the Boulder paleoweathering profile.	80
Figure A-1.	Plot of CaO versus distance from the Fountain Formation sediments along Boulder granodiorite paleoweathering profile.	90
Figure A-2.	Plot of Fe <sub>2</sub> O <sub>3</sub> versus distance from the Fountain Formation sediments along Boulder granodiorite paleoweathering profile.	91

Figure A-3.	Plot of Th versus distance from the Fountain Formation sediments along Boulder granodiorite paleoweathering profile.	92
Figure A-4.	Plot of Hf versus distance from the Fountain Formation sediments along Boulder granodiorite paleoweathering profile.	93
Figure A-5.	Plot of Nb versus distance from the Fountain Formation sediments along Boulder granodiorite paleoweathering profile.	94
Figure A-6.	Plot of Cr versus distance from the Fountain Formation sediments along Boulder granodiorite paleoweathering profile.	95
Figure A-7.	Plot of Co versus distance from the Fountain Formation sediments along Boulder granodiorite paleoweathering profile.	96
Figure A-8.	Plot of Y versus distance from the Fountain Formation sediments along Boulder granodiorite paleoweathering profile.	97
Figure A-9.	Plot of Zr/Y versus distance from the Fountain Formation sediments along Boulder granodiorite paleoweathering profile.	98
Figure A-10.	Plot of Co/Th versus distance from the Fountain Formation sediments along Boulder granodiorite paleoweathering profile.	99
Figure A-11.	Plot of La/Th versus distance from the Fountain Formation sediments along Boulder granodiorite paleoweathering profile.	100
Figure A-12.	Plot of Cr/Sc versus distance from the Fountain Formation sediments along Boulder granodiorite paleoweathering profile.	101

## List of Tables

Table 1. Modal analyses of fresh rock, weathered rock, and shales from the Boulder granodiorite paleoweathering profile.	11
--	----

## Introduction

Rare earth elements (REE) have very similar physical and chemical properties and are not easily fractionated during sedimentary processes (McLennan, 1981). The low solubilities and low concentrations of REE in the hydrosphere implies that they are transferred to the oceans as the suspended loads of rivers and streams (McLennan, 1981; Condie, 1991). This considered, REE are often assumed to be sensitive to source area composition and have been used as provenance indicators of fine-grained sedimentary rocks (McLennan, 1981; Condie, 1991; Crichton and Condie, 1993). In sedimentary studies, a remarkable similarity between REE patterns of fine-grained sediments derived from a variety of igneous sources has been observed (McLennan, 1981). It is thought that REE distributions of these sediments accurately reflects the average composition of the upper crust. The uniformity of the REE patterns has been attributed to efficient mixing of sediments during the mechanical processes of sedimentation (Duddy, 1980). Using trace element distributions of fine-grained sediments to determine the source material may yield important information about the relationship between sediments and their protolith, and this information may be used to constrain crustal compositions, tectonic settings, and the growth of continents (Taylor and McLennan, 1985; Condie, 1991; Crichton and Condie, 1993).

Recent studies have criticized the use of REE as provenance indicators for fine-grained sediments because too little is known about the effects on element fractionation of grain size, selective adsorption or solution of the REE in waters with variable pH, climatic influences, and the original mineralogy of the parent rock (Cullers, 1988; Duddy, 1980). There have been many studies of trace element behavior during the chemical weathering (Nesbitt, 1979; Duddy, 1980; Suttner et al., 1981; Cullers et al., 1987; Cullers, 1988; Johnsson et al., 1988). These studies show that REE are

remobilized during weathering but there is no net gain or loss of specific REE. Nesbitt (1979) suggested fractionation of REE in a weathering profile is due primarily to mineralogical control; however, changes in the REE distribution can be caused by differences in solubility of specific REE and changes in the geochemical environment. The extent to which REE are adsorbed onto clay minerals is sensitive to pH. REE are susceptible to removal in acidic solutions and remain fixed in basic solutions (Duddy, 1980; Cullers, 1987) and individual REE vary in their geochemical behaviors. The light REE (LREE) have been shown to be preferentially adsorbed on primary or secondary minerals (Nesbitt, 1979). Heavy REE (HREE) form stronger complexes with carbonate and organic ligands and therefore stay in solution more easily than LREE (Henderson, 1984). It is uncertain whether small, localized REE fractionations recognized in weathering profiles have an effect on the overall REE pattern of a shale or fine-grained sediment derived from the erosion and subsequent deposition of these profiles.

Whether or not REE are mobilized and fractionated during weathering and redeposition determines their usefulness as provenance indicators. The mobilization of REE has commonly been assumed to reflect mineralogical changes that occur during weathering (Nesbitt, 1979). If this is the case, it is important to determine what mineralogical changes occur during alteration and how these changes affect resulting sediments. REE in igneous rocks are hosted chiefly in accessory minerals. Common REE-bearing accessory minerals include zircon, apatite, allanite, sphene, and monazite (Henderson, 1984). Of the major rock-forming minerals, micas and amphiboles may contain moderate amounts of REE. Feldspars contain very small amounts of REE; however, due to the substitution of Eu for Ca, feldspars can house appreciable amounts of Eu (Taylor and McLennan, 1985). It is of interest to ascertain which minerals are hosting REE during progressive weathering and in transfer to derivative sediments. There are three methods by which the REE can be transferred to sediment from a

weathering profile: (1) REE can remain in the accessory minerals and be transferred in bulk to the sediments; (2) REE may be housed in relatively unstable accessory minerals which break down and release the REE to clay minerals as weathering progresses, and if so, the clays then carry the bulk REE concentration to the sediments; (3) and thirdly, REE may be transferred from a relatively unstable mineral to a secondary product of that mineral. This secondary product remains stable through the sedimentary process and preserves the REE signature of the source rock.

Although REE are thought to reside in the clay minerals of shales, a significant proportion of the non-opaque heavy minerals in sediments may be hosting REE and controlling REE distributions (Blatt and Sutherland, 1969; Gromet and Silver, 1984; Cullers et al., 1987; Condie, 1991). Cullers et al. (1987) noted that modern weathering products of granitoids contain an enrichment of heavy minerals in the clay and silt-sized fractions. Small amounts of these minerals could influence the REE distributions in the suspended load and sediments of streams. Both sphene and apatite have REE distributions similar to shales, but elevated by two orders of magnitude (Taylor and McLennan, 1985). Therefore, a small percentage of these minerals in a fine-grained sediment would influence the REE distributions. Shales from many diverse igneous rocks of post-Archean age have similar REE distributions (Taylor and McLennan, 1985; McLennan, 1981; Condie, 1991). This implies that, if REE do reside in the heavy minerals, these minerals must occur in the same proportions in the sediments and parent material. Knowing that chemical and mechanical variations occur during weathering and transportation, this does not seem like a feasible mechanism for the transfer of REE.

REE may be adsorbed onto clays from mineral phases that break down during weathering (Henderson, 1984). REE are housed in accessory minerals in the parent rock and upon weathering these minerals break down and may release their REE in solution. Assuming the REE are not complexed by fluids and selectively removed from

the system, they may be adsorbed onto clays with no net gains or losses of individual REE. In a study of different size fractions of soil and stream sediment derived from an intensely weathered granite, it was found that the trace element distributions of silt-sized material most closely represented those of the source rock (Cullers, 1988). This implies that REE may be hosted by the finer-grained material. Clay control of the REE distributions of fine-grained sediments is also supported by the similarity of the REE distributions of the sediments to those of illites, the principal clays in shales (Cullers et al., 1975 - fig. 2). The similarity of REE distributions in the suspended loads of rivers to those of shales and the correlations of the  $Al_2O_3$  and REE concentrations in shales also suggest clay control (Condie, 1991).

REE may be transferred from a relatively unstable host mineral into a secondary phase produced from that mineral during weathering and transported to the resulting sediments. A study by Banfield and Eggleton (1989) showed that apatite replacement by REE-bearing phases such as fluorencite enriched the weathered rock in REE with no gain or loss of individual REE (Ce anomalies were reported, however). The secondary phases are presumed stable in the weathering environment and are the primary REE hosts in the resulting sediment.

The purpose of the present study is to determine which minerals host REE throughout the weathering process in a paleoweathering profile. By analyzing the geochemical changes that occur during weathering, it is possible to determine whether REE are mobilized, and to what extent gains or losses of specific REE occur. A second objective is to determine the usefulness of REE as provenance indicators in sediments. Parent-rock REE distributions are compared to those of the weathered rock and to the shales that appear to be derived from the paleoweathering profile. The Eu anomaly of fine-grained sediments may reflect that of the source rock (Chrichton, 1992), and the large negative Eu anomaly common to post-Archean shales has been assumed to reflect the Eu anomaly of the exposed continental crust from which these

shales were derived (McLennan 1981). A third purpose of this study is to determine how the Eu anomaly of the sediments relates to that of the parent rock and whether the Eu anomaly develops during weathering.

## General Geology

A Pennsylvanian paleoweathering profile developed on a granodiorite of the Boulder Batholith was chosen for this study. The profile is well exposed along the main road through Flagstaff Mountain Park, near Boulder, Colorado (Fig. 1), and it is easy to sample from fresh to highly weathered rock. The most highly weathered granodiorite is in contact with the Permian Fountain Formation, which is considered to be the recycled and transported material from the weathered Boulder Batholith (Wahlstrom, 1948). This occurrence makes the profile ideal for studying the transfer of REE from the source material to derivative sediments.

There have been several previous studies of the Boulder paleoweathering profile (hereafter referred to as simply the weathering profile). A general geochemical overview of the profile was published by Wahlstrom (1948), and a study of the distribution of uranium and thorium during weathering of the granodiorite was published by Pfler and Adams (1972). A series of whole rock and mineral geochemical analyses from the Boulder Batholith are available in Gable (1980). R. L. Cullers (personal communication, May, 1993) has also sampled from the profile for REE analyses. These data have been useful for comparison to the results of this study.

The Boulder weathering profile is exposed along the Flagstaff Mountain road cut (Fig. 2). Fresh granodiorite is well preserved on the western end of the outcrop with the arkose and shales of the Fountain Formation overlying the weathered profile material to the east. Recent weathering is parallel to the present day soil surface and in



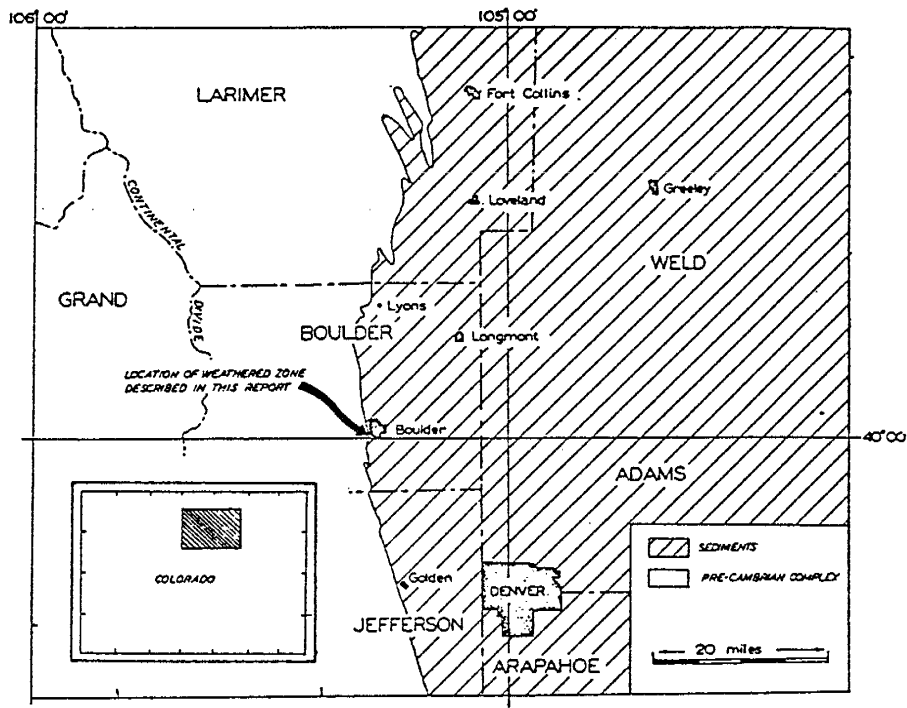


Figure 1. Index map showing location of the Boulder granodiorite weathering profile, north-central, Colorado (after Wahlstrom, 1948).

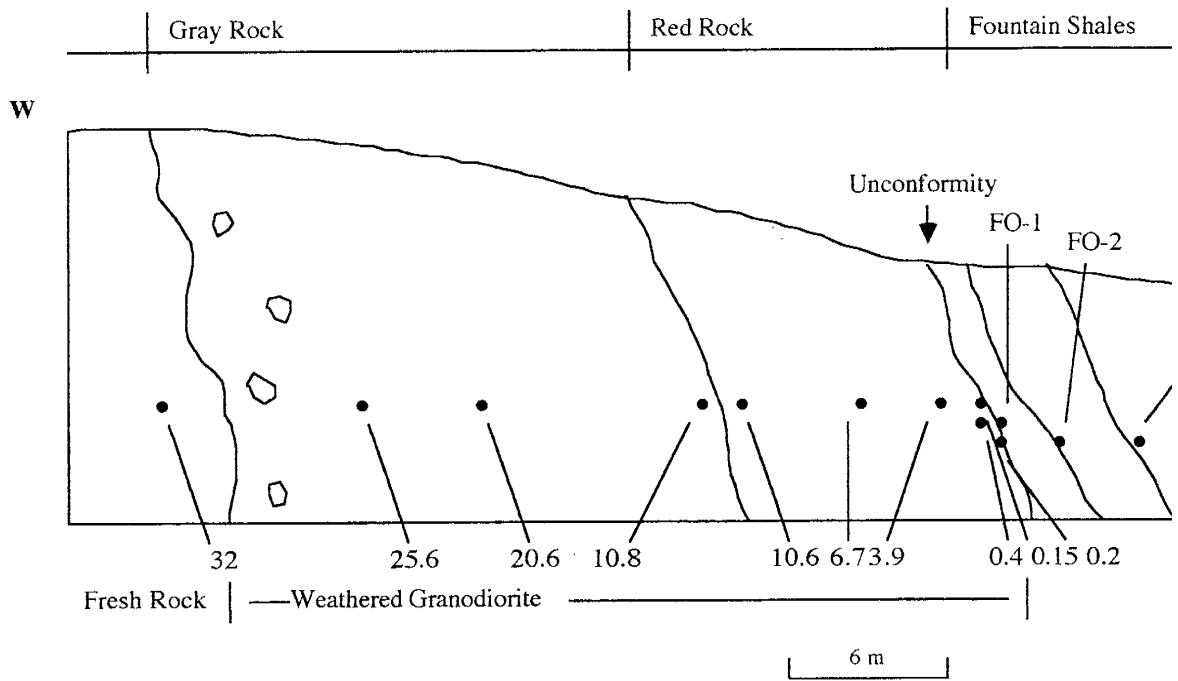


Figure 2.

Diagrammatic construction of the Boulder paleoweathering profile on Flagstaff Mountain west of Boulder, Colorado. Numbers represent sample locations measured in meters beneath the Permian unconformity.

places is superimposed on the paleoweathering profile. The modern weathering appears to have had no effect on the Pennsylvanian profile (Wahlstrom, 1948).

From the contact with the fresh rock, the weathered granodiorite extends laterally for approximately 30 m and can be divided into three main zones on a visual basis. The most weathered part of the granodiorite forms a red zone 10 m thick that grades from a very dark brown color nearest the sediments to a lighter pink as it becomes less enriched in iron-oxides. In this red zone, leaching is severe and there is evidence of collapse and compaction and the rock no longer displays a granitoid texture. It is cut by ubiquitous aplitic and pegmatitic dikes. The brown and pink zones are underlain by a distinct light gray bleached saprolite zone 15 - 18 m thick that grades into fresh rock. Within the saprolite are rounded masses of residual parent material that were not weathered as pervasively. The saprolite retains the original granitoid texture, although it is friable and appears more porous than the parent rock.

The unconformably overlying arkose interfingers with shale beds ranging from a few centimeters to more than 5 m thick, increasing in width with distance from the contact. The Permian paleoclimate has been interpreted as humid with moderate to high average temperatures consistent with severe chemical weathering (Wahlstrom, 1948).

## Methods

The field work for this study was completed during the summer of 1992. Samples of the weathered granodiorite and Permian shales were taken from the roadcut at intervals measured perpendicular to the contact with the Fountain Formation (Fig. 1). Due to the poorly consolidated nature of the weathered material, samples were easily removed from the outcrop with a geologic pick. A minimum of 1000 cm<sup>3</sup> was taken

for chemical analysis and 50 kg of material was taken from incipiently weathered rock for mineral separates. Although the majority of the profile yielded unconsolidated samples, there are sections of intact material used for density measurements and thin sections.

Samples were obtained from the brown-red zone directly adjacent to the shale contact and up to 6 m away, avoiding the cross-cutting dikes and two adjacent samples were taken from the gray-red contact (at 10.8 and 10.6 m) and up to 26 m from the Permian unconformity. Samples were taken from three separate shales of the Fountain Formation. From comparison to granodiorite previously analyzed at this location (R. L. Cullers, personal communication, May, 1993), the fresh rock initially sampled appears to be slightly altered and therefore, not representative of the parent material. For the purposes of this study, an average of two fresh rock samples collected by Cullers has been used as the parent rock composition.

Samples were ground and prepared for instrumental neutron activation analysis for the trace elements Hf, Ta, Sc, Co, Cr, Ba, Th and seven REE (La, Ce, Sm, Nd, Eu, Tb, Yb, and Lu). The whole-rock samples were irradiated at Texas A&M University, College Station, Texas and the University of Missouri at Columbia. Several duplicate samples were irradiated to check the precision and accuracy of the method. Element abundances were determined at New Mexico Tech using TEABAGS reduction software and Ge gamma-ray detectors. Samples were analyzed by XRF for the major elements SiO<sub>2</sub>, Na<sub>2</sub>O, TiO<sub>2</sub>, Fe<sub>2</sub>O<sub>3</sub>T, MnO, MgO, CaO, K<sub>2</sub>O, and P<sub>2</sub>O<sub>5</sub> and the trace elements Rb, Sr, Y, Zr, and Nb using a Rigaku XRF spectrometer. See Appendix C for complete details of analytical methods.

Density measurements were made of both weathered and unweathered rock. Samples were weighed and then coated with a clear nail polish because of their porous and friable nature. They were placed in a graduated cylinder and the volume of water displaced was measured. Numerous measurements were made and the density values

for each sample were averaged. Values varied between 2.68 g/cm<sup>3</sup> (fresh rock) and 2.22 g/cm<sup>3</sup> (weathered rock) (see Table 1). The incipiently and moderately weathered samples showed the lowest densities with values between 2.37 g/cm<sup>3</sup> and 2.22 g/cm<sup>3</sup>. Due to compaction and high Fe-oxide content, the density of the material increased with increased weathering to values of 2.4-2.5 g/cm<sup>3</sup>.

Mineral separates were obtained from one sample of incipiently weathered rock near the base of the fresh granodiorite (25.6 m). The minerals include sphene, apatite, feldspar, and biotite. A magnetic separator, manual picking, and paper shaking techniques were used to further purify the biotite and feldspar fractions. Sphene and apatite separates were obtained using heavy liquids (lithium metatungstate and methylene iodide).

### Petrographic Results

A total of 17 thin sections were made from the fresh rock, weathering profile and overlying shales. Thin sections were prepared from each of the weathered samples, two shale samples, and four samples of the parent granodiorite. Modal counts were made using standard point counting methods as described in Pettijohn et al. (1973) and results are presented in Table 1. Due to the unconsolidated nature of the weathered material, all but one of the samples were made as epoxy mounts and these thin sections may not be representative of the weathered material. However, when used in conjunction with the major element data, it was possible to closely approximate the modal contents by using normative mineral percentages.

The average point count of four thin sections of fresh granodiorite was taken to represent the parent rock (Table 1). This average shows good agreement with the

	Fresh Rock	25.6 m	20.6 m	10.8 m	10.4 m	6.7 m	3.9 m	.4 m	.15 m	.02 m
Quartz	24	30	33	27.3	15	18	16	14	18	15
K-Feldspar	16	10	8.2	8.3	8.6	7.5	6.9	8.8	5.6	5.3
Plagioclase	40	18	7.3	2.0	2.6	3.1	2.0	2.2	2	1.5
Biotite	13	10	15	12.6	13.3	12	5.2	3.3	2.3	2.1
Hornblende	1	0	0	0	0	0	0	0	0	0
Opaque	5.1	3.3	2.2	2.3	10.6	2.9	4.8	8.1	11	12
Apatite	0.45	0.36	0.36	0.6	1.0	0.88	0.88	0.82	0.3	0.34
Sphene	.40	.11	.02	0	0	0	0	0	0	0
Zircon	0.02	0.03	0.03	0.04	0.04	0.04	0.04	0.03	0.03	0.03
Allanite	0.001	0.1	0	0	0	0	0	0	0	0
Clays	tr	26	32	43.3	47.3	53	54	60	60	64
Carbonate	0	2.0	2.8	3.3	1.6	3.1	1.5	2.0	1.0	1.1
Density g/cm <sup>3</sup>	2.68	2.27	2.24	2.37	2.37	2.22	2.44	2.39	2.4	2.5

Table 1. Modal analyses of fresh rock, weathered rock, and Fountain Formation shales from the Boulder granodiorite paleoweathering profile.

modal percentages published by Wahlstrom (1948): 35% oligoclase, 25% microcline, 20% quartz, 16% biotite, 3% hornblende, and 1% minor minerals such as apatite, sphene, magnetite, and allanite.

In the fresh granodiorite, oligoclase is slightly altered by dissolution and etching along twin planes and grain boundaries and some clay replacement is present. Biotite forms both interlocking laths with adjacent minerals and relatively large flakes. There are small amounts of hornblende present in the rock, and trace amounts of sphene, apatite, allanite, and zircon. The sphene and apatite are intimately associated with biotite, occurring along grain edges and as inclusions within the biotite crystals. There are small amounts of carbonate present as patches in altered plagioclase grains.

The secondary minerals resulting from pre-Fountain weathering are clays, iron-oxides, hydrated micas, and carbonate. Montmorillonite, kaolinite, and illite are present throughout the profile in varying abundances (Wahlstrom, 1948), but were not identified as separate minerals in this study. Three primary stages of alteration can be defined along the profile. The initial stage of weathering (the light gray, bleached zone) occurs between the parent rock and approximately 10 m beneath the contact with the unconformably overlying Permian sediments. This zone is characterized by altered plagioclase, a high clay percentage, the appearance of minor amounts of iron-oxide as crusts on biotite, and the absence of hornblende. There is also an abundance of irregularly matted, poorly oriented flakes of clay that occur as a matrix for other minerals. In some cases, these clay matrices have pseudomorphically replaced feldspar grains and retain the original feldspar morphology, including relicts of twinned plagioclase. Sphene is still present at this stage of weathering, but it is partly altered to leucoxene. The quartz, microcline, biotite, apatite and zircon, remain relatively fresh in this portion of the profile. Carbonate occurs in significant amounts and is primarily associated with altered plagioclase. It is also present in veinlets that cut other minerals. Wahlstrom (1948) suggests that the carbonate was derived from altered minerals within

the profile and not precipitated from surface solutions. The relative mineral stability in incipiently weathered granodiorite is hornblende, sphene, plagioclase, biotite, microcline, and quartz, quartz being the most stable.

The second, or moderately weathered zone (the pinkish-red zone) occurs between 10 m and 1 m beneath the sediment-weathering profile contact. This zone is characterized by a significant increase in the amount of iron-oxides. These oxides form as crusts on biotite and are also interspersed with the clays. Sphene and its alteration products have been completely removed, the biotite is altering to vermiculite, and the plagioclase is almost entirely replaced by clay. Apatite and zircon are present throughout this portion of the profile, quartz and microcline remain intact, and carbonate is present in minor amounts.

The third and most highly weathered zone (dark red-brown rock) begins at 1 m beneath the contact with the Permian shales. In this highly weathered zone, the K-feldspar begins to show signs of alteration, exhibiting ragged edges and solution pits. Quartz remains resistant, although iron-oxide rinds and coatings are present. At the contact with the adjacent Fountain Formation, the clay percentages are quite high (Table 1, sample 0.02 m). The only original minerals remaining are remnants of quartz and microcline and the accessories apatite and zircon. Biotite has been completely altered to clay, hydrated mica, and iron-oxide. This zone also has a distinct compaction texture. The less resistant minerals, such as altered biotites and clays, have been deformed and envelope the more stable grains of quartz and microcline.

The Fountain Formation shales are fine-grained with angular to subangular clasts in a clay and iron-oxide matrix. The clasts are composed primarily of quartz, microcline, plagioclase feldspar, muscovite, and biotite. The grains appear relatively unweathered, and no trace minerals other than zircon were observed in thin section.



## GEOCHEMICAL RESULTS

### Major Element Distributions

Parent granodiorite and weathering profile major element concentrations have been plotted versus distance from the unconformably overlying Permian sediments. The Fountain Formation shales are placed arbitrarily along the distance axis. Plots included in the text are those elements which display representative behaviors, the remainder are located in Appendix A.

With the exception of two incipiently weathered samples (20.6 m, 10.8 m), there is a decrease in SiO<sub>2</sub> from 71 to 51 % along the weathering profile (Fig. 3). This decrease is pronounced across the gray-red contact at 10.7 m. SiO<sub>2</sub> reaches a minimum value at the sediment-weathering profile interface (0.02 m). The incipiently weathered samples showing high SiO<sub>2</sub> concentrations (20.6 m, 10.8 m) have a greater percentage of quartz in thin section than the fresh granodiorite (Table 1). The incipiently weathered sample taken closest to the parent rock (25.6 m) also has a greater percentage of quartz in thin section, however the SiO<sub>2</sub> concentration is low. Shale SiO<sub>2</sub> values range from 59 to 67 % and resemble the moderately and highly weathered granodiorite concentrations.

Na<sub>2</sub>O and CaO behave similarly as a function of distance along the weathering profile (Fig. 4 and Fig. A-1). Na<sub>2</sub>O and CaO values range from 0.2 to 2.94 % and 0.5 to 2.64 %, respectively. These oxides drop off abruptly from the fresh rock values at the onset of weathering. Na<sub>2</sub>O and CaO continue to decrease throughout the remainder of the profile, reaching a minimum at the unconformity. There is virtually no change in the Na<sub>2</sub>O or CaO content across the gray-red contact. Shale Na<sub>2</sub>O and

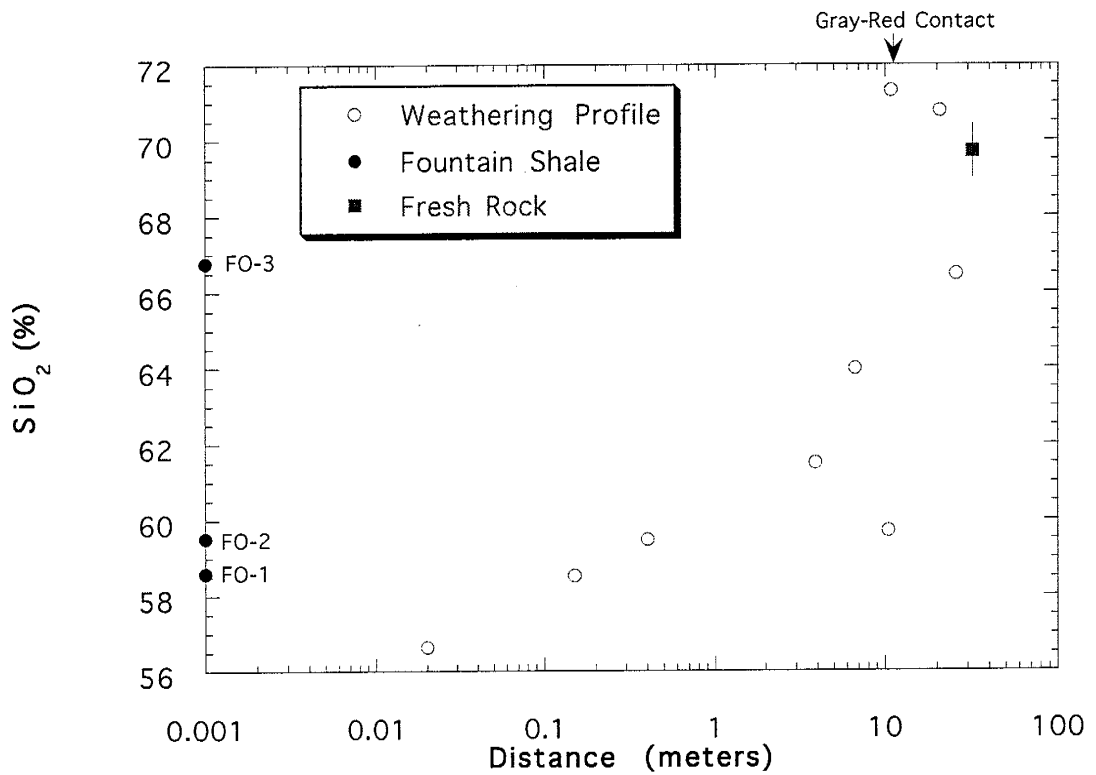


Figure 3. Plot of SiO<sub>2</sub> versus distance from the Fountain Formation sediments along the Boulder granodiorite paleoweathering profile. Shale samples FO-1, FO-2, FO-3 are arbitrary on the distance axis. Vertical line through parent rock represents range in composition of fresh granodiorite samples CR1-1 and CR

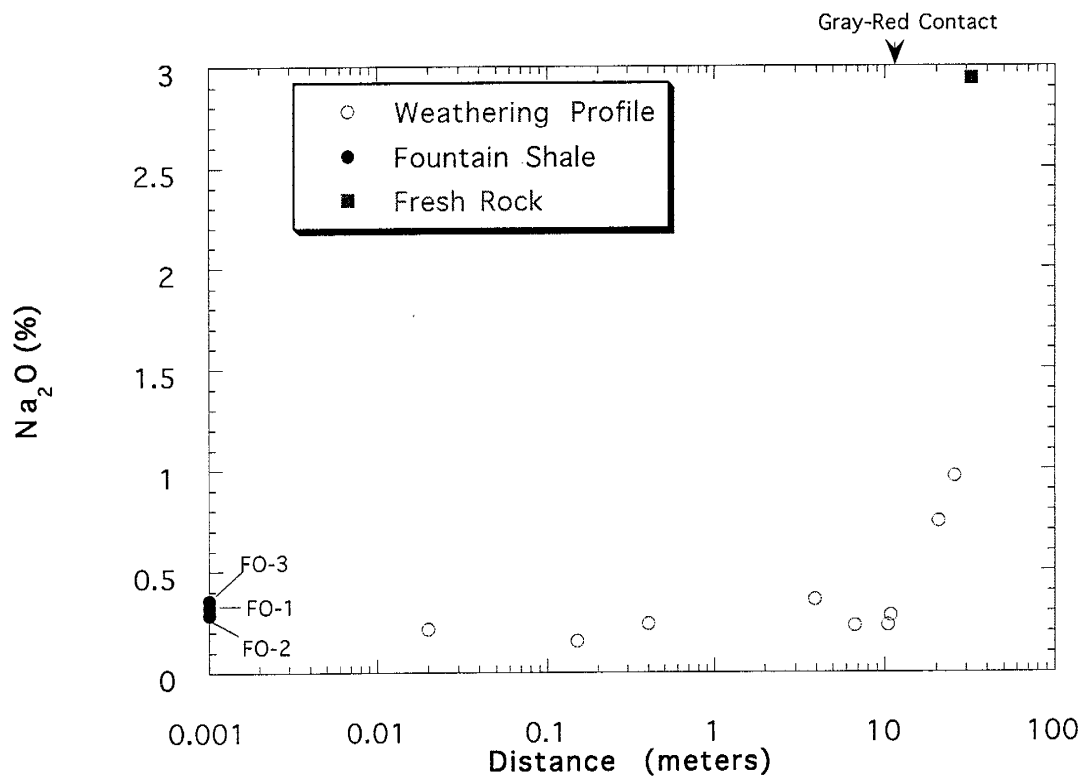


Figure 4. Plot of Na<sub>2</sub>O versus distance from the Fountain Formation sediments along the Boulder granodiorite paleoweathering profile. Other information given in Figure 3.

CaO values range from 0.3 to 0.4 % and 0.4 to 0.6 %, respectively, similar to the concentrations of these elements in the last meter of the weathering profile.

Al<sub>2</sub>O<sub>3</sub> and Fe<sub>2</sub>O<sub>3</sub>T also behave similarly in the weathering profile (Fig. 5 and Fig. A-2), where they range from 13 to 20 % and 2 to 10 %, respectively. There is an initial decrease in the Al<sub>2</sub>O<sub>3</sub> and Fe<sub>2</sub>O<sub>3</sub>T contents of the first three incipiently weathered samples (25.6m, 20.6m, 10.8 m) from fresh rock concentrations. The oxide concentrations increase throughout the remainder of the profile and reach a maximum at the unconformity. There is a pronounced increase in both Al<sub>2</sub>O<sub>3</sub> and Fe<sub>2</sub>O<sub>3</sub>T across the gray-red contact. The Fountain Formation shales have Al<sub>2</sub>O<sub>3</sub> values ranging from 19 to 21 %, similar to those of the highly weathered portion of the profile. The Fe<sub>2</sub>O<sub>3</sub>T concentrations of the shales range from 3 to 8 %, resembling the moderately and highly weathered granodiorite.

TiO<sub>2</sub> content varies from 0.3 to 0.8 % along the weathering profile (Fig. 6). The concentration remains relatively constant in the incipiently weathered rock, increases dramatically across the gray-red contact, and reaches a maximum in the highly weathered rock adjacent to the unconformity. TiO<sub>2</sub> values in the shales range from 0.6 to 0.8 % and are similar to the TiO<sub>2</sub> contents of the moderately and highly weathered granodiorite.

K<sub>2</sub>O values increase from 4 to 7 % along the profile and reach a maximum value in the highly weathered rock directly beneath the Permian unconformity (Fig. 7). There is a slight decrease in K<sub>2</sub>O across the gray - red contact. Shale K<sub>2</sub>O values range from 6-8 % approximating the K<sub>2</sub>O content of the moderately and highly weathered rock.

MgO concentrations vary from 1 to 2.5 % along the profile (Fig. 8). The MgO content increases from fresh rock concentration to the incipiently weathered sample (25.6 m), then decreases in the bleached rock ( 20.6 m, 10.8 m). There is a

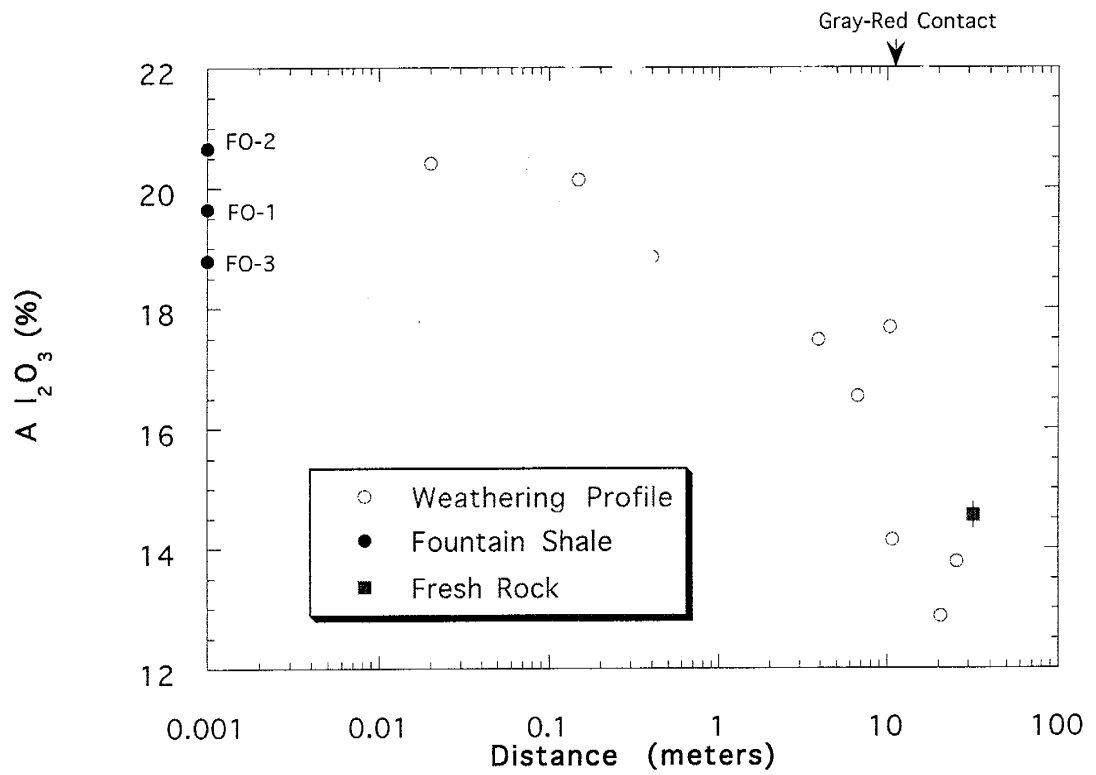


Figure 5. Plot of  $Al_2O_3$  versus distance from the Fountain Formation sediments along the Boulder granodiorite paleoweathering profile. Other information given in Figure 3.

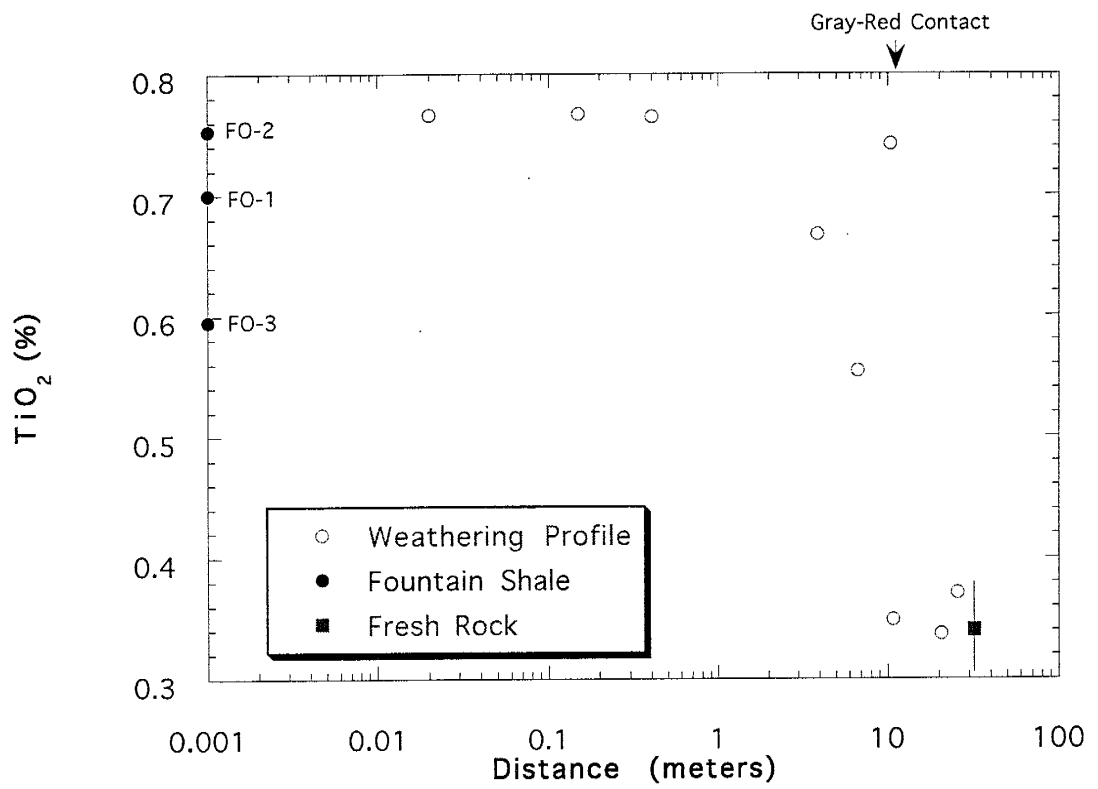


Figure 6. Plot of TiO<sub>2</sub> versus distance from the Fountain Formation sediments along the Boulder granodiorite paleoweathering profile. Other information given in Figure 3.

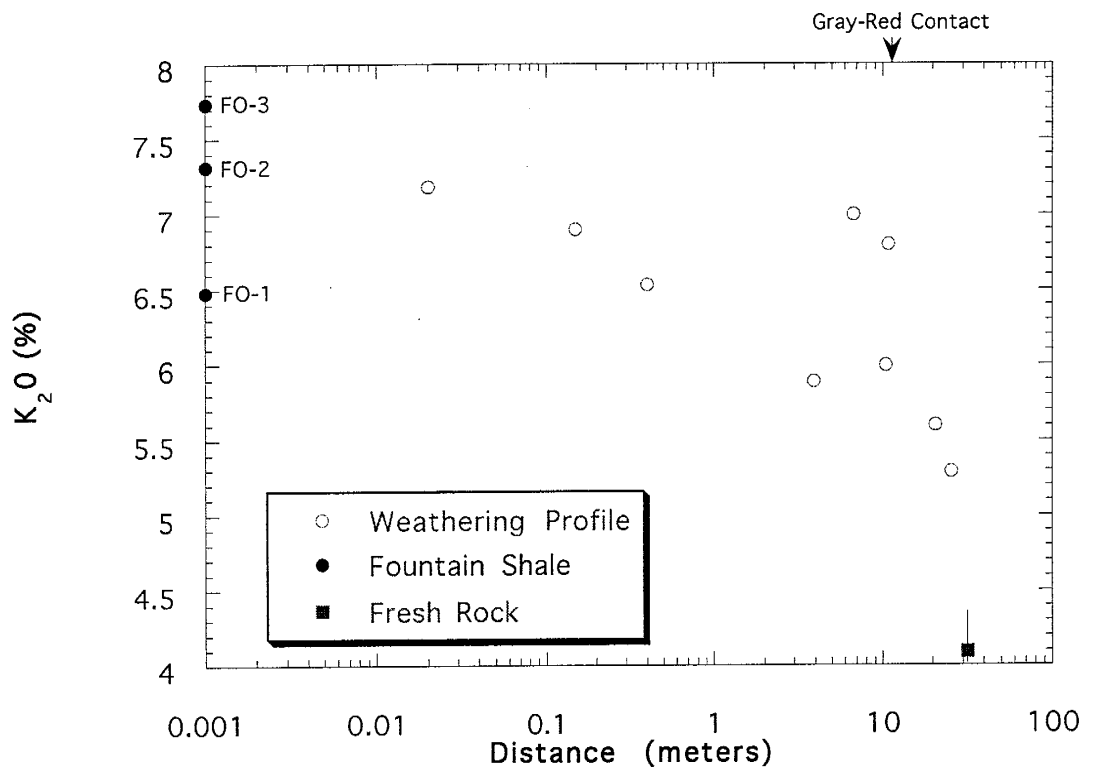


Figure 7. Plot of K<sub>2</sub>O versus distance from the Fountain Formation sediments along the Boulder granodiorite paleoweathering profile. Other information given in Figure 3.

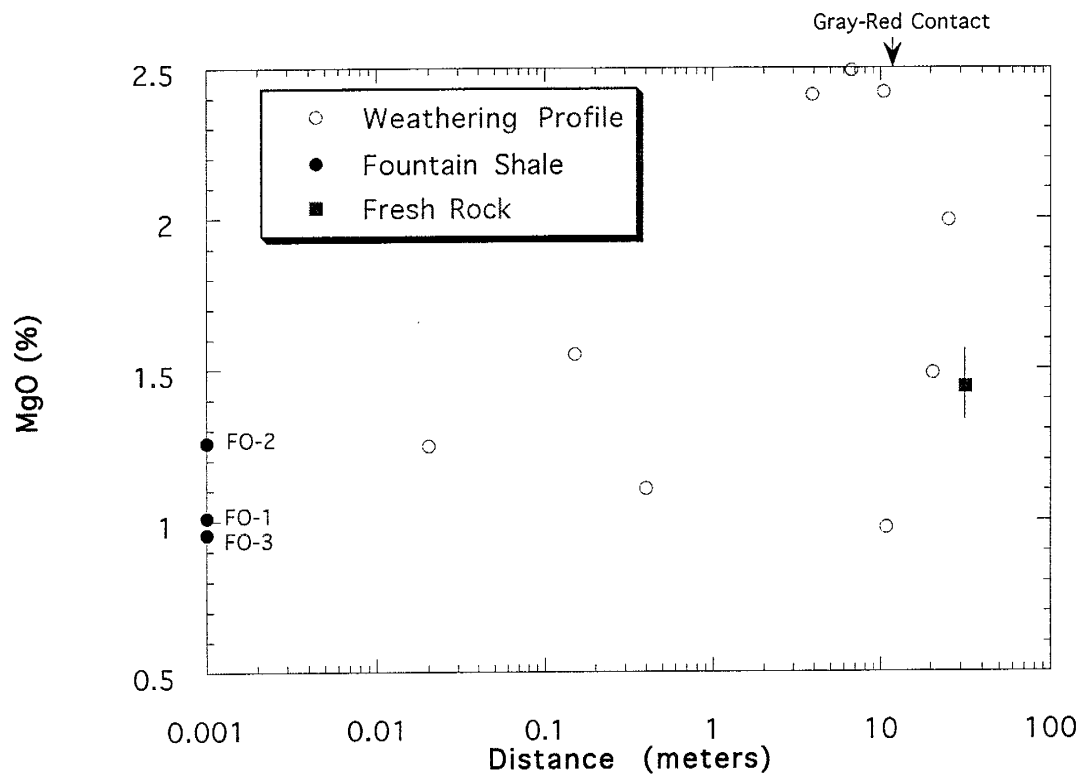


Figure 8. Plot of MgO versus distance from the Fountain Formation sediments along the Boulder granodiorite paleoweathering profile. Other information given in Figure 3.



pronounced increase in MgO across the gray-red contact and values reach a maximum approximately 7 m beneath the unconformity, followed by a decrease in the last meter of the profile. The shale MgO values range from 1 to 1.25 % , resembling those of the most highly weathered granodiorite.

P<sub>2</sub>O<sub>5</sub> values range from 0.1 to 0.4 % along the weathering profile (Fig. 9). With exception of the first two incipiently weathered samples (25.6m, 20.6 m), P<sub>2</sub>O<sub>5</sub> concentrations increase throughout the bleached zone into the red, moderately weathered granodiorite, and reach a maximum 10 m beneath the Permian unconformity. One meter below the unconformity there is a decrease in the P<sub>2</sub>O<sub>5</sub> content. P<sub>2</sub>O<sub>5</sub> concentrations of the shale range from 0.1 to 0.14 % , resembling those of the most highly weathered material.

In summary, during progressive weathering of the granodiorite, SiO<sub>2</sub>, Na<sub>2</sub>O<sub>3</sub>, and CaO contents decrease. These elements reach their lowest values in the most highly weathered portion of the profile, 0.4 to 0.02 m beneath the unconformity. Al<sub>2</sub>O<sub>3</sub>, Fe<sub>2</sub>O<sub>3</sub>T, TiO<sub>2</sub>, and K<sub>2</sub>O contents increase with increased weathering, reaching maximum concentrations in the highly weathered granodiorite, 0.4 to 0.02 m beneath the unconformity. The behavior of MgO and P<sub>2</sub>O<sub>5</sub> is more variable. Both of these oxides have maximum values in the moderately weathered rock , 7 to 10 m beneath the Permian unconformity. Across the gray-red contact there is a decrease in the SiO<sub>2</sub> and K<sub>2</sub>O concentrations, and Al<sub>2</sub>O<sub>3</sub>, Fe<sub>2</sub>O<sub>3</sub>T, TiO<sub>2</sub>, MgO, and P<sub>2</sub>O<sub>5</sub> increase from the bleached to the red rock. However, there is virtually no change in Na<sub>2</sub>O and CaO across the contact.

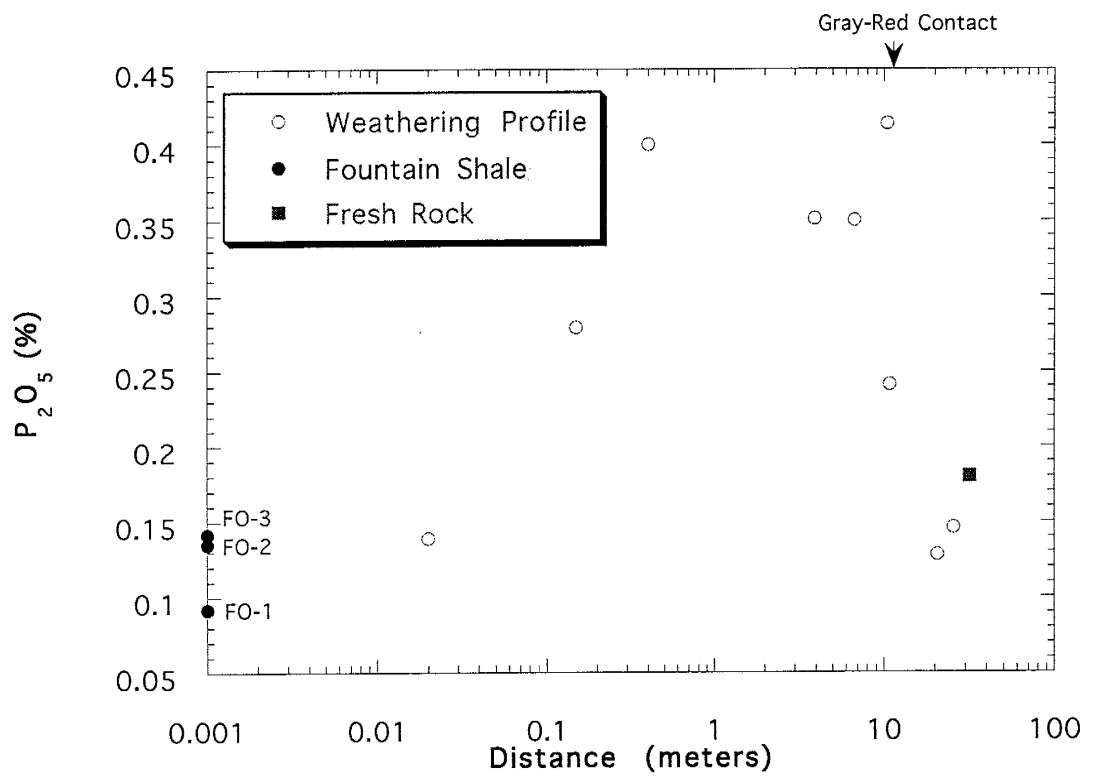


Figure 9. Plot of  $P_2O_5$  versus distance from the Fountain Formation sediments along the Boulder granodiorite paleoweathering profile. Other information given in Figure 3.

## Chemical Weathering Indices

Several chemical weathering indices have been proposed to quantify rock alteration (Nesbitt and Young, 1982; Harnois, 1988; Chittleborough, 1991). These indices are based on the progressive removal of elements during weathering. The CIA index of alteration is used in this study. It is a useful method of determining the degree to which feldspars have been altered, and may indicate to what extent weathering has removed K, Na, and Ca from clays (Taylor and McLennan, 1985). It is calculated by dividing  $(Al_2O_3)$  by  $(Al_2O_3+K_2O+Na_2O+CaO) \times 100$  with Al, K, Na, and Ca in molar proportions (Nesbitt and Young, 1982). The CaO content represents that of the silicate minerals only, excluding apatite and carbonate. The CIA variation as a function of distance along the Boulder weathering profile is shown in Figure 10. The CIA increases rapidly from a fresh granodiorite value of 52 throughout the incipiently and moderately weathered rock, reflecting chiefly alteration of plagioclase. A value of 70 is reached approximately 10 m beneath the Permian sediment contact where CIA values level off. Fountain Formation shale CIA indices range from 66 to 70. Extremely weathered clays have CIA values near 100 (Taylor and McClennan, 1985). Neither the weathering profile nor the Fountain sediments are altered to the point that K, Na, or Ca have been leached from the clays.

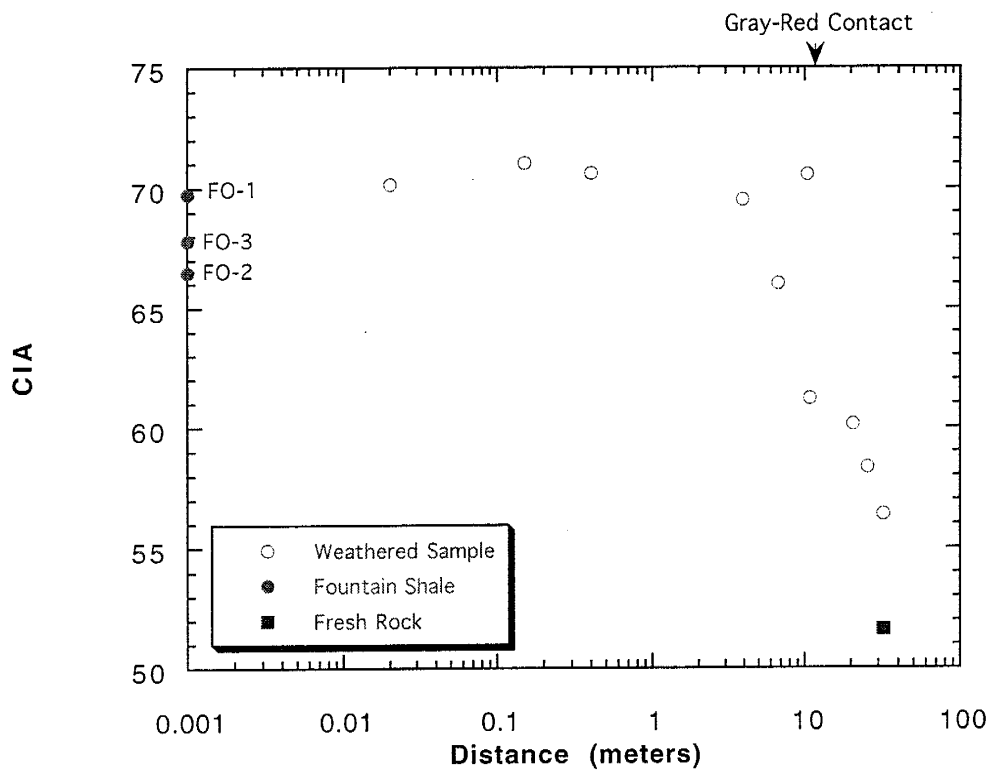


Figure 10. Plot of CIA index versus distance from the Fountain Formation sediments along the Boulder granodiorite paleoweathering profile. CIA is defined as  $(Al_2O_3)/(Al_2O_3+K_2O+Na_2O+CaO)*100$  with oxides in molar proportions and CaO representing that of silicates only (Nesbitt and Young, 1982). Other information given in Figure 3.

## Trace Element Distributions

Representative trace element distributions during weathering of the Boulder granodiorite are shown in Figures 11 through 19, the remaining trace element plots are located in Appendix A. The element concentrations have been plotted versus distance from the overlying Permian sediments and the Fountain Formation shales have been placed arbitrarily on the distance axis.

The Rb content varies from 174-284 ppm along the weathering profile (Fig 11). There is a slight increase in Rb from the fresh granodiorite through the incipiently weathered rock and a notable jump in concentration occurs across the gray-red contact. The Rb concentration changes little throughout the moderately and highly weathered rock, dropping slightly beneath the sediment contact. The Fountain shale Rb concentrations range from 388-411 ppm, much higher than in the weathering profile or fresh rock.

From the parent rock value, Sr decreases through the incipiently and moderately weathered rock, to a depth of 3.9 m and does not change appreciably across the gray-red contact. The Sr concentration varies from 200 to 1045 ppm in the weathering profile (Fig. 12). The significant increase to 1045 ppm occurs approximately 1 m beneath the unconformity after which Sr values decrease rapidly. The shales have Sr concentrations ranging from 300-400 ppm, similar to the incipiently and moderately weathered portions of the profile.

The Ba content of the weathering profile ranges from 615 to 1375 ppm (Fig. 13). Ba increases from the parent rock value through the bleached zone, reaching a maximum at the gray-red zone contact. There is a large decrease in Ba across the

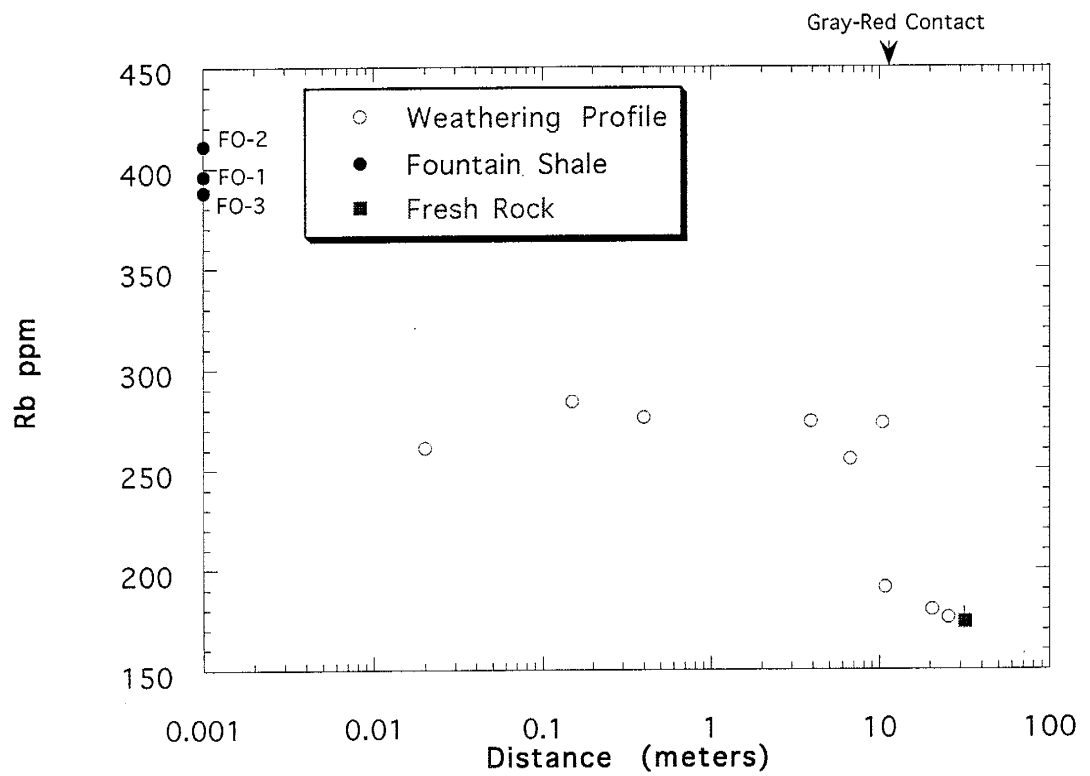


Figure 11. Plot of Rb versus distance from the Fountain Formation sediments along the Boulder granodiorite paleoweathering profile. Other information given in Figure 3.

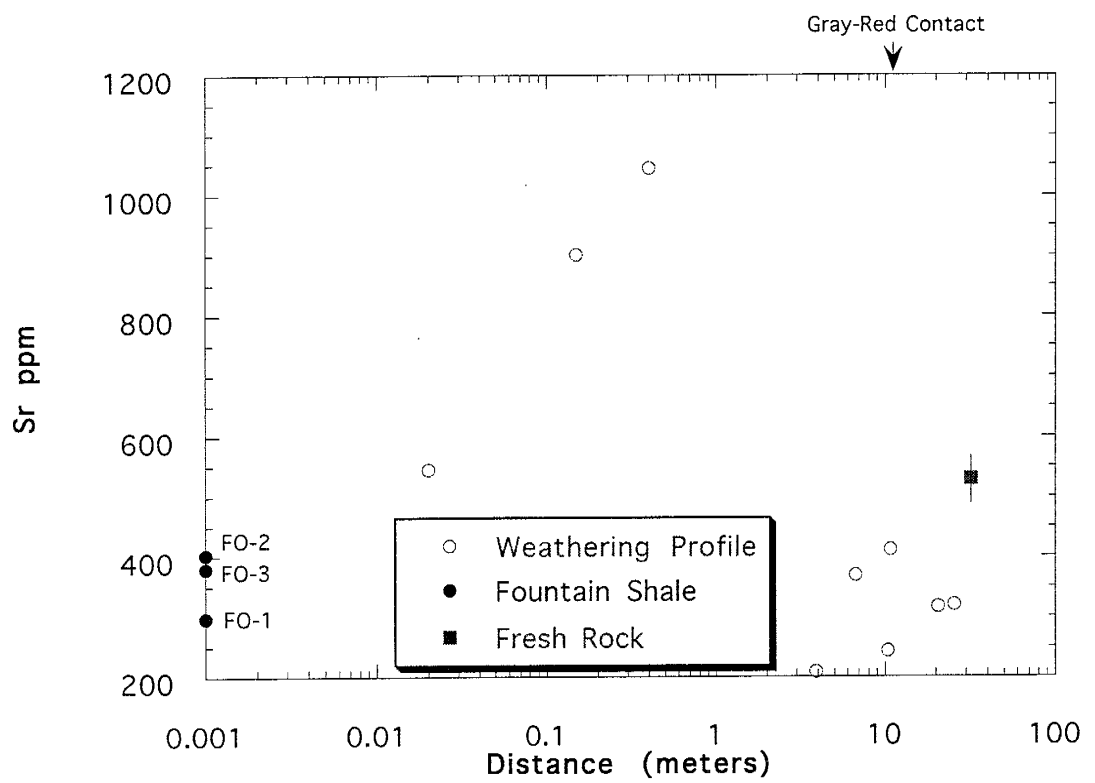


Figure 12. Plot of Sr versus distance from the Fountain Formation sediments along the Boulder granodiorite paleoweathering profile. Other information given in Figure 3.

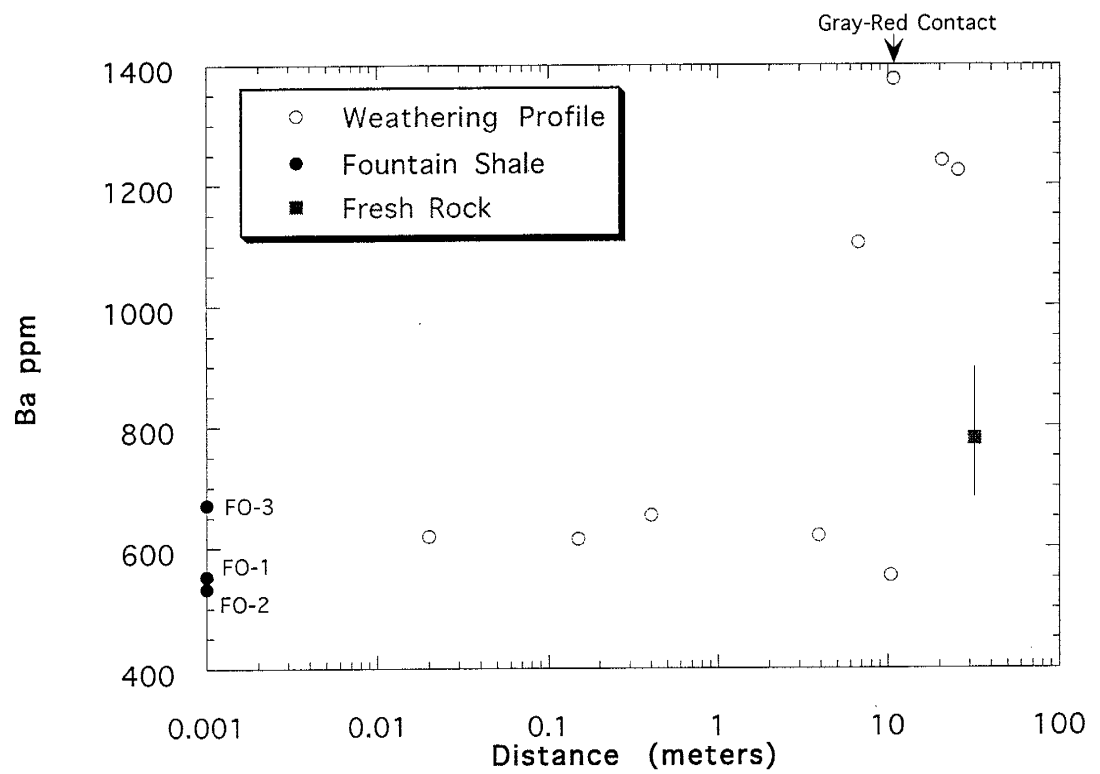


Figure 13. Plot of Ba versus distance from the Fountain Formation sediments along the Boulder granodiorite paleoweathering profile. Other information given in Figure 3.



contact into the red, moderately weathered material. With exception of one higher concentration (at 6.7 m), the Ba content of the moderately and highly weathered rock is relatively constant and lower than the fresh rock. The Ba contents of the Fountain shales range from 530 to 670 ppm and closely resemble the Ba concentrations of the highly weathered granodiorite.

Th increases from the fresh granodiorite in the incipiently and moderately weathered rock with virtually no change across the gray-red contact. There is an abrupt increase in Th approximately 1 m beneath the unconformity followed by a slight drop. The Th values range from 5 to 20 ppm along the weathering profile (Fig. A-3). The shales have Th concentrations ranging from 22 - 43 ppm. Two of the shale samples have Th values higher than those along the weathering profile and the third shale sample has a lower Th content, resembling that of the most highly weathered material.

Zr in the weathering profile varies from 109-218 ppm (Fig. 14) when it increases from the fresh rock through the bleached zone and reaches a maximum approximately 10 m beneath the Permian unconformity. Zr values decrease slightly through the remainder of the profile. The shale Zr concentrations range from 195 to 390 ppm with two of the shale samples having Zr concentrations higher than those of the weathering profile and the third sample with a concentration similar to the most altered rock.

Hf concentrations vary from 4-9 ppm along the weathering profile (Fig. A-4). The Hf behavior is similar to that of Zircon, increasing from the incipiently and moderately weathered rock and decreasing at 1 m beneath the Permian unconformity. Unlike Zr, Hf reaches a maximum in the last meter of the profile. The shale Hf concentrations range from 4 to 13.8 ppm. As with Zr, two shales have Hf values higher than those along the profile. The third shale has a concentration close to that of the fresh rock.

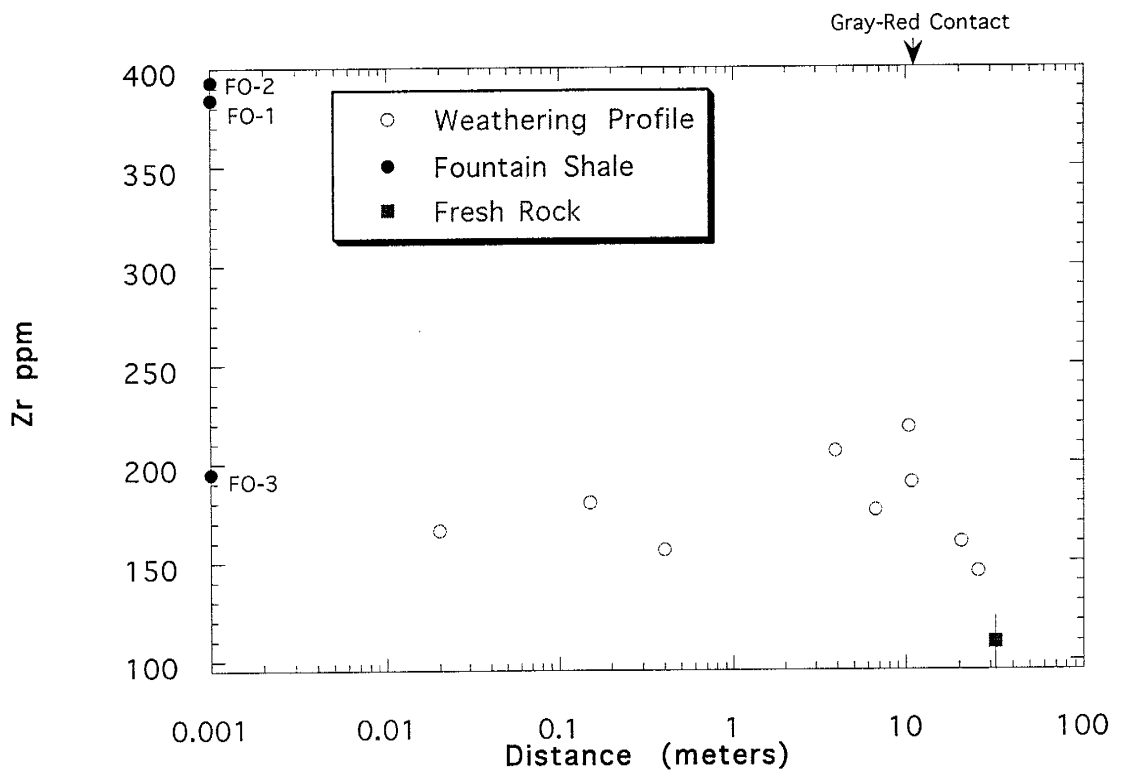


Figure 14. Plot of Zr versus distance from the Fountain Formation sediments along the Boulder granodiorite paleoweathering profile. Other information given in Figure 3.

Ta and Nb exhibit similar behavior as weathering increases along the profile (Fig. 18 and Fig. A-5). Values for Ta and Nb range from 0.4 - 1.2 ppm and 6.0 -12.4 ppm, respectively. Following a decrease in the first two incipiently weathered samples (25.6 m, 20.6 m), the Ta and Nb concentrations increase slightly along the profile. Approximately 1 m beneath the Permian unconformity, there is a moderate increase in both elements and a maximum concentration is reached just below the sediments. The shale Ta values range from 1.1 to 2.6 ppm. Two of the shales have Ta values higher than the weathering profile and one has a Ta value near that of the highly weathered granodiorite. Nb values for the shales range from 24-27 ppm, higher than those for any portion of the weathering profile, and thus it appears that Ta and Nb become fractionated from each other during erosion and deposition.

Sc concentration in the weathering profile ranges from 6 to 18 ppm (Fig. 16). Sc content increases throughout the incipiently weathered rock and reaches a maximum in the moderately weathered granodiorite approximately 7 m beneath the overlying sediments. Sc decreases through the remainder of the profile, with lowest values below the contact with the Fountain sediments. The shale Sc values range from 7-14 ppm. Two of the shales have Sc contents similar to that of the most highly weathered portion of the profile and the third shale has a lower Sc content resembling that of the incipiently weathered rock.

Cr behaves similarly to Sc, increasing through the incipiently weathered rock and across the gray-red contact. The Cr concentration ranges from 46 to 103 ppm along the weathering profile (Fig. A-6). The 103 ppm maximum occurs approximately 10 m beneath the overlying sediments. With exception of a large drop in one sample at 7 m, there is a steady decrease in Cr through the moderately and highly weathered rock to the Permian unconformity. Shale Cr values range from 25-63 ppm. Two shales have values close to that of the most altered granodiorite and the third shale has a value lower than those recorded along the profile.

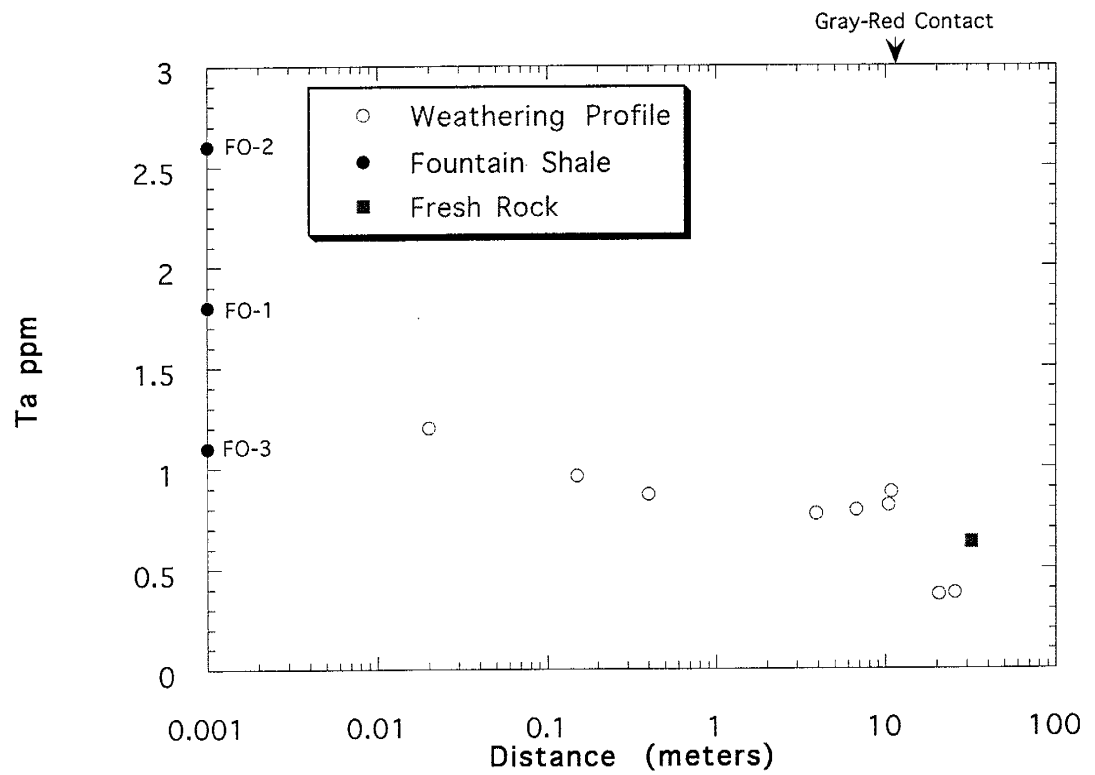


Figure 15. Plot of Ta versus distance from the Fountain Formation sediments along the Boulder granodiorite paleoweathering profile. Other information given in Figure 3.

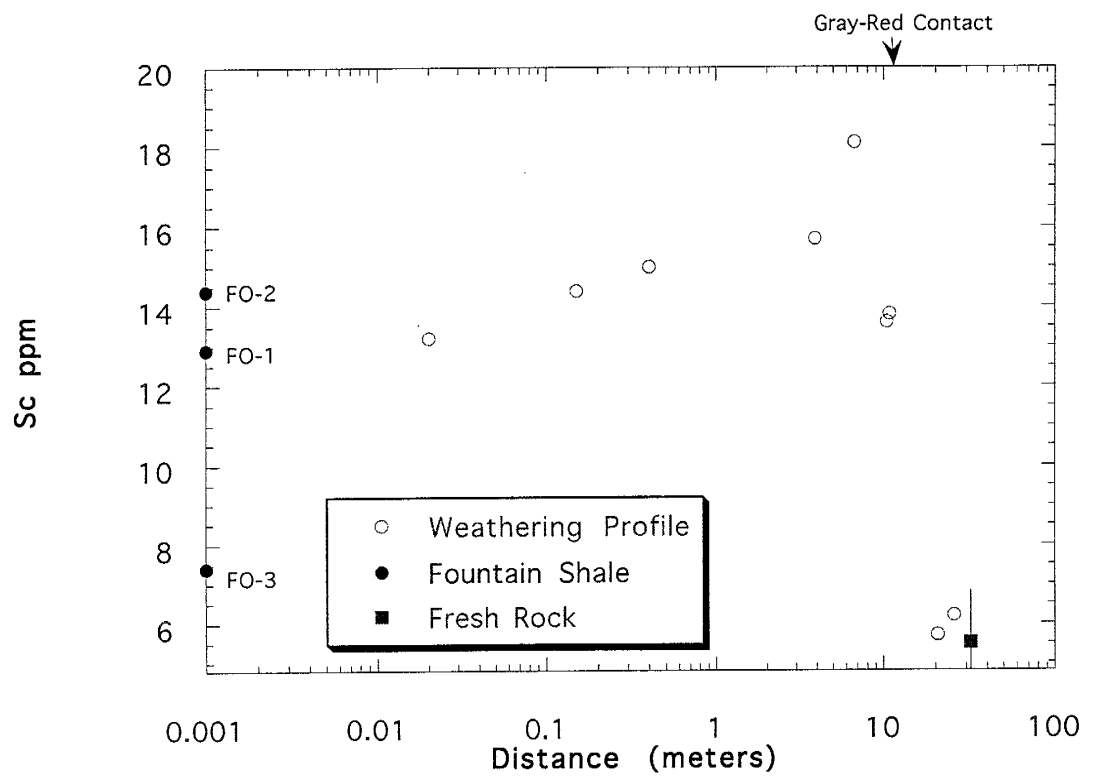


Figure 16. Plot of Sc versus distance from the Fountain Formation sediments along the Boulder granodiorite paleoweathering profile. Other information given in Figure 3.

Co increases from the fresh rock concentration of 9 ppm through the incipiently and moderately weathered rock, and reaches a maximum of 21 ppm approximately 4 m beneath the Permian unconformity (Fig. A-7). The Co content decreases throughout the last portion of the profile, reaching parent rock concentrations adjacent to the Fountain sediments. Shale Co values range from 5 to 12 ppm. Two of the shales have concentrations similar to that of the most highly weathered rock and the third shale has a concentration lower than that of the fresh granodiorite.

Y varies between 14 and 34 ppm along the profile (Fig. A-8). Y values increase from the fresh granodiorite through the incipiently and moderately weathered rock and shale Y values range from 40 to 57 ppm, higher than in the weathering profile.

La, Eu, and Yb are representative of REE variations as a function of distance along the outcrop and are shown in Figures 17 through 19. With exception of the sample at 20.6 m, in which all REE concentrations are low, these elements increase through the incipiently and moderately weathered rock. The LREE (La, Ce, Nd, Sm, and Eu; represented by La) reach maximum values approximately 1 m beneath the Permian unconformity, after which they decrease. The HREE (Yb and Lu; represented by Yb) reach maximum values 4 m beneath the overlying sediments and decrease through the remainder of the profile. Tb has a slightly different behavior from the other REE. This element increases until 0.15 meters before decreasing slightly to the sediment contact.

In summary, Rb, Ba, Th, Zr, Hf, Ta, Nb, Sc, Y, and Cr concentrations increase with increased weathering and Ba, Zr, and Cr reach maximums approximately 10 m beneath the Permian unconformity. Sc reaches a maximum at 7 m and Y reaches a maximum in the incipiently weathered rock at 25.6 m. Rb, Hf, Ta, and Nb reach their highest values in the uppermost meter of the weathered granodiorite. Sr decreases in concentration as weathering progresses, but shows an abrupt increase at a depth of 1

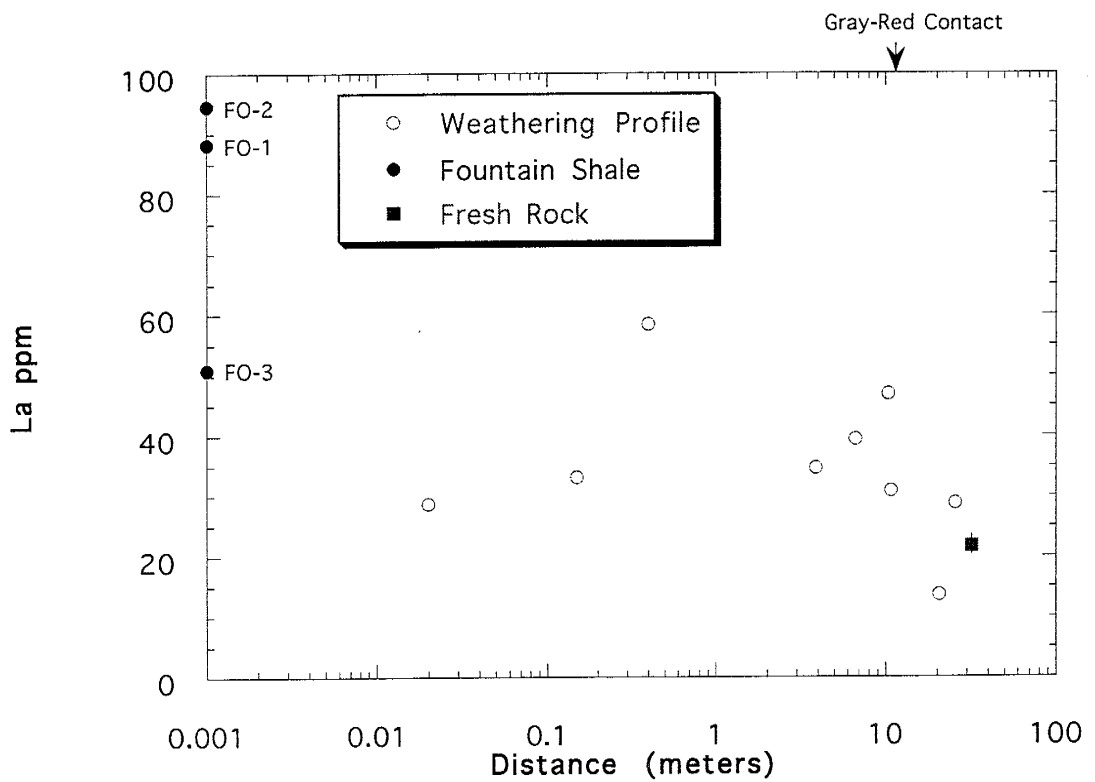


Figure 17. Plot of La versus distance from the Fountain Formation sediments along the Boulder granodiorite paleoweathering profile. Other information given in Figure 3.

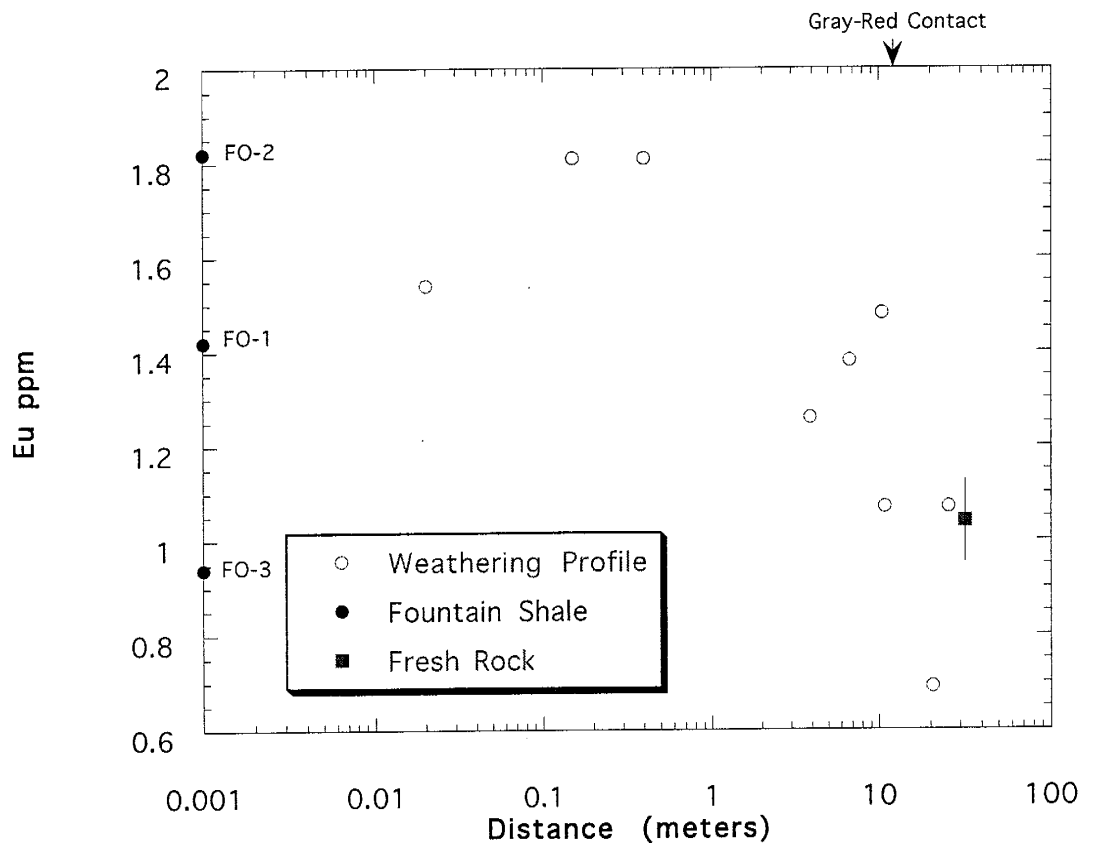


Figure 18. Plot of Eu versus distance from the Fountain Formation sediments along the Boulder granodiorite paleoweathering profile. Other information given in Figure 3.



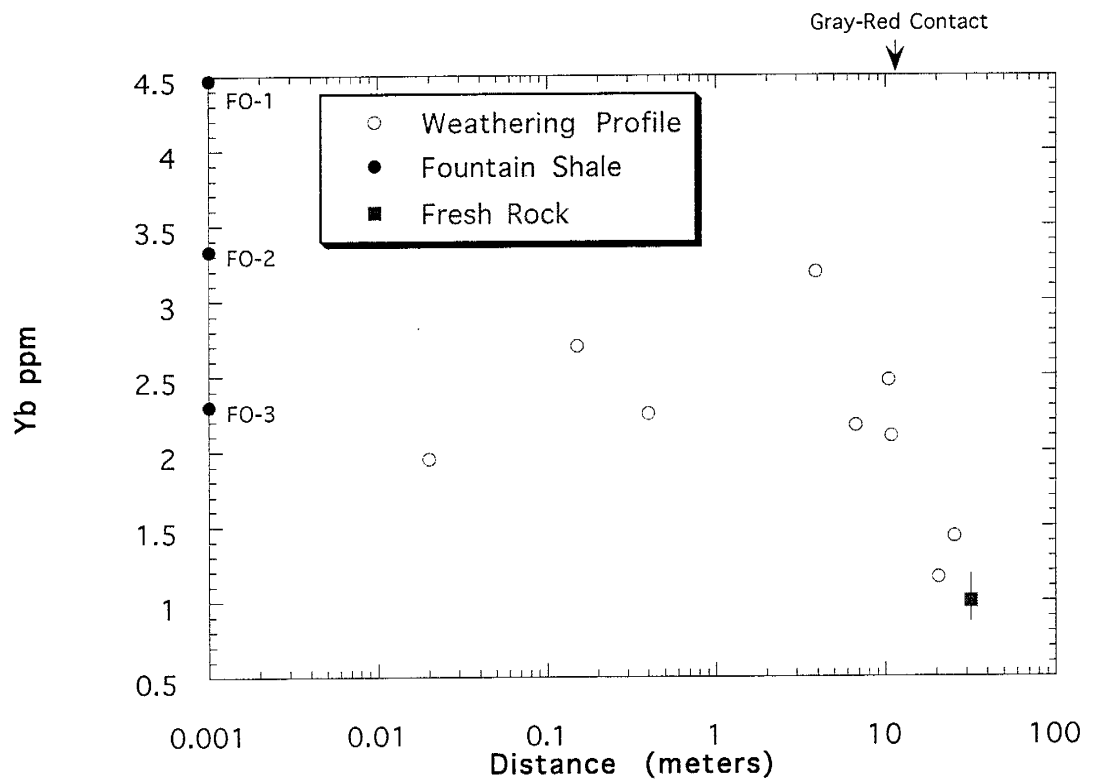


Figure 19. Plot of Yb versus distance from the Fountain Formation sediments along the Boulder granodiorite paleweathering profile. Other information given in Figure 3.

m. Co increases until the last meter of the profile, where concentrations drop to the sediment contact. The REE increase in concentration throughout the incipiently and moderately weathered granodiorite. LREE reach maximum values approximately 1 m beneath the overlying sediments after which the concentration decreases. The HREE reach maximum values at approximately 4 m beneath the sediment contact followed by a decrease to the Permian unconformity.

Element ratios were calculated for the parent granodiorite, bulk weathering profile, most highly weathered rock, and Fountain Formation shales. Figures 20 through 24 show representative element ratio variations with distance from the Permian unconformity, the remainder of the plots are located in Appendix A.

Cr/Th decreases with an increase in weathering, dropping from a value of 9 in the fresh granodiorite to 4 in the uppermost meter of the profile (Fig. 20). Cr/Th ratios in the Fountain shales have values close to 1, lower than along the profile or in the fresh rock.

Following a slight increase from a parent value of 8, Zr/Y decreases through the moderately and highly weathered rock to a minimum value of 5 in the uppermost meter of the weathering profile (Fig. A-9). The Fountain shale Zr/Y ratios are variable with 2 shales (sample FO-1 and FO-2) having Zr/Y ratios of 7 to 8. The third shale (FO-3) has a Zr/Y ratio of 5.

Co/Th and La/Th ratios decrease with distance from the fresh granodiorite with values ranging from 2 to 0.5 and 4 to 2 respectively (Figs. A-10 and A-11). The Co/Th ratio is 0.3 in the Fountain shales and the La/Th ratio is 2, resembling these ratios in the uppermost meter of the weathering profile.

There is a slight increase in the Cr/Sc ratio from the fresh rock value of 8 in the first two incipiently weathered samples (25.6 m, 20.6 m) (Fig. A-12). Cr/Sc decreases in the moderately and highly weathered rock, reaching a minimum of 5 in the

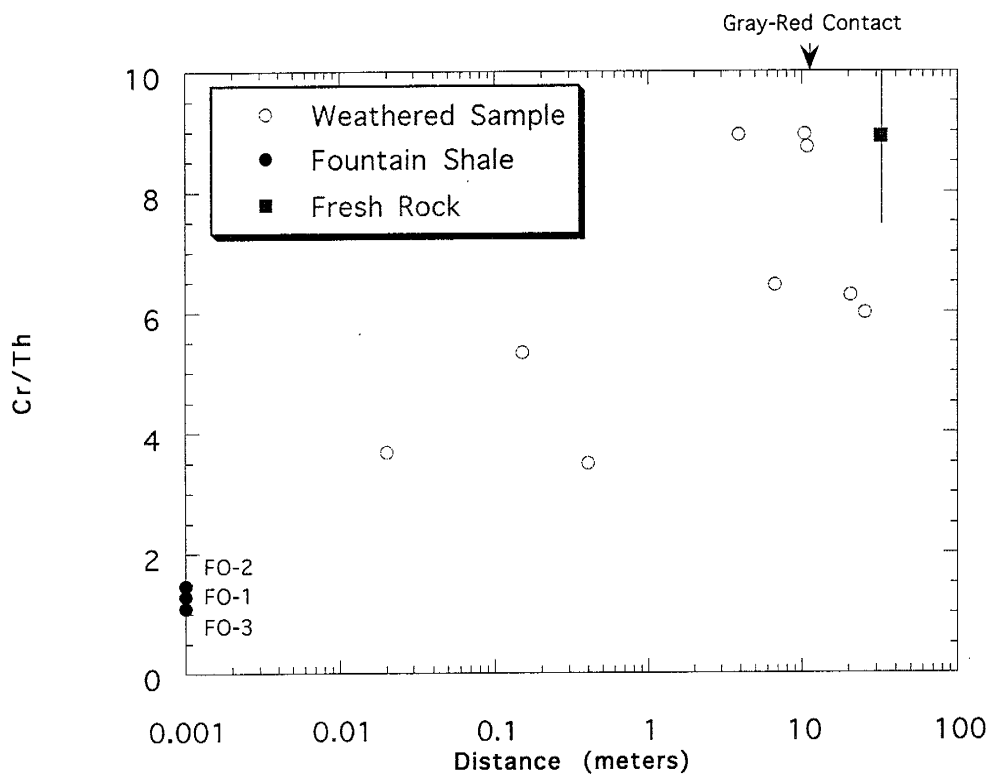


Figure 20. Plot of Cr/Th versus distance from the Fountain Formation sediments along the Boulder granodiorite paleoweathering profile. Other information given in Figure 3.

uppermost meter of the profile. Fountain shale Cr/Sc ratios range from 3 to 4, resembling the Cr/Sc ratios in the most altered granodiorite.

The La/Sc ratio is variable with distance, however shows an overall decreasing trend from fresh to weathered rock. Values range from 5 to 2 as weathering increases. With exception of three samples (25.6 m, 10.8 m, and 0.4 m) the weathering profile La/Sc ratios remain low (approximately 2), dropping from the fresh rock value of 4. The Fountain shale La/Sc ratios of 7 are higher than along the weathering profile or in the parent granodiorite.

Zr/Cr and Th/Sc ratios remain relatively constant as weathering increases (Figs. 21 and 22). The Zr/Cr ratio ranges from 2.7 to 2 and Th/Sc ranges from 1.5 to 0.9 in the weathering profile. The Fountain shale Zr/Cr and Th/Sc ratios are much higher than in the fresh or weathered rock with values of 6 to 8 and 3, respectively.

The Ti/Nb ratio increases with distance from a parent granodiorite value of 214 to values of 380 to 460 in the uppermost meter of the weathering profile (Fig 23). Fountain shale Ti/Nb ratios range from 160 to 210, lower than in the weathered granodiorite and resembling the ratio in the parent rock.

In summary, Cr/Th, Zr/Y, Co/Th, La/Th, Cr/Sc, and La/Sc decrease as a function of distance along the profile, attaining minimum values in the highly weathered rock. Shale Cr/Th, Co/Th, La/Th, and Cr/Sc ratios resemble those in the uppermost meter of the profile. Zr/Y ratios are variable in the shales and La/Sc ratios are higher than in the fresh or weathered granodiorite. Zr/Cr and Th/Sc values remain unchanged from the fresh granodiorite to the weathered rock and have Fountain shale values that are higher than in the weathering profile. . The Ti/Nb ratio increases as the degree of weathering increases and the Fountain shale Ti/Nb ratio is similar to that of the fresh granodiorite.

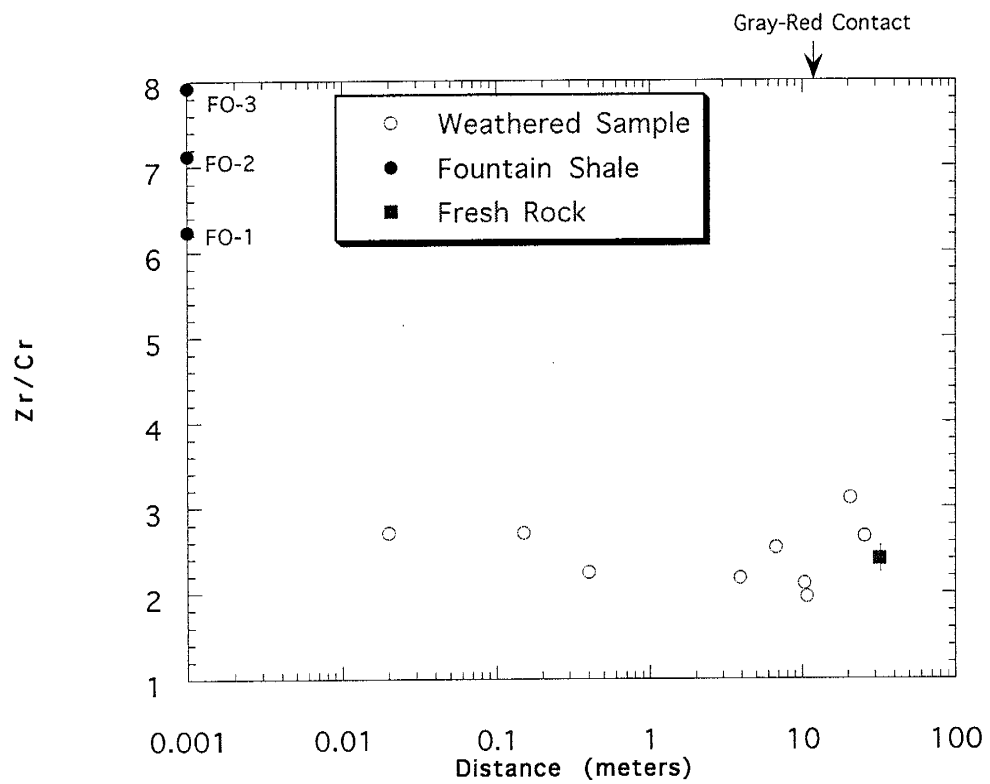


Figure 21. Plot of Zr/Cr versus distance from the Fountain Formation sediments along the Boulder granodiorite paleoweathering profile. Other information given in Figure 3.

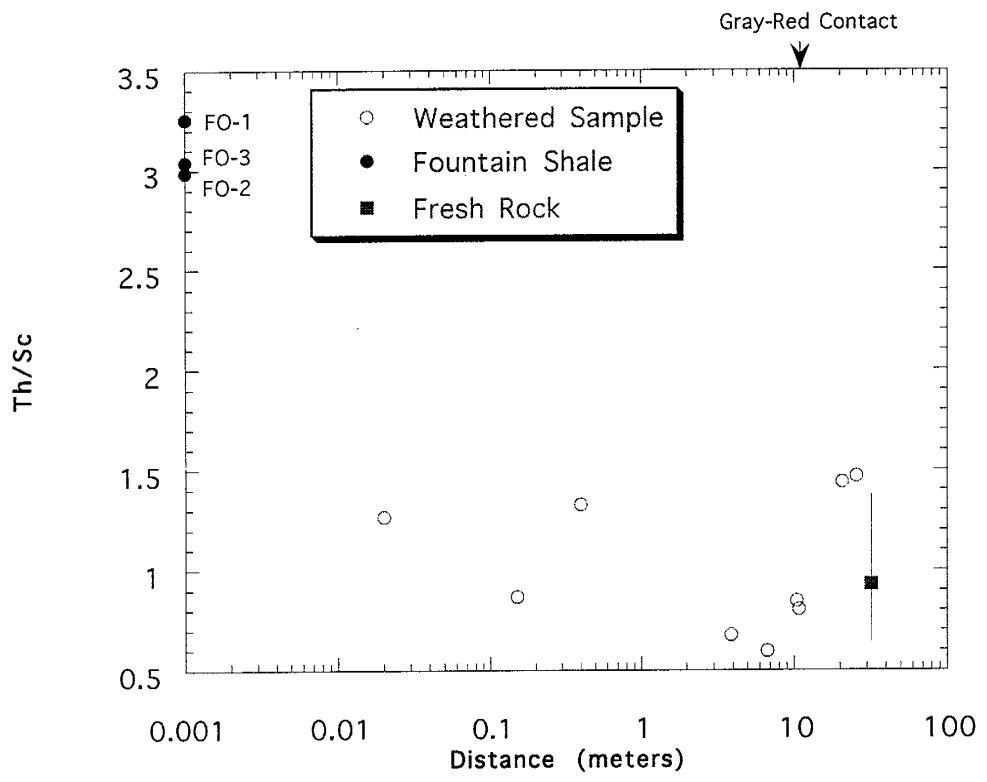


Figure 22. Plot of Th/Sc versus distance from the Fountain Formation sediments along the Boulder granodiorite paleoweathering profile. Other information given in Figure 3.

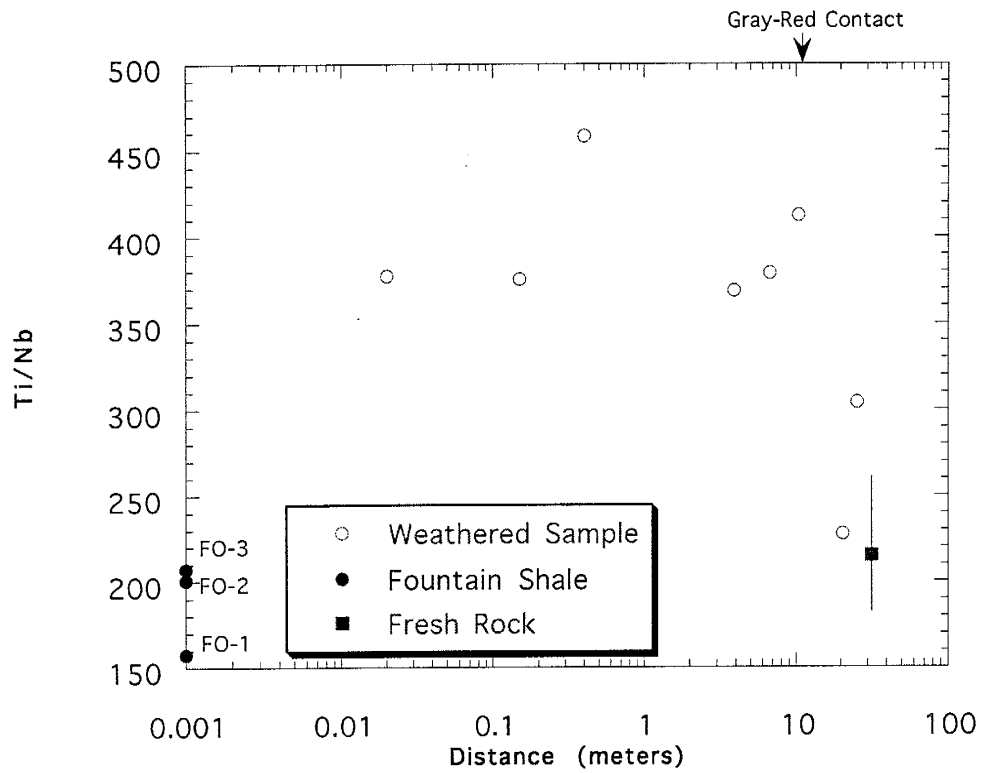


Figure 23. Plot of Ti/Nb versus distance from the Fountain Formation sediments along the Boulder granodiorite paleoweathering profile. Other information given in Figure 3.

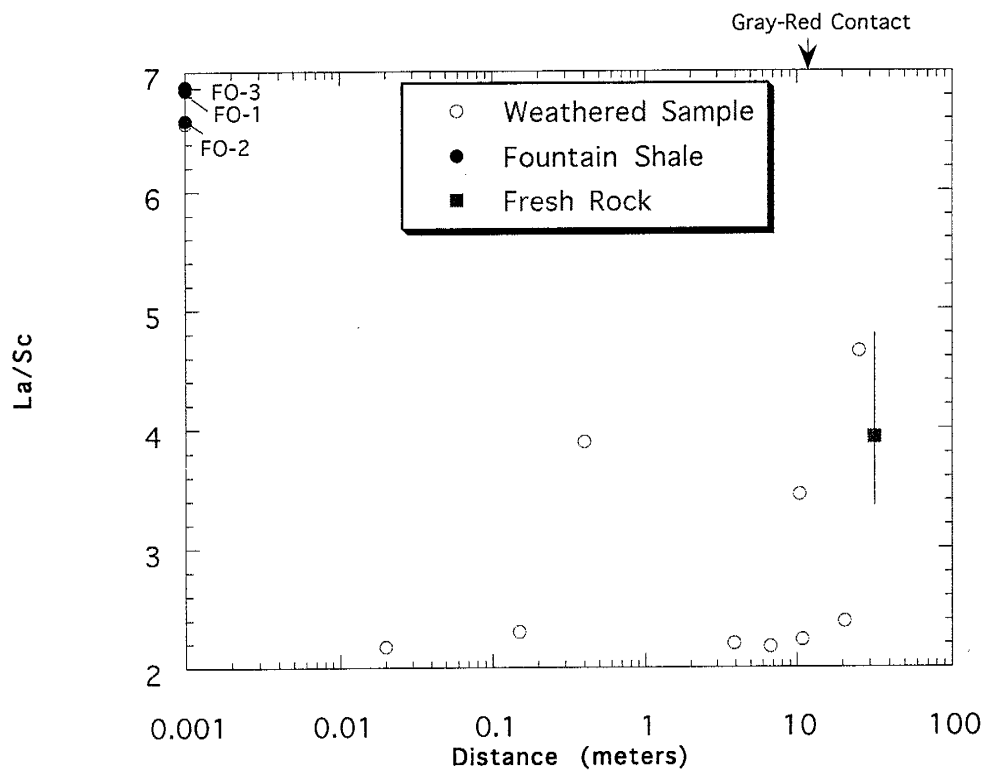


Figure 24. Plot of La/Sc versus distance from the Fountain Formation sediments along the Boulder granodiorite paleoweathering profile. Other information given in Figure 3.



## REE Distributions

Chondrite-normalized REE distributions of the weathering profile and parent granodiorite are shown in Figure 25. The fresh rock average is LREE enriched (100x chondrite) and exhibits a slight, positive Eu anomaly. With the exception of the 20.6 m sample, the weathering profile REE distributions fall in a coherent group, enriched relative to the parent rock. The 20.6 m sample is depleted in LREE, very slightly depleted in HREE, compared to the fresh granodiorite, and it has developed a small negative Eu anomaly. With this exception, all of the weathered samples are enriched in REE relative to the parent and have significant negative Eu anomalies. The weathering process has not produced progressive REE enrichment along the entire weathering profile, and there is some fractionation of the LREE and HREE.

The weathering profile REE concentrations have been normalized to the fresh rock average in Figure 26. Slope variations and the development of the large negative Eu anomaly are readily apparent. With the onset of weathering (at 25.6 m) the REE, excluding Eu, are enriched relative to the parent rock with little or no fractionation. At this point in the weathered profile, Eu has not increased from the parent rock concentration. The REE distributions in the remainder of the weathering profile have slopes and Eu concentrations that differ from the fresh granodiorite. From 10.8 m through 3.9 m, the REE begin to show fractionation from one another. These samples show HREE enriched patterns and are slightly LREE depleted with pronounced negative Eu anomalies. Samples from the most highly weathered material (approximately 1 m depth) show more variable REE behavior. The sample at 0.4 m is enriched in LREE and depleted in HREE. The samples at 0.15 m and 0.02 m are

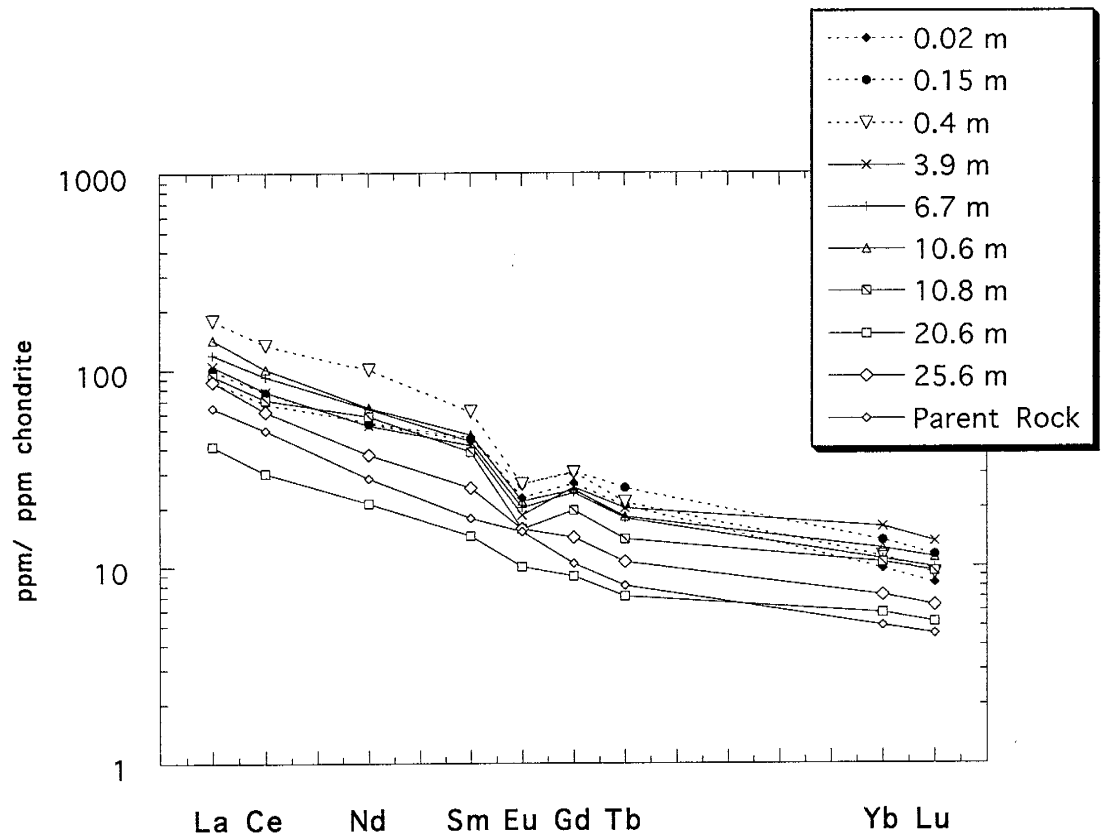


Figure 25. Chondrite-normalized REE distributions of parent granodior and weathered samples from the Boulder granodiorite paleoweathering profile. Chondrite values from Haskin et al. (1968). Gd estimated by  $Gd_n = (Sm_n \times Tb_n^2) \cdot 33$ .

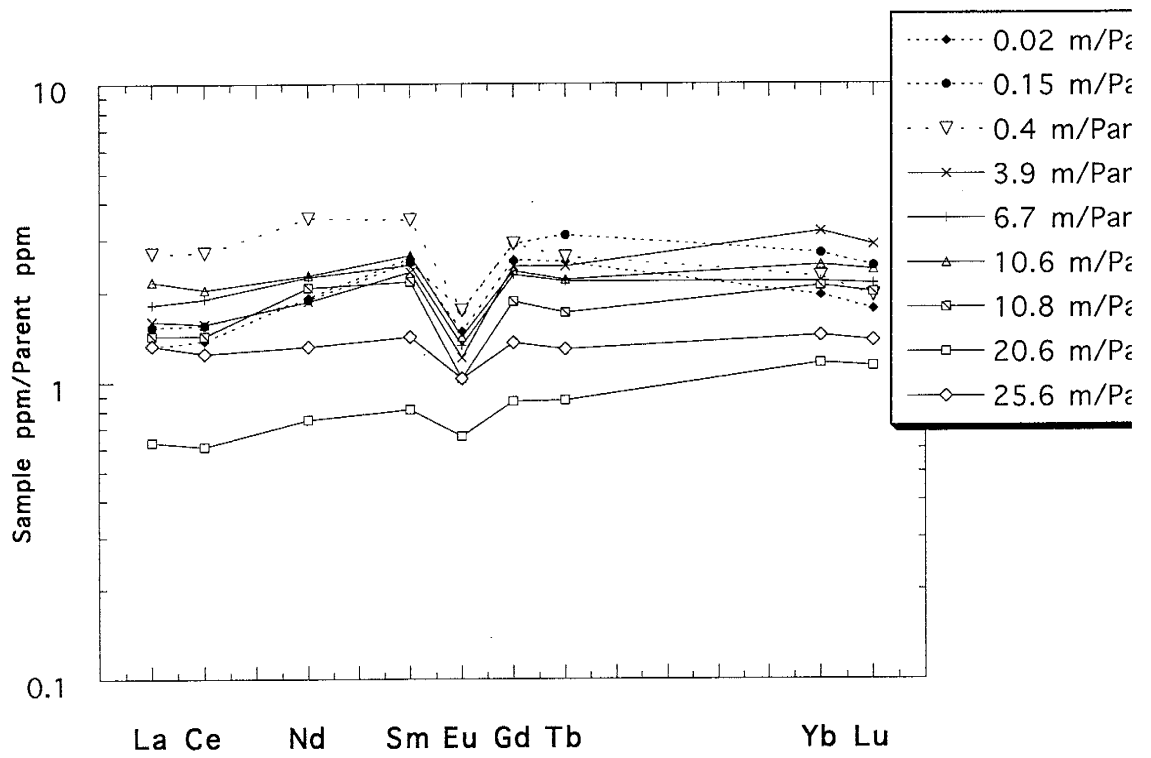


Figure 26. Parent-normalized REE distributions of weathered samples from Boulder granodiorite paleoweathering profile.

depleted in LREE and also slightly depleted in HREE. The negative Eu anomalies are well-developed in the last meter of the weathering profile. As mentioned previously, sample 20.6 m has an anomalous REE distribution; both LREE and slightly HREE depleted relative to the fresh granodiorite.

The chondrite-normalized REE distributions in Fountain Formation shales are enriched relative to the fresh granodiorite (Fig. 27) and show large, negative Eu anomalies. The shale and parent rock REE distributions, however, have similar slopes with little or no element fractionation. This relationship is also apparent in Figure 28 where shale REE concentrations have been normalized to the fresh rock values. FO-1 has a slight LREE enrichment relative to the parent rock (FO-1  $(La/Yb)_n = 16$ ; fresh rock  $(La/Yb)_n = 13$ ).

The chondrite-normalized La/Yb ratio (hereafter  $(La/Yb)_n$ ) of a sample is a measure of the slope of the REE distribution. With exception of a large increase approximately 1 m beneath the Permian unconformity, the  $(La/Yb)_n$  ratio decreases with distance along the profile (Figure 29). The high  $(La/Yb)_n$  ratio of the 0.4 m sample reflects a large LREE enrichment. Two of the Fountain Formation shales have  $(La/Yb)_n$  ratios similar to that of the fresh granodiorite. The third shale (FO-1) has a higher ratio due to LREE enrichment.

The variation of the Eu anomaly with distance along the weathering profile is shown in Figure 30.  $Eu/Eu^*$  decreases rapidly from the fresh rock to approximately 10 m depth. There is a slight increase in  $Eu/Eu^*$  at 0.15 m. The Fountain Formation shales have  $Eu/Eu^*$  values between 0.4 and 0.5, lower than that of the parent rock or weathering profile.

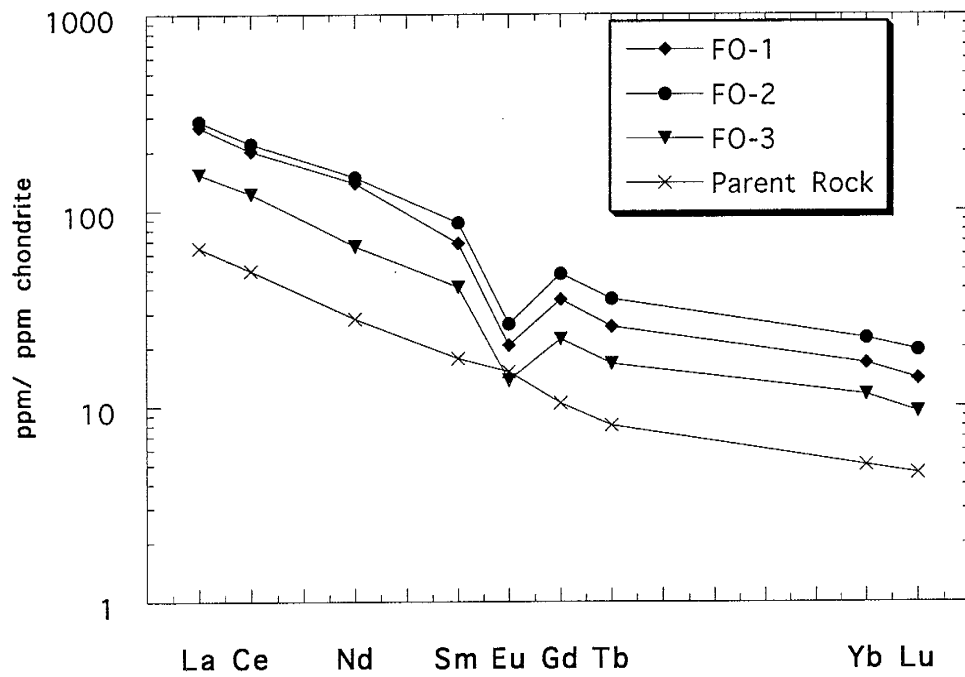


Figure 27. Chondrite-normalized REE distributions of parent granodior and Fountain Formation shales. Chondrite values from Haskin et al. (1968). Gd estimated by  $Gd_n = (Sm_n \times Tb_n^2)^{.33}$ .

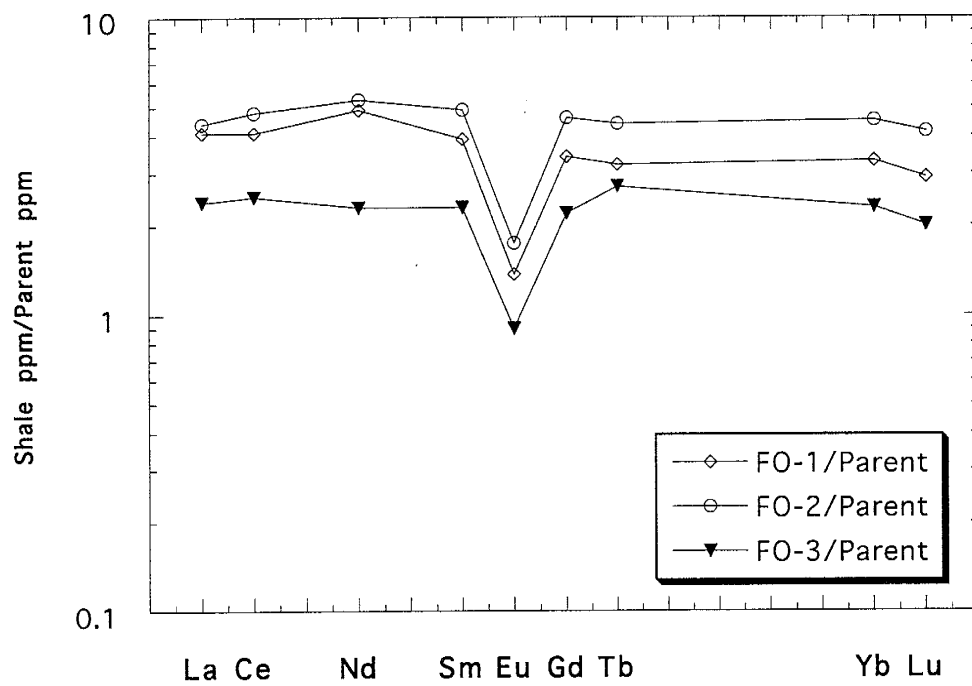


Figure 28. Parent-normalized REE distributions of Fountain Formation shales.

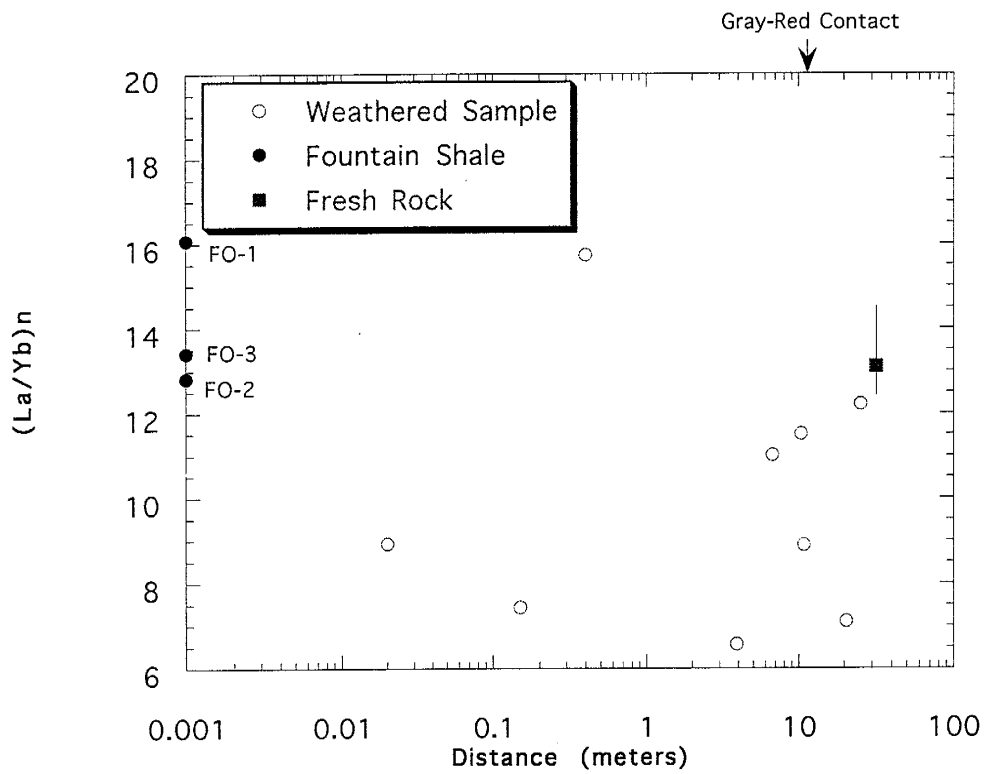


Figure 29. Plot of  $(La/Yb)_n$  versus distance from the Fountain Formation sediments along the Boulder granodiorite paleoweathering profile. Other information given in Figure 3.

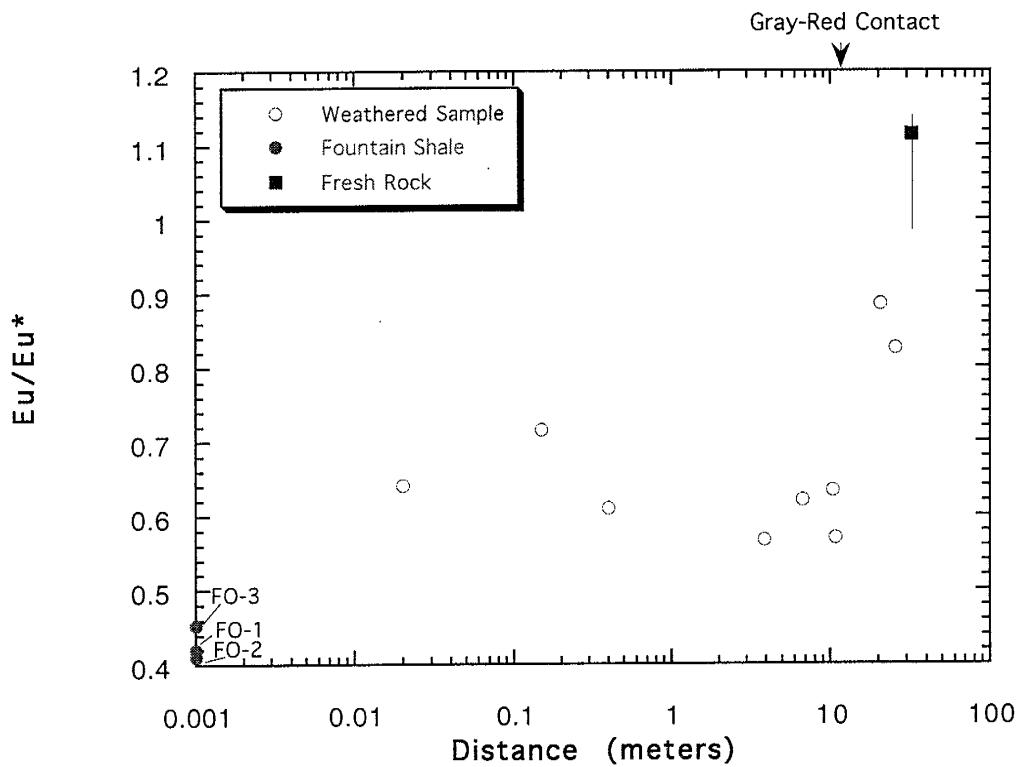


Figure 30. Plot of  $\text{Eu}/\text{Eu}^*$  versus distance from Fountain Formation sediments along the Boulder granodiorite paleoweathering profile.  $\text{Eu}/\text{Eu}^* = \text{Eu}_n / (\text{Sm}_n \times \text{Gd}_n)^{1/2}$ . Gd estimated by  $\text{Gd}_n = (\text{Sm}_n \times \text{Tb}_n^2)^{.33}$ . Other information given in Figure 3.



## DISCUSSION

### Element Losses and Gains During Weathering

Two graphical methods were employed to evaluate gains and losses of chemical components during weathering, based on accompanying composition and volume changes. The first method, published by Gresens (1967) and simplified by Grant (1986) considers gains and losses of chemical constituents relative to a line of equal concentration, or isocon. This line is determined by assuming weathering has been either a constant mass or constant volume process, or that one or more elements have remained immobile. The amount of displacement of elements from these isocons is a measure of their gain or loss relative to the parent rock.

Representative samples from the weathering profile have been plotted on the isocon plots in Figures 31 through 36. These graphs are generated by plotting the element concentration of the parent rock (x axis) against the element concentration of a weathered sample (y axis). The data are scaled following the method proposed by Grant (1986), allowing widely varying element concentrations to be plotted on the same diagram. Constant mass, volume, and alumina lines were calculated using equations provided by Grant (1986). The constant alumina isocon was included because previous studies have shown aluminum to be one of the least mobile constituents during the weathering of granitic rocks (Duddy, 1980; Harriss and Adams, 1966). Due to evidence of volume changes in the highly weathered portion of the profile (Wahlstrom, 1948) and mass changes during alteration, the constant alumina isocon may be the most useful line of reference.

A second graphical method for determining changes in the absolute abundances of elements was published by Brimhall and Dietrich (1987). Using the Brimhall

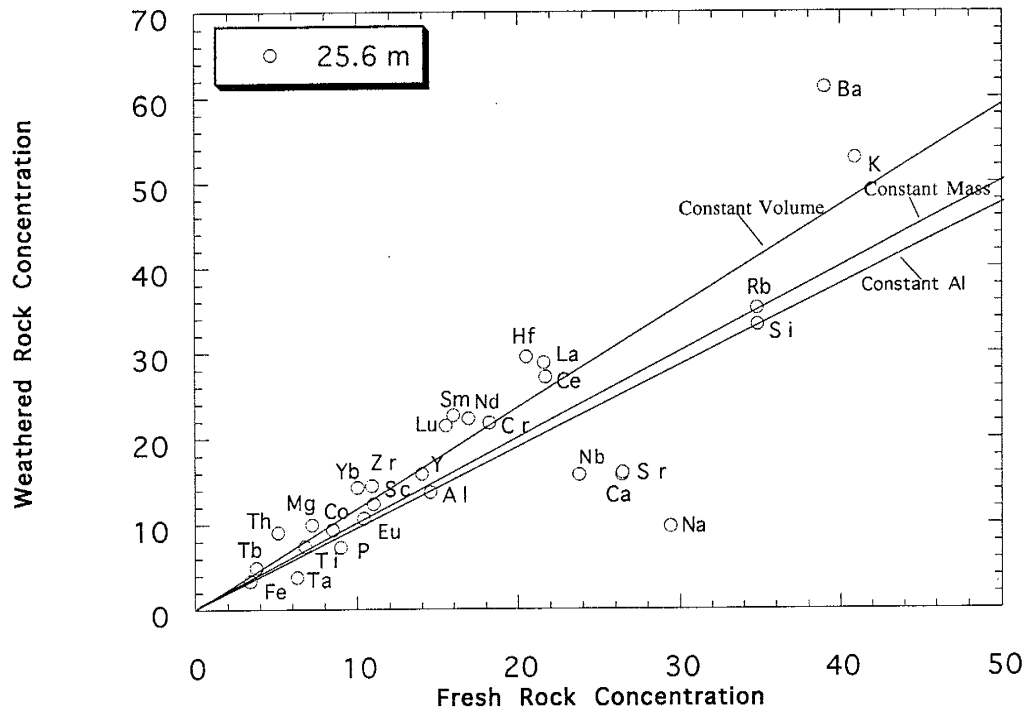


Figure 31. Isocon plot of the weathered rock element concentration versus fresh rock concentration at 25.6 m. Constant mass, constant volume, and constant alumina isocons are shown. Plotting method after Grant (1986). Scaling values (1 unless otherwise specified): 100, Lu; 50, P; 20, Ti; 10, Ca, Na, K, Ta, Eu, Tb; 5, Mg, Hf, Sm; 2.5, Nb; 2, Sc; 0.5, Si, Ce; 0.4, Cr; 0.2, Rb; 0.1, Zr; 0.05, Sr, Ba.

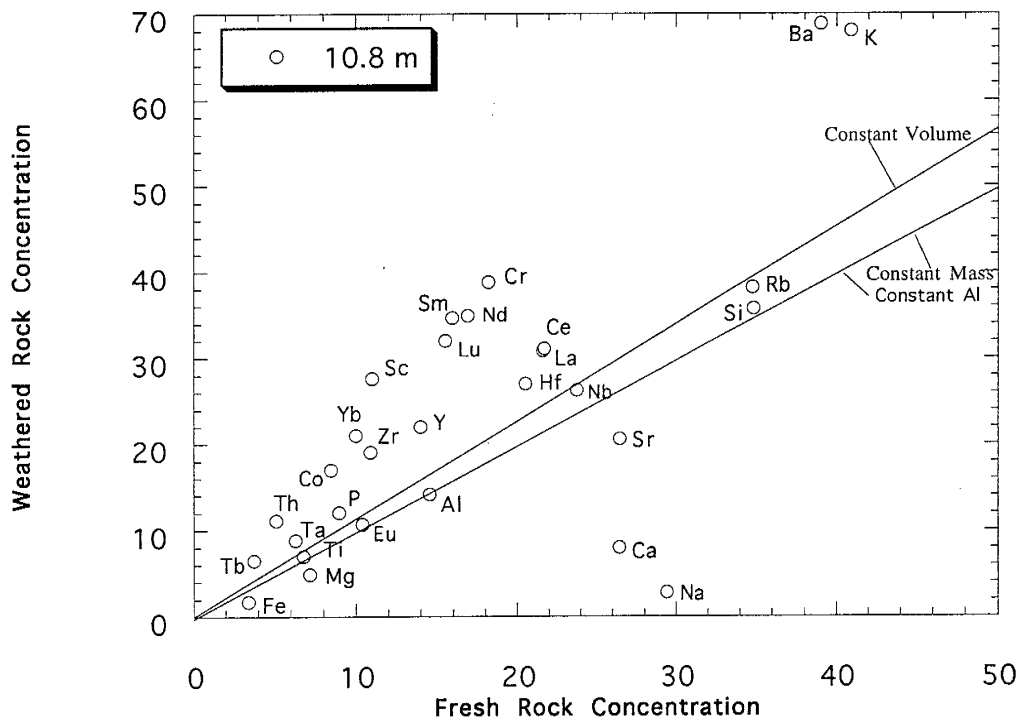


Figure 32. Isocon plot of the weathered rock element concentration versus fresh rock concentration at 10.8 m. Constant mass, constant volume, and constant alumina isocons are shown. Plotting method after Grant (1986). Other information given in Figure 31.

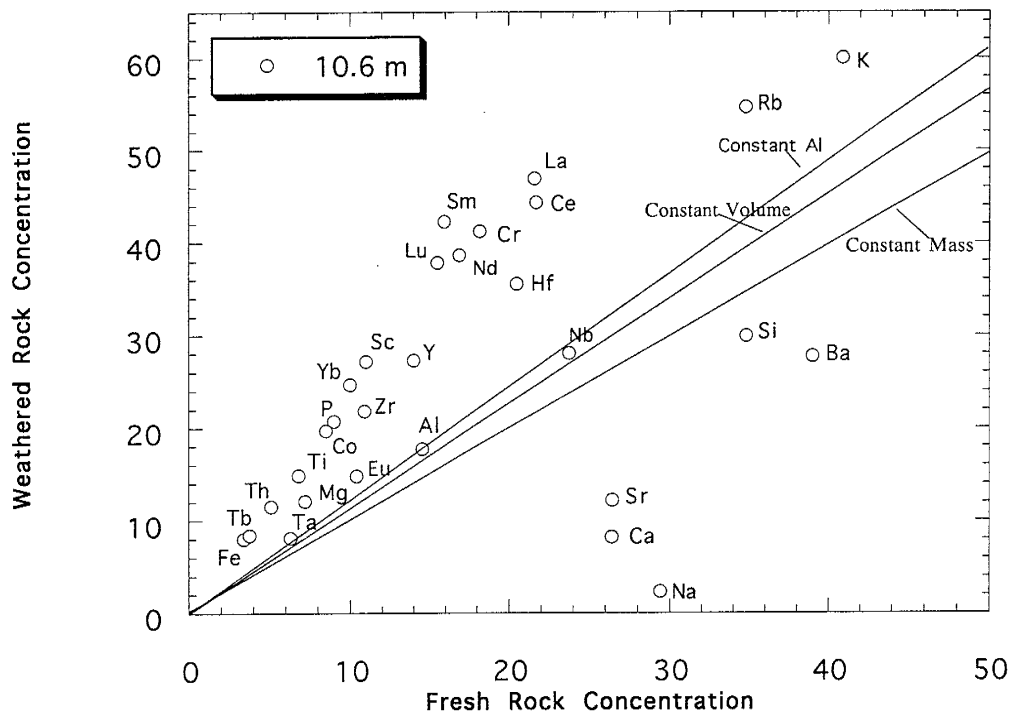


Figure 33. Isocon plot of the weathered rock element concentration versus fresh rock concentration at 10.6 m. Constant mass, constant volume, and constant alumina isocons are shown. Plotting method after Grant (1986). Other information given in Figure 31.

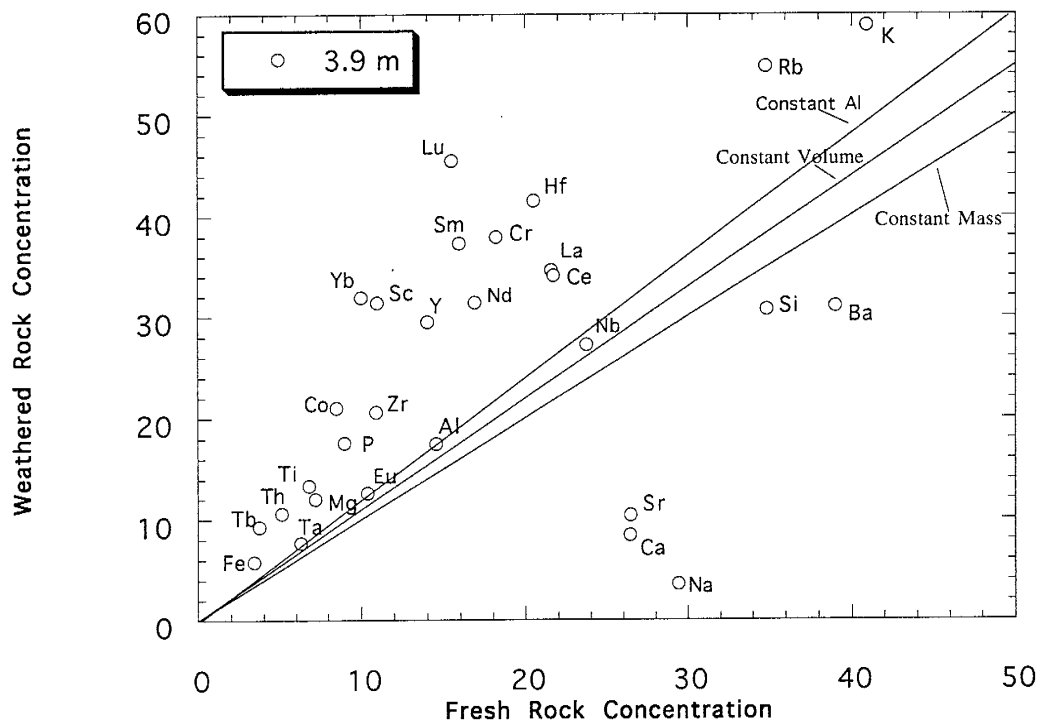


Figure 34. Isocon plot of the weathered rock element concentration versus fresh rock concentration at 3.9 m. Constant mass, constant volume, and constant alumina isocons are shown. Plotting method after Grant (1986). Other information given in Figure 31.

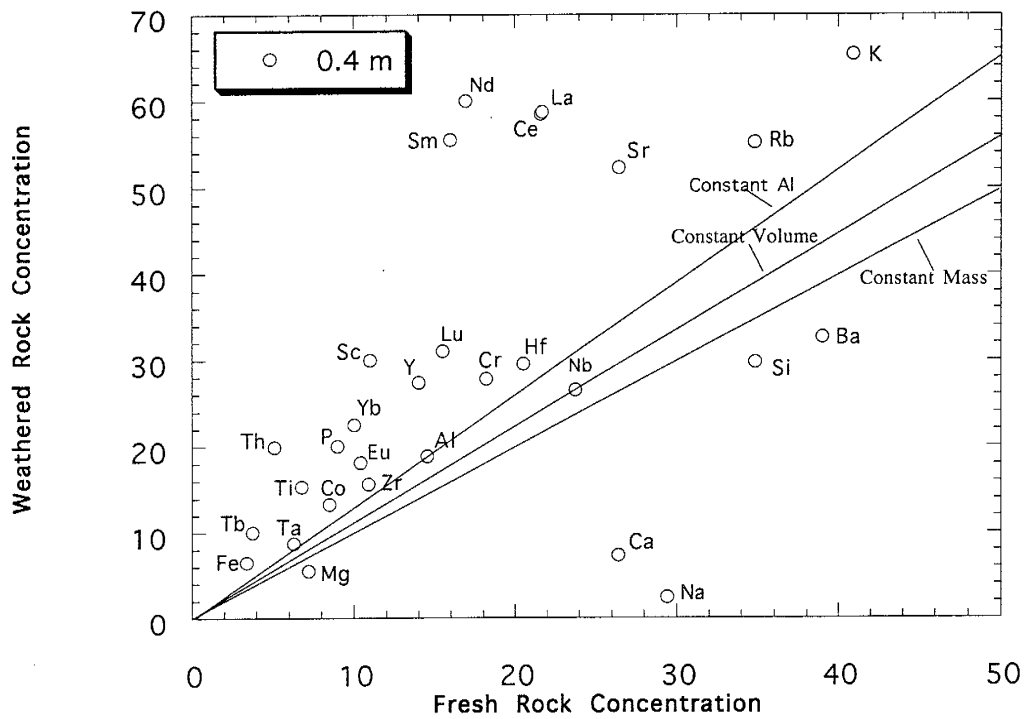


Figure 35. Isocon plot of the weathered rock element concentration versus fresh rock concentration at 0.4 m. Constant mass, constant volume, and constant alumina isocons are shown. Plotting method after Grant (1986). Other information given in Figure 31.

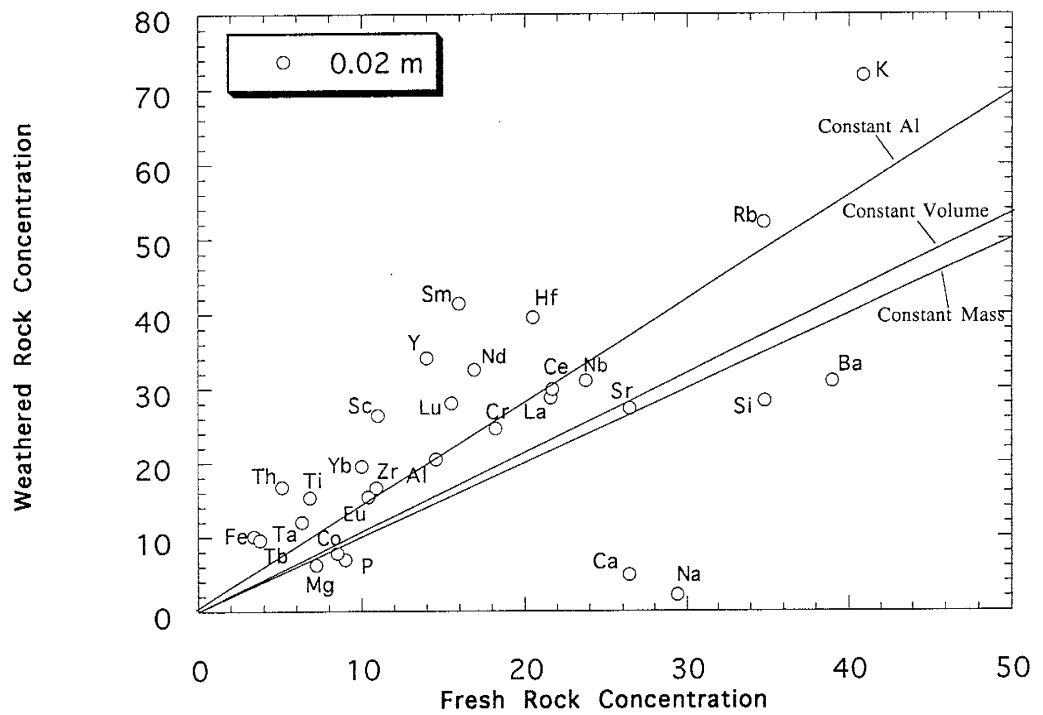


Figure 36. Isocon plot of the weathered rock element concentration versus fresh rock concentration at 0.02 m. Constant mass, constant volume, and constant alumina isocons are shown. Plotting method after Grant (1986). Other information given in Figure 31.

approach, the chemical gains and losses are determined by utilizing changes in rock density during weathering. On the Brimhall-style plot, three types of element behaviors can be defined: those that are residually enriched (neither enriched nor depleted relative to the parent rock concentration); elements that are enriched relative to fresh rock ; and those that are leached and removed from the system.

To construct a Brimhall-style plot, rock density ratios (density of the parent rock divided by the density of the weathered sample) are plotted against element ratios (the ratio of an element concentration in the weathered rock to the parent rock) (Figs. 37 through 41). For each sample, data points fall above, on, or below a line of residual enrichment. Equations for calculating this line are given in Brimhall and Dietrich (1987). To minimize the scatter of data , a residual enrichment range has been defined by assuming  $Al_2O_3$  to be immobile.  $Al_2O_3$  values fall between 0.3 above or below the residual enrichment line and any other element falling within this range is also considered immobile. With a few exceptions the results from the isocon and Brimhall-style plots are in good agreement.

In the incipiently weathered material (represented by the sample taken at 25.6 m) there is a substantial loss of CaO,  $Na_2O$ , and Sr. These elements fall below all three Gresens isocons and below the residual enrichment range on the Brimhall plots. Ca, Na, and Sr are housed in plagioclase, where Sr substitutes for Ca (Fritz, 1988). The loss of these elements is thought to be due to the removal of plagioclase during the early stages of weathering. Consistent with this interpretation is the fact that there is a dramatic decrease in plagioclase from 40% in the parent rock to 18% in the first incipiently weathered sample (Table 1). Ta, Nb, and  $P_2O_5$  are also depleted relative to fresh granodiorite. These elements fall below the Gresens isocons and below the residual enrichment range on the Brimhall-style plot. Ta and Nb depletion may reflect the removal of sphene, and to a lesser extent, hornblende (sphene may contain up to 330 ppm Ta and hornblende may contain up to 7.2 ppm Ta (Wedepohl, 1978). Sphene



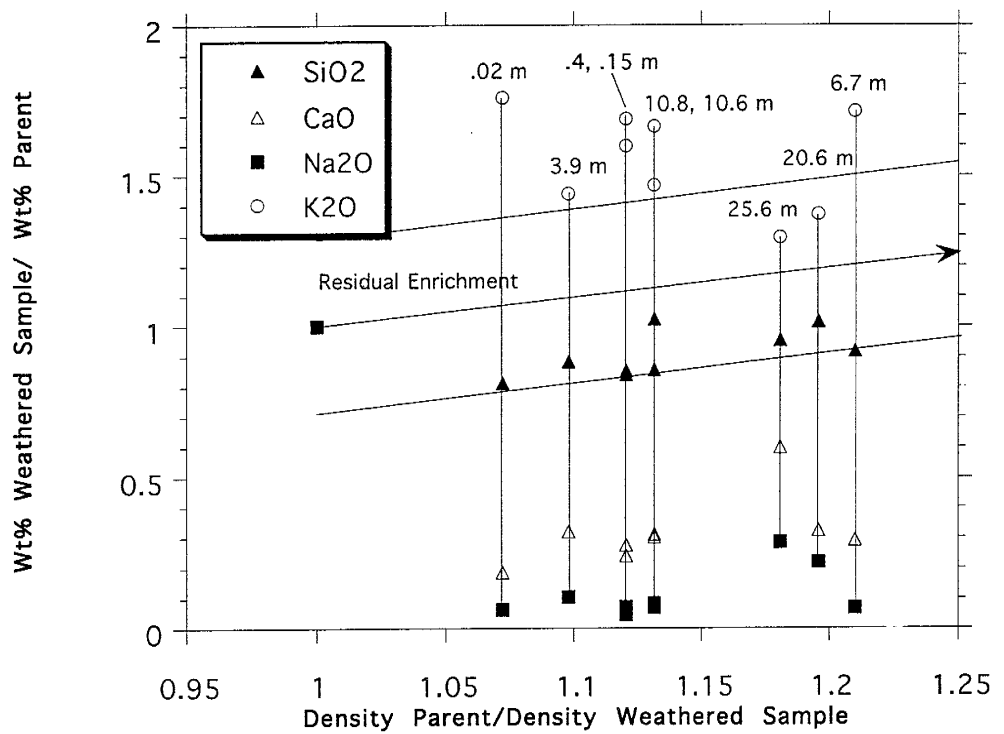


Figure 37. Brimhall plot of weathered rock-parent rock concentration ratio versus parent rock-weathered rock density ratio for SiO<sub>2</sub>, CaO, Na<sub>2</sub>O, K<sub>2</sub>O. Residual enrichment line and range are shown. Plotting technique after Brimhall and Dietrich (1987).

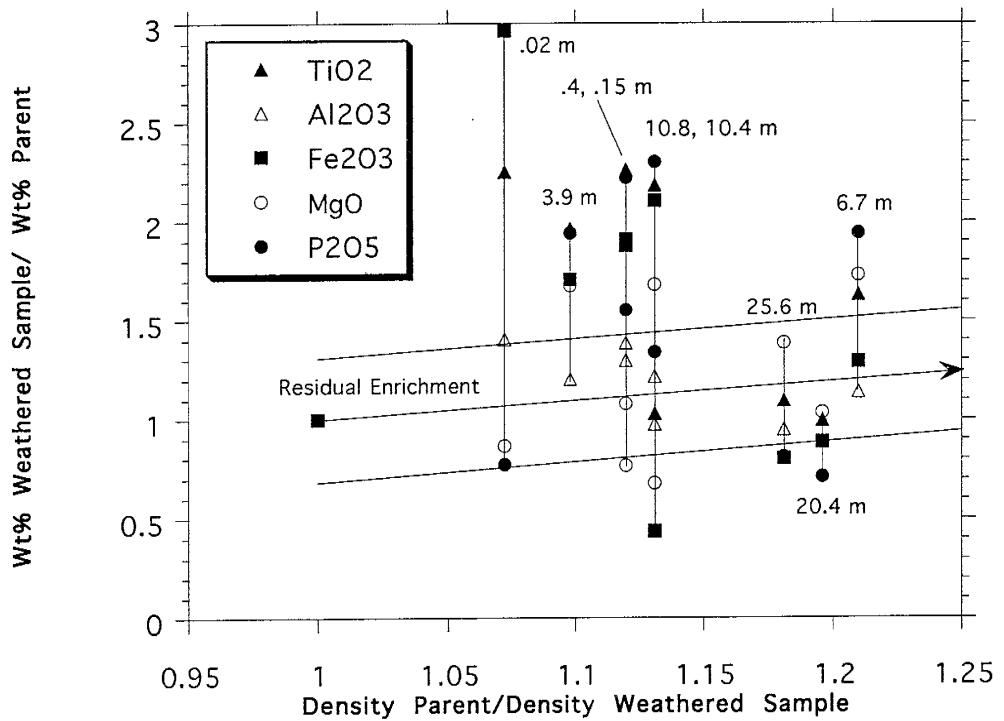


Figure 38. Brimhall plot of weathered rock-parent rock concentration ratio versus parent rock-weathered rock density ratio for  $TiO_2$ ,  $Al_2O_3$ ,  $Fe_2O_3$ ,  $MgO$ ,  $P_2O_5$ . Residual enrichment line and range are shown. Plotting technique after Brimhall and Dietrich (1987).

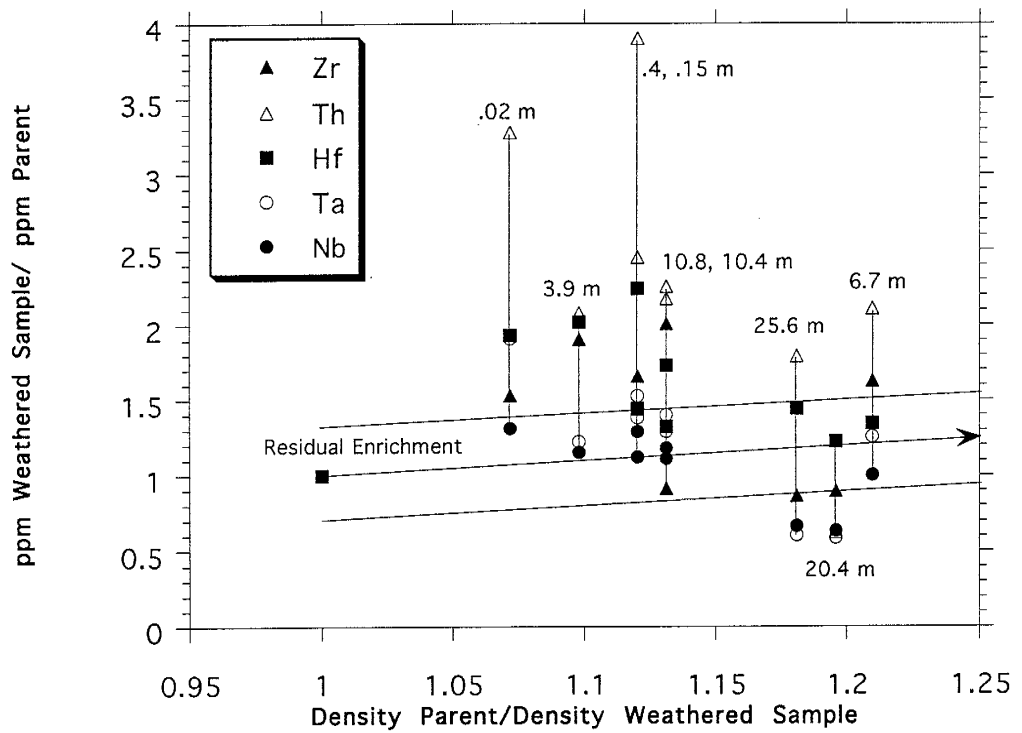


Figure 39. Brimhall plot of weathered rock-parent rock concentration ratio versus parent rock-weathered rock density ratio for Zr, Hf, Th, Ta, and Nb. Residual enrichment line and range are shown. Plotting technique after Brimhall and Dietrich (1987).

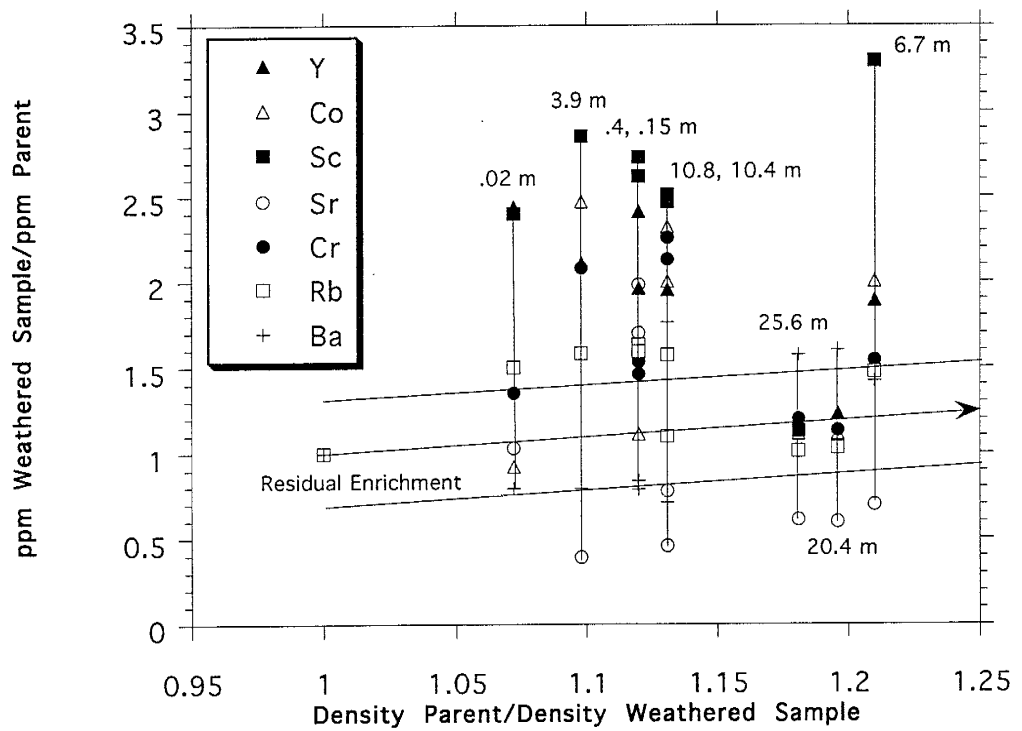


Figure 40. Brimhall plot of weathered rock-parent rock concentration ratio versus parent rock-weathered rock density ratio for Y, Co, Sc, Sr, Cr, Rb, Ba. Residual enrichment line and range are shown. Plotting technique after Brimhall and Di. (1987).

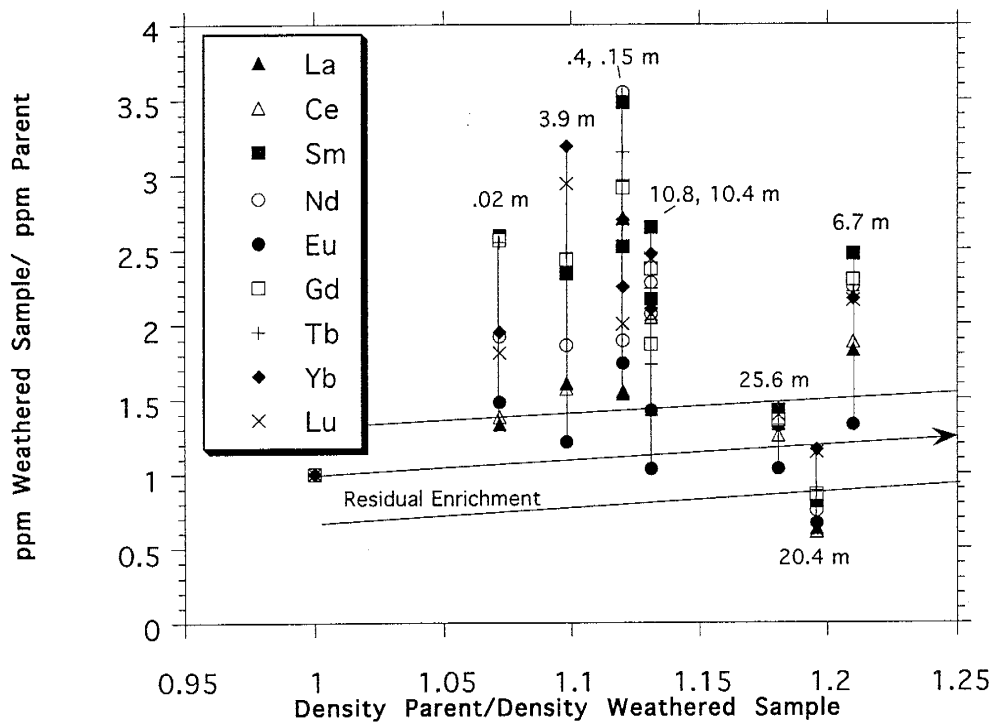


Figure 41. Brimhall plot of weathered rock-parent rock concentration ratio versus parent rock-weathered rock density ratio for La, Ce, Sm, Nd, Eu, Gd, Tb, Yb, Lu. Residual enrichment line and range are shown. Plotting technique after Brimhall and Dietrich (1987).

decreases from 0.4 to 0.1 % at the onset of weathering and hornblende is lost entirely (Table 1). The decrease in  $P_2O_5$  is due to a decrease in the percentage of apatite present, which almost exclusively controls the  $P_2O_5$  concentration (Wedepohl 1978).  $Fe_2O_3T$  is depleted on the Brimhall-style plot, but falls along all three isocons. The  $Fe_2O_3T$  content of the bleached rock at 10.8 m beneath the Permian unconformity is also depleted relative to the parent rock. Therefore, although  $Fe_2O_3T$  falls along the isocons, it is likely that the sample at 25.6 m is depleted in this element. The discrepancy between the graphical methods may be explained by the lack of data points in the incipiently weathered rock. The loss of  $Fe_2O_3T$  may be due to a slight decrease in the percentage of Fe-oxides at 25.6 meters together with the breakdown of hornblende.

$SiO_2$ ,  $Al_2O_3$ ,  $TiO_2$ , Y, Cr, Sc, Eu, Tb, and Rb remain immobile during the early stages of weathering (as represented by the 25.6 m sample). These elements fall along the constant mass, constant volume, and constant Al isocons and within the residual enrichment range on the Brimhall plots. Cr,  $TiO_2$ , Sc, and Rb concentrations may be controlled by biotite which has not been altered in the early stages of weathering (Cullers, 1988).

Also in the incipiently weathered rock, Th, Zr, Hf, MgO, Co,  $K_2O$ , Ba, and REE (except Eu and Tb) are enriched relative to fresh granodiorite. These elements fall above all three isocons and above the residual enrichment range on the Brimhall plots. The enrichments of these elements may be caused by a relative increase in the proportions of the minerals in which these elements are housed. In a weathering study of another granitoid, Harriss and Adams (1966) noted an apparent Th and  $K_2O$  enrichment due to the concentration of resistate minerals and microcline in which Th and  $K_2O$  are housed. This concentration reflects the removal of other constituents such as plagioclase. K-feldspar is likely to house most of the Ba in granitic rocks (Nesbitt et al., 1980). Therefore, the enrichment of Ba could also reflect the removal of

plagioclase and the corresponding increase in K-feldspar per unit volume. Other than clays, which increase by 26%, thin section data do not show a large increase in any mineral between the parent rock and the first stages of weathering.

Samples taken from either side of the gray-red contact (between 10.8 and 10.6 m) were plotted on isocon and Brimhall plots to determine the geochemical changes that occur at this break along the profile. At 10.8 m,  $\text{Na}_2\text{O}$ ,  $\text{CaO}$ ,  $\text{Sr}$ , and  $\text{Fe}_2\text{O}_3$  remain depleted, falling below all three isocons and below the residual enrichment range on the Brimhall plot. The  $\text{Na}_2\text{O}$ ,  $\text{CaO}$ , and  $\text{Sr}$  losses reflect a further decrease in plagioclase. Only 2% of the plagioclase from the parent rock remains in this sample (Table 1). The low  $\text{Fe}_2\text{O}_3$  content may be a reflection of a slight decrease in the amount of Fe-oxides, and perhaps the loss of hornblende. Ta and Nb are no longer depleted relative to the parent rock. These elements fall near the isocons and within the residual enrichment range. Ta and Nb may have been released into solution during weathering of sphene and then adsorbed onto clays (Wedepohl, 1978).  $\text{SiO}_2$ ,  $\text{TiO}_2$ ,  $\text{Al}_2\text{O}_3$ ,  $\text{MgO}$ ,  $\text{P}_2\text{O}_5$ , Zr, Hf, Ta, Nb, Rb, Eu, and La are neither enriched nor depleted relative to the parent rock at this stage of weathering. With the exception of La, Zr, and Hf, these elements fall near the isocons and within the residual enrichment range. La, Zr, and Hf fall above all three isocons, but within the Brimhall residual enrichment range. Th, Co, Y, Sc, Ba,  $\text{K}_2\text{O}$ , Cr, and REE (except Eu) are enriched relative to the fresh rock, falling above the isocons and above the residual enrichment range. This enrichment may reflect the further concentration of the residual state and clay minerals in which these elements are housed.

On the red side of the bleached-red contact, sample 10.6 m,  $\text{Sr}$ ,  $\text{CaO}$ , and  $\text{Na}_2\text{O}$  remain depleted relative to the Al isocon and fall below the residual enrichment range. Ba is no longer enriched, falling below the Al isocon and below the residual enrichment range on the Brimhall plot. Ta,  $\text{Al}_2\text{O}_3$ , Nb,  $\text{SiO}_2$ , and Eu fall within the residual enrichment range,  $\text{SiO}_2$  falls below the isocons, and Eu lies above the isocons. These

elements are considered to be immobile at this stage. Fe<sub>2</sub>O<sub>3</sub>T, K<sub>2</sub>O, TiO<sub>2</sub>, MgO, P<sub>2</sub>O<sub>5</sub>, Zr, Th, Hf, Y, Co, Sc, Cr, Rb, and REE (except Eu) are enriched relative to the parent rock, falling above all three isocons and above the residual enrichment range.

In summary, across the gray-red contact there is an enrichment of Fe<sub>2</sub>O<sub>3</sub>T, TiO<sub>2</sub>, MgO, P<sub>2</sub>O<sub>5</sub>, Zr, Hf, La and Rb. The increase in Fe<sub>2</sub>O<sub>3</sub>T and TiO<sub>2</sub> corresponds to an increase in Fe-Ti oxides. In thin section, there is a large increase in the percent of Fe-Ti oxides from 10.8 to 10.6 m ( 2.3 to 10.6 % Fe-Ti oxides) (Table 1). Cr, Sc, and Co also remain enriched. These elements follow iron during weathering (Cullers, 1988), therefore this enrichment may also be a reflection of the increase in Fe-Ti oxides. In the red, moderately weathered rock, Ba and K<sub>2</sub>O no longer exhibit similar behavior. Ba is depleted relative to the parent rock and K<sub>2</sub>O remains enriched. The Ba depletion may reflect a slight loss of K-feldspar as Ba is known to be preferentially released into solution during weathering (Wedepohl, 1978; Cullers, 1988). Thin section analysis shows a decrease from the parent rock K-feldspar content of 16 % to 10.4% in this sample (Table 1). Fritz (1988) also noted a loss of Ba during weathering of a granite. The P<sub>2</sub>O<sub>5</sub> enrichment corresponds to an increase in apatite. The remainder of the element behaviors do not vary from the gray to the red rock.

The sample taken at 3.9 m is representative of the moderately weathered portion of the profile. CaO, Na<sub>2</sub>O, Sr, and Ba remain depleted relative to the isocons and to the residual enrichment range. The Ba depletion may reflect the further alteration of K-feldspar to clay minerals. In thin section, there is 6.9 % K-feldspar in the moderately weathered rock compared to 10% in the incipiently weathered rock (Table 1). SiO<sub>2</sub>, Ta, Al<sub>2</sub>O<sub>3</sub>, Eu, and Nb are neither enriched nor depleted relative to the parent rock at this stage. These elements (with the exception of SiO<sub>2</sub>, which lies below the Al isocon) fall close to the constant Al isocon and close to the residual enrichment line on the Brimhall plots. TiO<sub>2</sub>, Fe<sub>2</sub>O<sub>3</sub>T, K<sub>2</sub>O, MgO, P<sub>2</sub>O<sub>5</sub>, Zr, Th, Hf, Y, Co, Sc, Cr, Rb,



and REE (except Eu) are enriched relative to the fresh rock concentration. These elements fall above the isocons and the residual enrichment range. As constituents are removed during weathering, there is further enrichment of resistate minerals and clays in which these elements are housed.

The sample taken at 0.4 meters differs significantly from the majority of the highly weathered rock. CaO, Na<sub>2</sub>O, SiO<sub>2</sub>, MgO, and Ba are depleted relative to the isocons and to the residual enrichment range. The MgO depletion may reflect the alteration of biotite. From thin section data, there is only 3.3 % biotite remaining in this sample. The Ba depletion may reflect the further alteration of K-feldspar. Ta, Nb, and Al<sub>2</sub>O<sub>3</sub> are neither enriched nor depleted relative to the parent rock. These elements fall near the constant aluminum and constant volume isocons and within the residual enrichment range. K<sub>2</sub>O, TiO<sub>2</sub>, Fe<sub>2</sub>O<sub>3</sub>T, P<sub>2</sub>O<sub>5</sub>, Th, Y, Co, Sc, Cr, Sr, Rb, and the REE fall above the residual enrichment range on the Brimhall plots and above all three isocons. The LREE and Sr are especially enriched, plotting as a separate group above the isocons.

In the most highly weathered rock along the profile, represented by the sample at 0.02 m, CaO, Na<sub>2</sub>O, SiO<sub>2</sub>, Ba, and P<sub>2</sub>O<sub>5</sub> are depleted relative to the isocons and fall below the residual enrichment range on the Brimhall plots. The depletion of P<sub>2</sub>O<sub>5</sub> reflects a drop in apatite. Al<sub>2</sub>O<sub>3</sub>, MgO, Nb, Co, Sr, Cr, La, Ce, Eu are neither enriched nor depleted relative to the parent rock. These elements fall near the isocons and within the residual enrichment range. Previously in the profile, MgO losses may reflect the alteration of biotite. At this stage, however, Mg may have been adsorbed onto clay minerals and no longer is depleted relative to the parent rock (Wedepohl, 1978). K<sub>2</sub>O, TiO<sub>2</sub>, Fe<sub>2</sub>O<sub>3</sub>T, Zr, Th, Y, Sc, Rb, REE (except La, Ce, Eu) are enriched relative to all three isocons and fall above the residual enrichment range. At this point in the weathering process the clay percentage has reached a maximum.

In summary, the major and trace element behavior throughout the weathering profile of the Boulder granodiorite is a complex process. The mobility of the elements seem to be dependent upon where the element is housed in the parent rock, the ability of these elements to go into solution, form complexes, or be adsorbed onto clays. Ca, Na, and Sr are very mobile elements and easily transported during weathering (Nesbitt et al., 1980) and these elements are readily lost as plagioclase is altered and removed from the system (with the noted exception of an increase in Sr in the highly weathered rock). The decrease in Ta and Nb in the incipiently weathered rock appears to be due to the removal of hornblende and sphene. These elements are conserved in the remainder of the profile probably in minor phases formed during weathering. The biotite and Fe-Ti oxides may house the majority of the Fe<sub>2</sub>O<sub>3</sub>T, TiO<sub>2</sub>, Co, Cr, and Sc. These elements are enriched as weathering increases. It is likely that this enrichment is due to both the increase in Fe-Ti oxides as weathering progresses, and an increase of other minerals they are housed in as different constituents of the rock are removed. K<sub>2</sub>O and Ba are housed primarily in the potassium feldspar and this mineral remains unaltered in the incipiently weathered rock. There is an increase in the concentration of K<sub>2</sub>O and Ba at the onset of weathering due to an increase in K-feldspar per unit volume. There is a loss of Ba in the moderately weathered rock, possibly reflecting the greater ease with which this element goes into solution relative to K. Zr, Hf, Th, P<sub>2</sub>O<sub>5</sub>, and REE are housed in the accessory minerals apatite, sphene, zircon, and allanite. The Zr, Hf, and P<sub>2</sub>O<sub>5</sub> concentrations are controlled by the zircon and apatite percentage of the rock. These minerals remain largely unweathered throughout the profile. The increases in Th and REE as weathering progresses may be due to the enrichments of the minerals in which they are housed (such as zircon or clays) as other constituents are removed.

## Mass Balance Calculations

REE analyses were obtained for plagioclase, biotite, sphene, and apatite separates from the fresh granodiorite and one incipiently weathered sample (25.6 m). Due to small grain size, measurable amounts of zircon and allanite were not obtained. Published REE data for these minerals (Sawka, 1988; Gromet and Silver, 1983) were used in the mass balance calculations. The variability of REE distributions for zircons and allanites from a variety of granites and granodiorites is small (Sawka, 1988; Gromet and Silver, 1983). It was therefore assumed that the use of published values for these minerals in mass balance calculations would not cause appreciable error. Mineral separate data, published values, and modal percentages were used for mass balance calculations of each sample along the weathering profile. Mineral contributions to the REE contents of parent rock and representative incipient, moderate, and highly weathered samples are shown in Figures 42 through 45. Data for the remainder of the samples are included in Appendix D .

Approximately 80 percent of the total REE in the parent rock are housed in sphene with apatite and clays supplying approximately 10 %, and biotite 5% (Fig. 42). Allanite contributes between 2 and 3 % of the LREE and negligible amounts of the HREE and zircon contributes 3% HREE and negligible amounts of LREE. The REE contributions of the feldspars are low, ( 0.1%) excluding Eu. Plagioclase contains approximately 5% of the Eu, whereas K-feldspar contains only 0.5 % Eu.

In the incipiently weathered rock (25.6 m, Fig. 43), sphene contributes only 10% of the LREE and 20-30% of the HREE. 70 to 80% of the total REE are supplied by the clays. The amount of REE supplied by biotite, apatite, allanite, zircon and

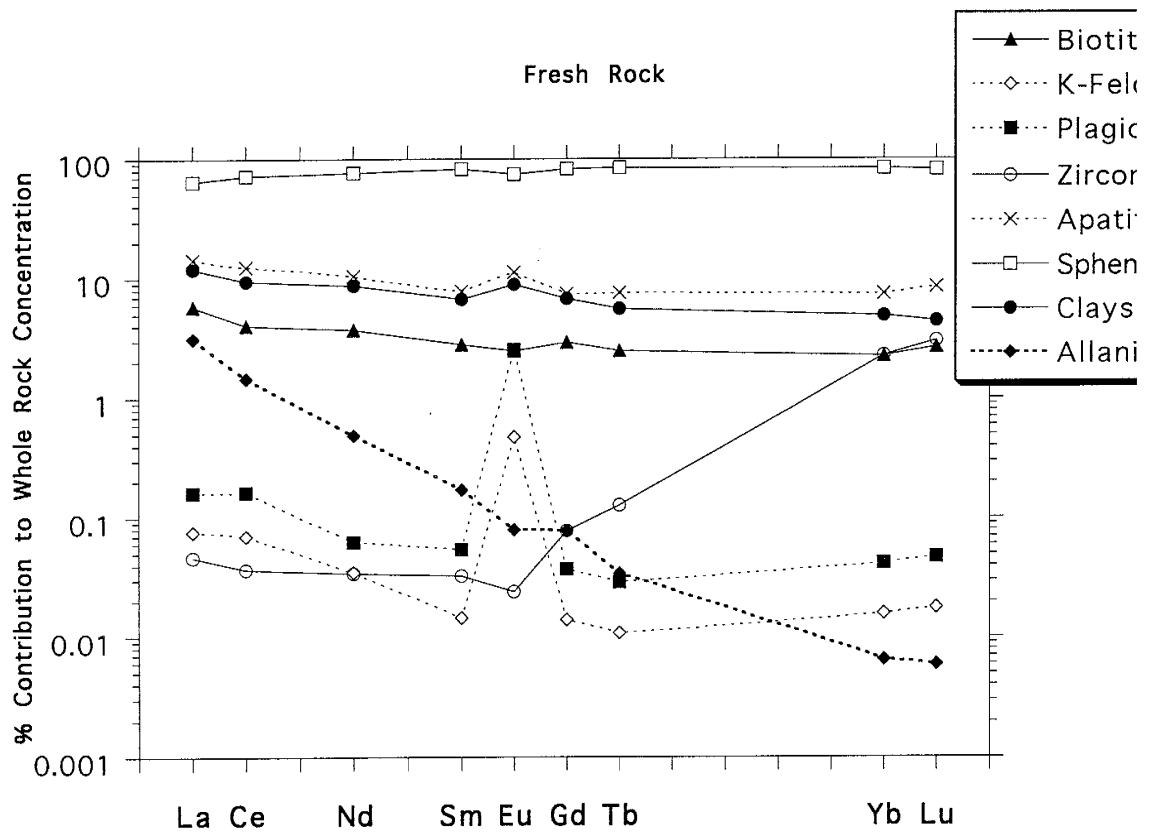


Figure 42. Plot of the percent contribution of minerals to whole-rock REE content for parent rock from the Boulder paleoweathering profile. Mineral compositions given in Appendix D. Zircon and allanite compositions from Gromet and Silver (1983).

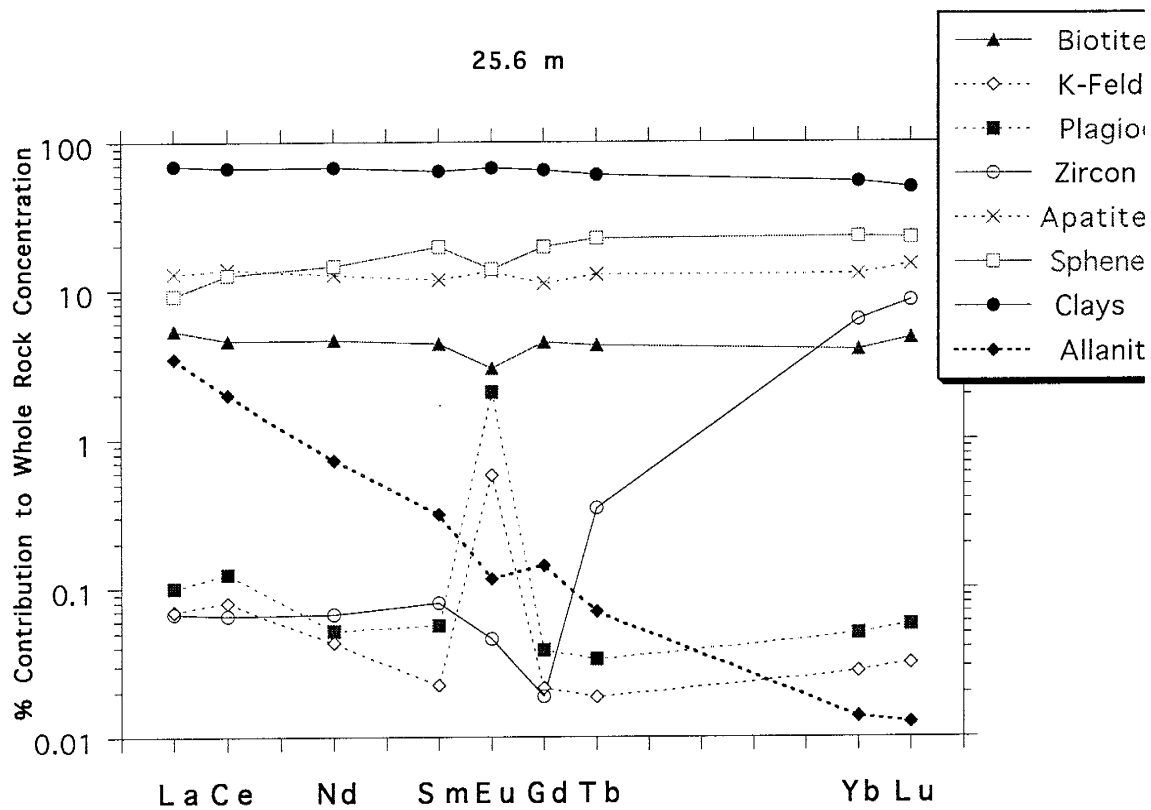


Figure 43. Plot of the percent contribution of minerals to whole-rock REE content for weathered rock (25.6 m from sediment-granodiorite interface) from the Boulder granodiorite paleoweathering profile. Mineral compositions given in Appendix D. Zircon and allanite compositions from Gromet and Silver (1

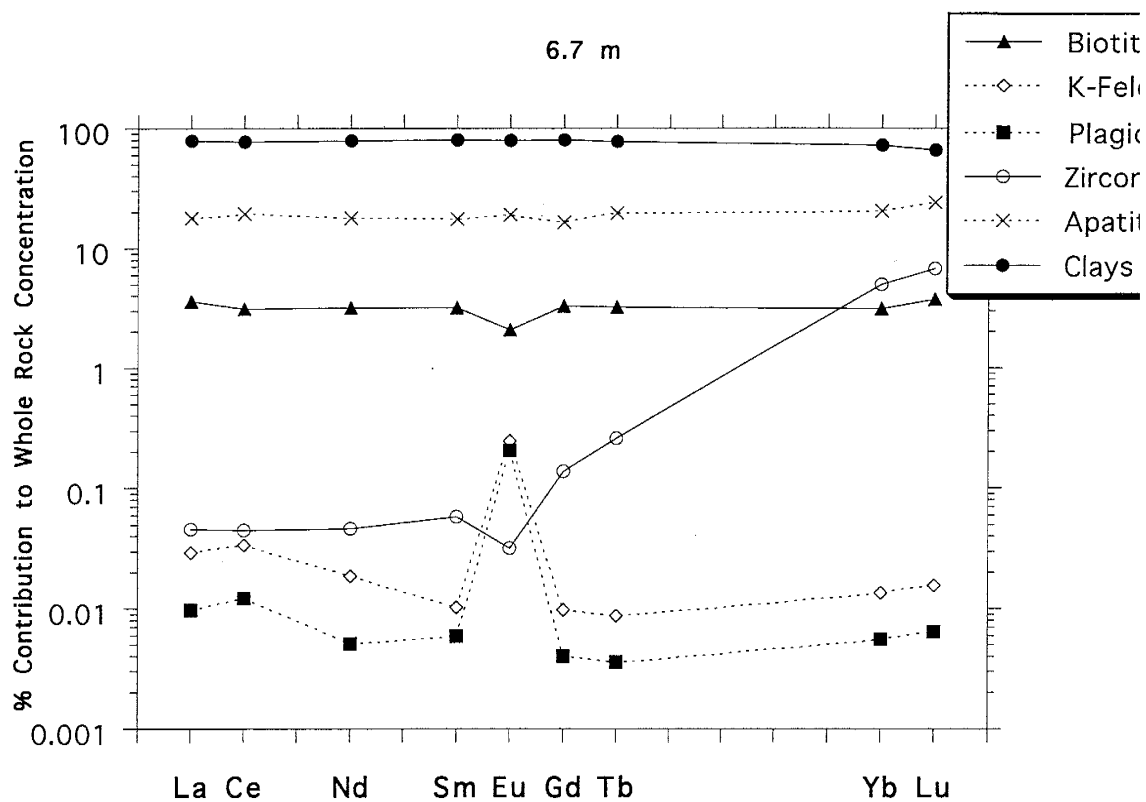


Figure 44. Plot of the percent contribution of minerals to whole-rock REE content for weathered rock (6.7 m from sediment-granodiorite interface) from the Boulder granodiorite paleoweathering profile. Mineral compositions given in Appendix D. Zircon and allanite compositions from Gromet and Silver (1983).

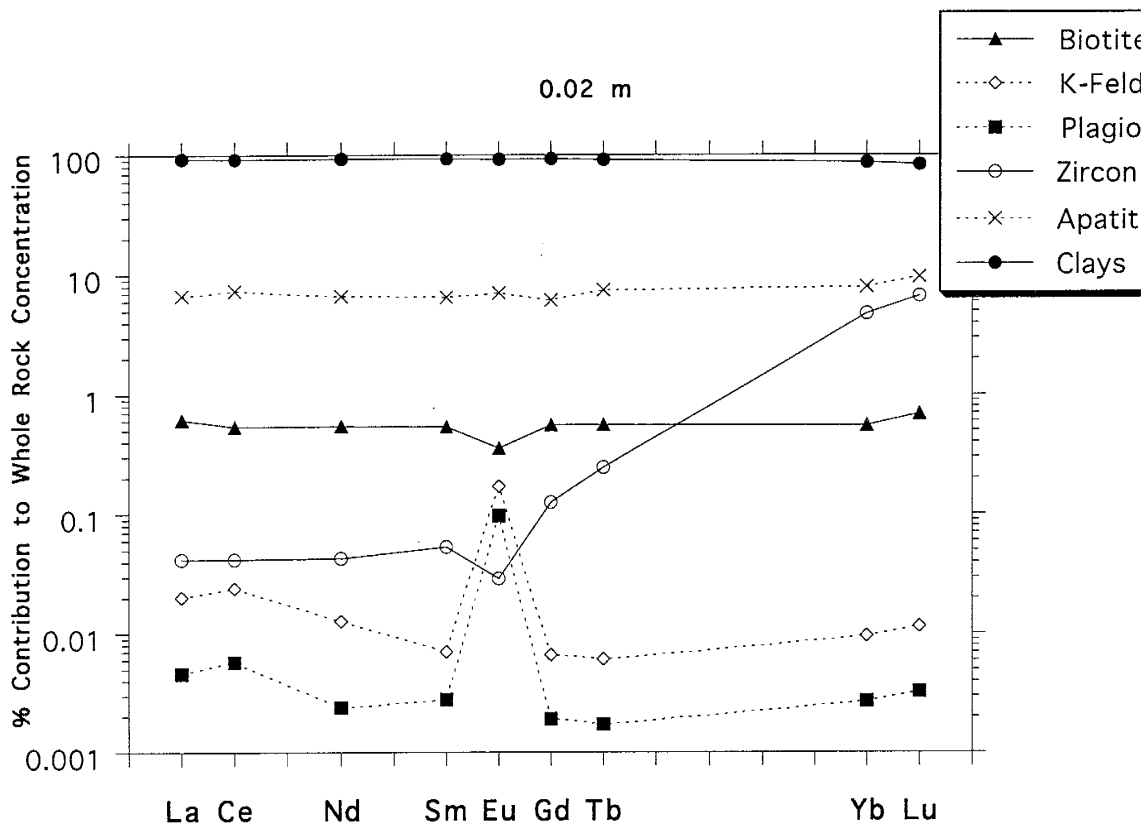


Figure 45. Plot of the percent contribution of minerals to the whole-rock REE content for weathered rock (0.02 m from the sediment-granodiorite interface) from the Boulder granodiorite paleoweathering profile. Mineral composition given in Appendix D. Zircon and allanite compositions from Gromet and Silver (1983).

feldspars is approximately the same in the incipiently weathered rock and the parent granodiorite.

In the moderately weathered rock ( represented by the sample 6.7 m, Fig. 44 ), more than 80% of the whole-rock REE content is supplied by clays. Apatite contributes approximately 10 to 12 % of the REE, and biotite contributes 5 %. In the moderately weathered rock, sphene and allanite appear to have been destroyed and thus, no longer contribute to the whole-rock REE distribution. Zircon supplies slightly more than 5% of the HREE and only 0.05% of the LREE in this sample. The plagioclase and K-feldspar contribute very small amounts of REE and approximately 0.1% of the Eu.

In the most highly weathered rock along the profile (represented by the sample at 0.02 m, Fig. 45), clays are supplying over 90% to the whole-rock REE content. Apatite contributes less than 10% of the REE and biotite less than 1 %. Zircon contributes approximately 5% to the overall HREE and negligible amounts of LREE and plagioclase and potassium feldspar contribute negligible amounts of REE.

Figures 46 through 48 show the percent contributions of the constituent minerals to whole rock La, Eu, and Yb as a function of distance along the outcrop. In the parent rock, the majority of the La is housed in sphene (Fig. 46). As weathering begins and sphene is progressively altered, La is transferred to clay minerals. This transition begins at the onset of weathering and is completed approximately 20 m beneath the Permian unconformity. In the highly weathered rock, clays are supplying the majority of the La. Only small amounts of La are housed in apatite and biotite and zircon and feldspars contribute negligible amounts of La to the whole-rock.

Yb concentrations exhibit a distribution similar to La, as shown in Figure 47. In the fresh rock, the majority of the Yb is housed in sphene and is transferred to clay minerals at the onset of weathering. As with La, this transfer takes place approximately 20 m beneath the Permian unconformity. The contribution to whole-



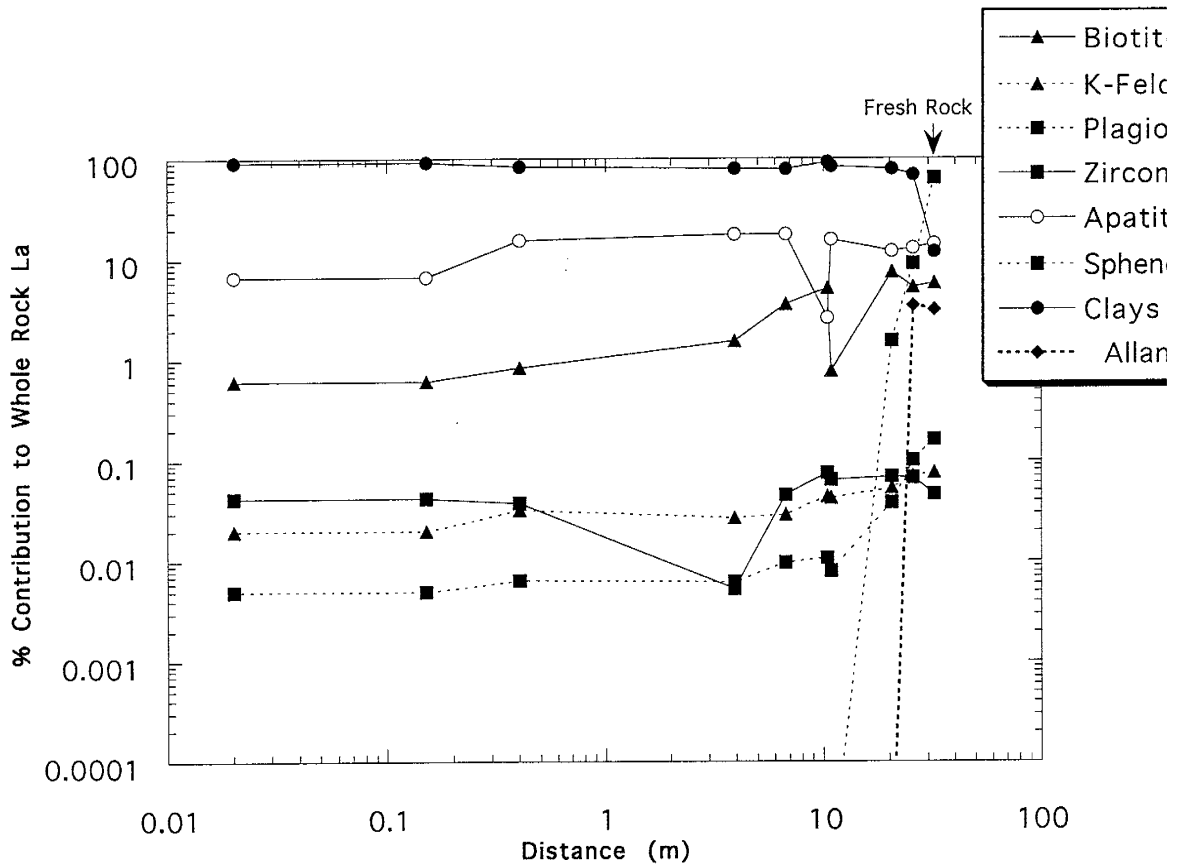


Figure 46. Plot of the percent contribution of minerals to the whole-rock La concentration versus distance from Fountain Formation sediments along the Boulder granodiorite paleoweathering profile.

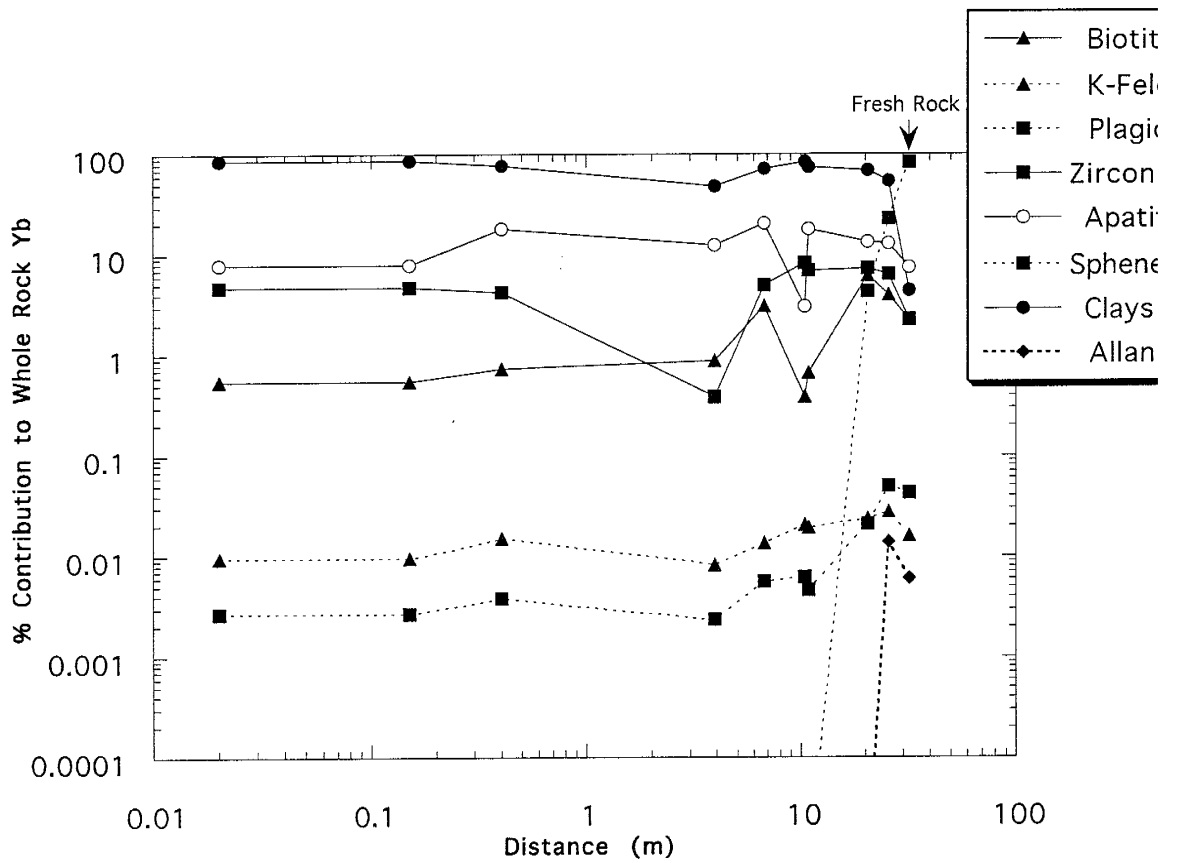


Figure 47. Plot of the percent contribution of minerals to the whole-rock Yb concentration versus distance from Fountain Formation sediments along the Boulder granodiorite paleoweathering profile.

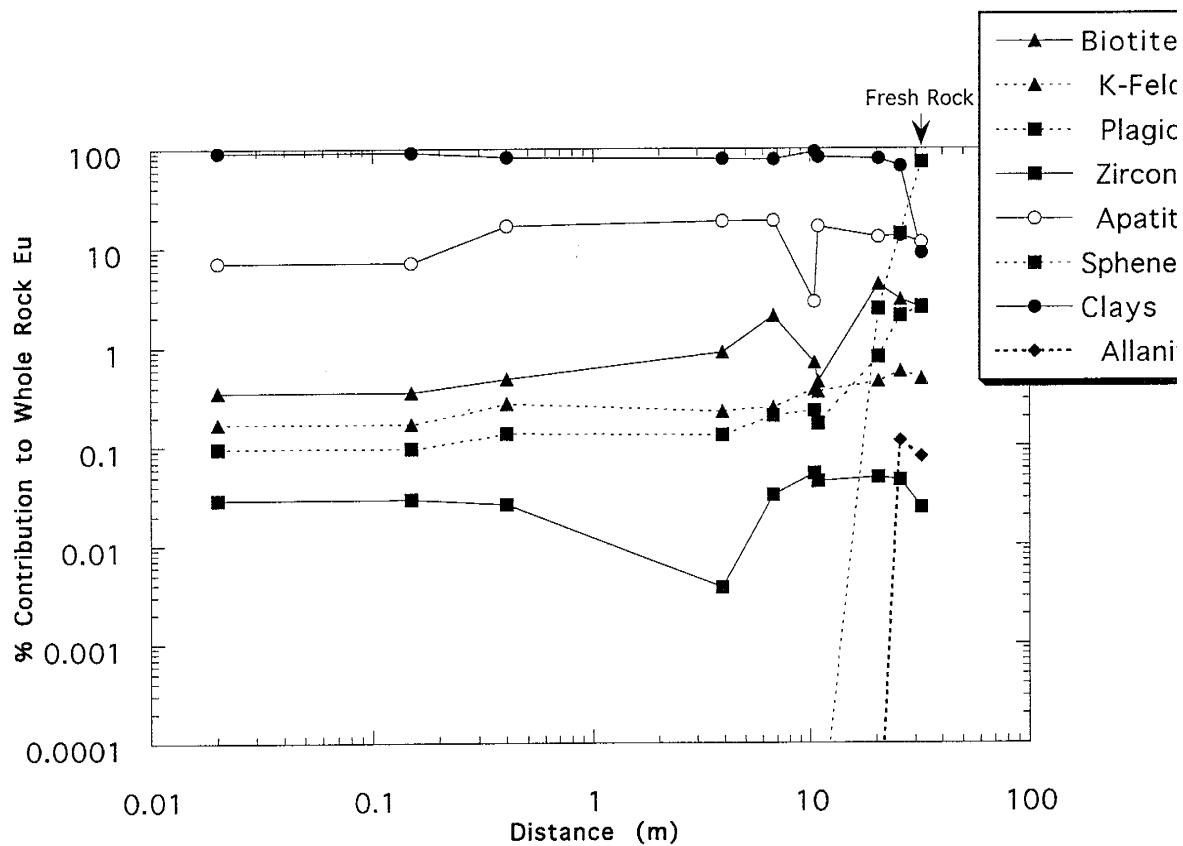


Figure 48. Plot of the percent contribution of minerals to the whole-rock Eu concentration versus distance from Fountain Formation sediments along the Boulder granodiorite paleoweathering profile.

rock Eu versus distance plot shows the same general trends as for La and Yb (Fig. 48). The relatively large contribution (5%) of plagioclase to the unweathered granodiorite Eu content is also evident from this graph.

The contribution to whole-rock La from apatite increases slightly in the moderately weathered rock (to approximately 12 %) and decreases to 8% in the uppermost meter of the profile. The increase in the amount of La supplied by apatite in the moderately weathered rock is probably due to the removal of other constituents during weathering and the subsequent decrease is likely due to the slight alteration of apatite in the highly weathered granodiorite. There is a noticeable decrease (approximately 5%) in the amount of La, Eu, and Yb supplied by apatite across the gray-red contact. This decrease does not reflect a decrease in the percentage of apatite across the contact, as apatite increases from 0.6 to 1.0 % in thin section (Table 1). There is, however, a large increase in the amount of La supplied by biotite across this contact.

The amount of La supplied by biotite decreases with an increase in the degree of weathering to less than 1% in the uppermost meter of the profile. As previously mentioned, there is a 5% increase in the amount of La supplied by biotite across the gray-red contact. The amount of Eu contributed by biotite decreases to 0.5 % during weathering and Yb shows an overall decrease to 0.7% in the uppermost meter of the profile. There is a noticeable decrease in the amount of La, Yb, and Eu supplied by biotite in sample 10.8 m, which may be due to the smaller percentage of biotite from the previous sample (Table 1). The decrease in the contribution to whole-rock La, Eu, and Yb from biotite with distance is most likely a result of alteration of biotite to clays and the subsequent transfer of REE.

The contribution to whole-rock La and Yb from feldspar drops to less than 0.05% in the uppermost meter of the profile. The contribution from plagioclase to whole-rock Eu decreases to 0.1% in the highly weathered granodiorite due to alteration.

K-feldspar contributes 0.5% Eu in the fresh rock which decreases to 0.3% of the Eu in the uppermost meter of the profile.

The contribution to fresh rock La and Eu from zircon is 0.8% and 0.5%, respectively, and remains constant in the highly weathered rock following a decrease to 0.01% at 3.9 m. Zircon contributes 2-3% of the whole-rock Yb and increases to 8% in the highly weathered rock following a decrease to 0.8% at 3.9 m. The sample at 3.9 m does not contain appreciably less zircon in thin section (Table 1).

In summary, mass balance calculations show that the majority of the REE are housed in sphene in the parent granodiorite. As weathering begins, the sphene breaks down and its constituent REE are transferred to clay minerals. This process occurs over a section of less than 1 m in the weathering profile.

### REE Fractionation During Weathering

An important difference between the parent granodiorite and the altered rock of the Boulder weathering profile is the variation in slope of the chondrite-normalized REE patterns (Fig. 25). As previously discussed, the weathered granodiorite has developed a large negative Eu anomaly and, with exception of sample 0.4 m, there appears to be LREE depletion and HREE enrichment as the degree of weathering increases. In addition to the chondrite-normalized REE distributions, the trend of decreasing  $(La/Yb)_n$  during weathering indicates LREE depletion and HREE enrichment (Fig. 29). Mass balance calculations show that the majority of the REE throughout the weathering profile are being supplied by clay minerals. It is therefore likely that the REE fractionation is a result of preferential adsorption onto clays. The process by which HREE may become preferentially enriched and the LREE depleted during

weathering involves the geochemical behaviors of specific REE, weathering environment, and the availability of REE to the system.

Primary factors influencing the mobility of REE during progressive weathering are: their abundance and location in the unaltered rock, the REE concentration of the fluids introduced into the system during weathering, and the amount of adsorption on secondary (Henderson, 1984). REE in the Boulder granodiorite were originally housed in the relatively unstable mineral sphene. As sphene underwent alteration, REE were mobilized and transferred to the clays. Chondrite-normalized REE distributions for the Boulder weathering profile (Fig. 25) show that the REE distributions of weathered samples are enriched relative to the parent rock. The REE also have been fractionated from one another during alteration. Along with progressive total REE enrichment, there is a relative increase in the HREE as a function of distance along the profile (Fig. 25, 26).

Studies show that solution pH is important in determining REE mobility (Nesbitt, 1979; Henderson, 1984). In a low pH environment, REE are more likely to go into solution and be transported, either as free ions or as complexes (Henderson 1984). As the pH of a system increases, REE may precipitate or be adsorbed onto clays. Nesbitt (1979) found that the mobility of REE during the weathering of a granodiorite could be explained by changes in fluid pH. Soluble elements, including REE, are removed in a low pH weathering environment. As the solution becomes more basic, the REE are precipitated or adsorbed on clays.

The adsorption of specific REE on clay minerals has also been shown to be pH dependent (Duddy, 1980). HREE form more soluble complexes with bicarbonate and organic materials and are therefore more likely to be carried in solution than LREE (Henderson, 1984). This results in a greater availability of HREE to be adsorbed by clays. Nesbitt (1979) suggested that HREE enrichment during the weathering of a granodiorite is due to the preferential formation of complexes by HREE and the ease

with which they are transported in solution. The relative HREE enrichment of the Boulder profile may also be a result of this phenomenon.

Approximately 1 m beneath the Permian unconformity, there is a significant LREE enrichment, disrupting the trend of steadily increasing HREE. There is no corresponding deficit of LREE along the profile. An enrichment of LREE requires a source of these elements. The fluid moving through the weathering profile may be considered as a possible source of LREE, causing the LREE enrichment 1 m beneath the Permian unconformity. Work done on the REE content of rivers and streams shows that chondrite-normalized REE patterns of river waters are similar to that of NASC, North American Shale Composite (Henderson, 1984). The distribution is LREE-enriched, HREE-depleted and has a negative Eu anomaly (Henderson, 1984, Figure 9.6). Another possible source of the LREE is the mineral apatite which loses LREE as weathering proceeds (Fig. 46). The LREE may be more susceptible to leaching from the apatite than the HREE, which are known to form stronger complexes, and hence the LREE may have been transported in solution and redeposited beneath the Permian unconformity.

#### Provenance of Shales from the Fountain Formation

In conjunction with REE distributions, key element ratios have been considered useful as provenance indicators for fine-grained clastic sediments. Commonly used ratios include: Cr/Th, Zr/Y, Zr/Cr, Th/Sc, Ti/Nb, Co/Th, La/Th, Cr/Sc, La/Sc, Eu/Eu\* (Chrichton, 1992; McLennan and Taylor, 1991; Taylor and McLennan, 1985). Whether these ratios are transferred unchanged from the source rock to the weathering profile, and ultimately to the sediments, determines their usefulness as provenance

indicators. Element ratio variations with distance along the weathering profile are shown in Figures 20 through 24 and Appendix A.

As previously shown, Cr/Th, Zr/Y, Co/Th, La/Th, Cr/Sc, La/Sc, and Eu/Eu\* decrease as a function of distance along the profile, attaining minimum values in the highly weathered rock. The Ti/Nb ratio increases as the degree of weathering increases and Zr/Cr and Th/Sc ratios remain unchanged from the fresh granodiorite to the weathered rock.

Cr/Th, Co/Th, La/Th, Eu/Eu\*, and Cr/Sc ratios are lower in the shales than the parent rock. Co/Th, La/Th, and Cr/Sc ratios in the shales are similar to these ratios in the highly weathered rock in the uppermost meter of the profile and Cr/Th and Eu/Eu\* ratios are lower in the shales than either the profile or the parent rock. Zr/Y ratio is variable in the shales, samples FO-1 and FO-2 have values similar to that of the fresh granodiorite and the moderately weathered rock. Shale FO-3 has a Zr/Y ratio similar to that of the uppermost meter of the profile. La/Sc, Zr/Cr, and Th/Sc ratios are higher in the shales than the parent rock and Ti/Nb is similar in the shales to values in the fresh granodiorite.

Element ratios in the parent rock differ from ratios in both the weathering profile and in the Fountain shales and the fractionation of these ratios during weathering limits their usefulness as provenance indicators. Three ratios, Co/Th, La/Th, and Cr/Sc, are similar in the uppermost meter of the weathering profile to ratios in the shales. This similarity may indicate that there has been no significant change in the ratios through the mechanical processes of sorting and deposition. Zr/Cr and Th/Sc ratios remain unchanged from the parent rock through the weathering profile, but differ in the shales. This suggests these ratios may be useful as provenance indicators, but the shales were not derived solely from the Boulder granodiorite. If this is so, the similarity between the Ti/Nb ratio in the parent rock and the shales may be a coincidence.



The REE distributions of the weathering profile differ from those of the parent rock and the adjacent shales. As seen from the  $(La/Yb)_n$  plot (Fig. 29), there is an increase in HREE as weathering proceeds. The REE distributions of the shales are similar (with the exception of a slight LREE enrichment in FO-1) to those of the parent rock, but are elevated in magnitude and show large, negative Eu anomalies. Two of the shales (FO-2, FO-3) have  $(La/Yb)_n$  values similar to that of the parent rock. The third shale (FO-1) has a value higher than the parent and most similar to the sample at 0.4 m from the sediment contact.

As discussed earlier, the results of this study show that a large negative Eu anomaly can develop during the weathering process. Therefore,  $Eu/Eu^*$  should not be used as a provenance indicator for fine-grained clastic sediments.

The results of this study illustrate that caution must be exercised when using element ratios or REE as provenance indicators for fine-grained sediments. It appears that none of the element ratios are transferred unchanged through the weathering process to the shales in the Boulder weathering profile. The chondrite-normalized REE distributions are similar in the parent granodiorite and the Fountain shales, but differ from the bulk weathering profile (with the exception of the first incipiently weathered sample, 25.6 m) and the uppermost meter of highly weathered granodiorite. The similarity between the REE distributions of the fresh granodiorite and the shales may be coincidental. Somewhere in the mechanical processes of erosion, transportation and deposition the REE have been redistributed in clays and reflect the distribution of the parent rock. It is possible that this redistribution occurred in the uppermost portion of the weathering profile, was at least partially eroded prior to the deposition of the shales. It is also possible that the Boulder granodiorite was not the only source for the Fountain shales. The appearance of relatively unweathered grains and muscovite in thin section, suggest additional sources for the shales during deposition and the influence of additional material to the shales would affect the REE distributions.

## Diagenesis

In an effort to completely understand the distribution of REE in the Boulder weathering profile and Fountain Formation sediments, it is important to differentiate the effects of weathering and diagenesis on REE behavior. Unfortunately, the influence of diagenesis on REE mobility is poorly understood. Recent studies have documented that REE are redistributed during diagenesis of carbonate rocks and during the early diagenesis of near shore sediments (Sholkovitz, et.al., 1989; Elderfield and Sholkovitz, 1987; Schieber, 1988).

In a study by Nesbitt and Young (1989), weathering trends documented on a geochemically similar modern weathering profile were compared to those of the Boulder profile. Deviations among the trends suggest that both early and late stage diagenesis may have occurred on the Boulder weathering profile. The precipitation of carbonate in the incipiently weathered granodiorite is likely the result of early diagenesis. It is also thought that there has been late stage K-metasomatism throughout the profile causing the conversion of other minerals (i.e. kaolinite and degraded K-feldspar) to illite and K-feldspar. The carbonate precipitation during early diagenesis does not appear to have affected the decreasing CaO trend resulting from the breakdown of plagioclase. However, in part, the trend of increasing K<sub>2</sub>O may be explained by the addition of K during late-stage metasomatism.

It is uncertain what effect the early and late-stage diagenesis would have on the REE distribution of the weathered granodiorite. With exception of sample 20.6 m and 0.4 m there does not appear to be an anomalous gain or loss of REE that may have resulted from either stage of diagenesis. Whether the variations in sample 20.6 m and 0.4 m are a result of diagenetic overprinting or some other process is unknown. Perhaps by comparing trends in REE distributions of modern weathering profiles to

those of the Boulder profile it would be possible to distinguish the changes in REE distributions that occur during weathering and those that occur due to diagenesis.

## Conclusions

Weathering of the Boulder granodiorite results in a substantial loss of CaO, Na<sub>2</sub>O, and Sr, due to the breakdown of plagioclase. REE (except Eu), Rb, Th, Zr, Hf, Sc, Co, Cr, and Y increase throughout the majority of the weathering profile, while Al<sub>2</sub>O<sub>3</sub>, Ta, and Nb are conserved during weathering. SiO<sub>2</sub> is conserved through the incipiently and moderately weathered granodiorite, however, there is a slight loss of SiO<sub>2</sub> in the highly weathered rock. Eu remains immobile until approximately one meter beneath the Permian unconformity, where it becomes enriched relative to the parent rock. The relative immobility of Eu compared to the remainder of the REE is responsible for the development of a large negative Eu anomaly in the weathering profile. There may be some loss of Eu due to the breakdown of plagioclase. Ba is enriched in the incipiently weathered rock, but is depleted as weathering progresses. MgO behavior is variable throughout the incipiently and moderately weathered granodiorite and there is a loss of MgO in the uppermost meter of the profile. Across the gray-red contact there is a significant increase in Fe<sub>2</sub>O<sub>3</sub>T and TiO<sub>2</sub> which appears to be due to the increase in iron oxides. This increase iron oxides is responsible for the color change between the gray and the red rock. Approximately one meter beneath the Permian unconformity there is a sudden increase in the LREE, Eu, and Sr content.

The REE distributions in the unweathered Boulder granodiorite are primarily controlled by sphene. Greater than 70% of the REE in the parent rock are housed in the

sphene with lesser amounts in housed in other accessory minerals, biotite, and feldspars. Sphene alters rapidly at the onset of weathering and the REE are transferred to clay minerals. Clays control the REE distribution of the moderately and highly weathered portions of the profile. There is some fractionation of the REE as weathering progresses with an enrichment of HREE and depletion of LREE relative to the parent rock. The LREE concentration decreases along the profile to sample 0.4 m where there is a sudden increase in concentration. LREE are the first to be removed in an acidic environment and HREE form stronger complexes and are more likely to stay in solution. The HREE enrichment of the majority of the Boulder profile may be explained by the greater availability of HREE in solution to be adsorbed by clays. The LREE enrichment at 0.4 meters beneath the sediment contact may be due to the influx of surface waters rich in LREE.

Shale REE distributions are similar to those of the parent rock, although they are enriched and show large, negative Eu anomalies. The element ratios of the shales, weathering profile, and parent rock are dissimilar. The Zr/Cr and Th/Sc ratios are transferred unchanged from the parent rock through the weathering profile, however are not inherited by the shales. Ratios that are similar in the shales and the parent rock may be a coincidence and caution should be exercised when using element ratios as provenance indicators. It is shown conclusively that the negative Eu anomaly of the Boulder profile is developed during weathering and therefore the Eu/Eu\* of a fine-grained sediment should not be inferred to reflect that of the source rock.

From this study, it is seen that REE are mobilized during weathering. The REE are enriched relative to the parent rock and are fractionated from one another during progressive alteration, and the negative Eu anomaly forms during the weathering process. Ratios that have commonly been used as provenance indicators vary in the parent rock, weathering profile, and the shales.

## Appendix A

Selected plots of major element, trace element, and trace element ratio behaviors.

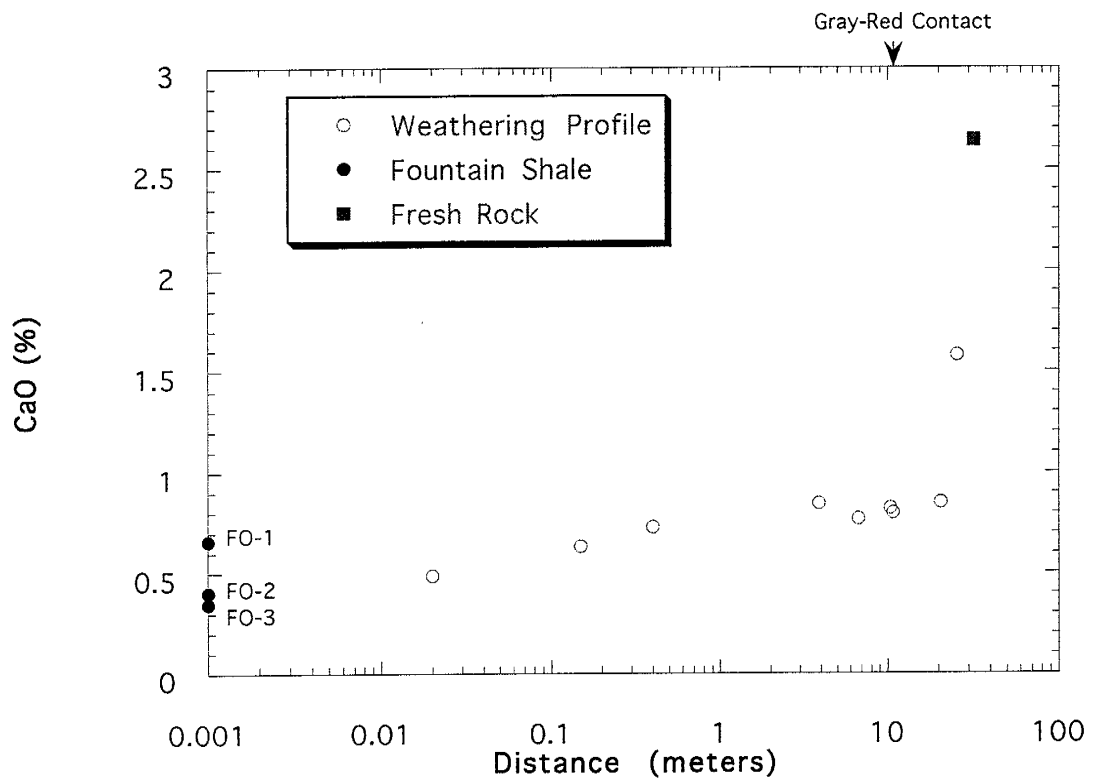


Figure A-1. Plot of CaO versus distance from the Fountain Formation sediments along the Boulder granodiorite paleoweathering profile. Other information given in Figure 3.

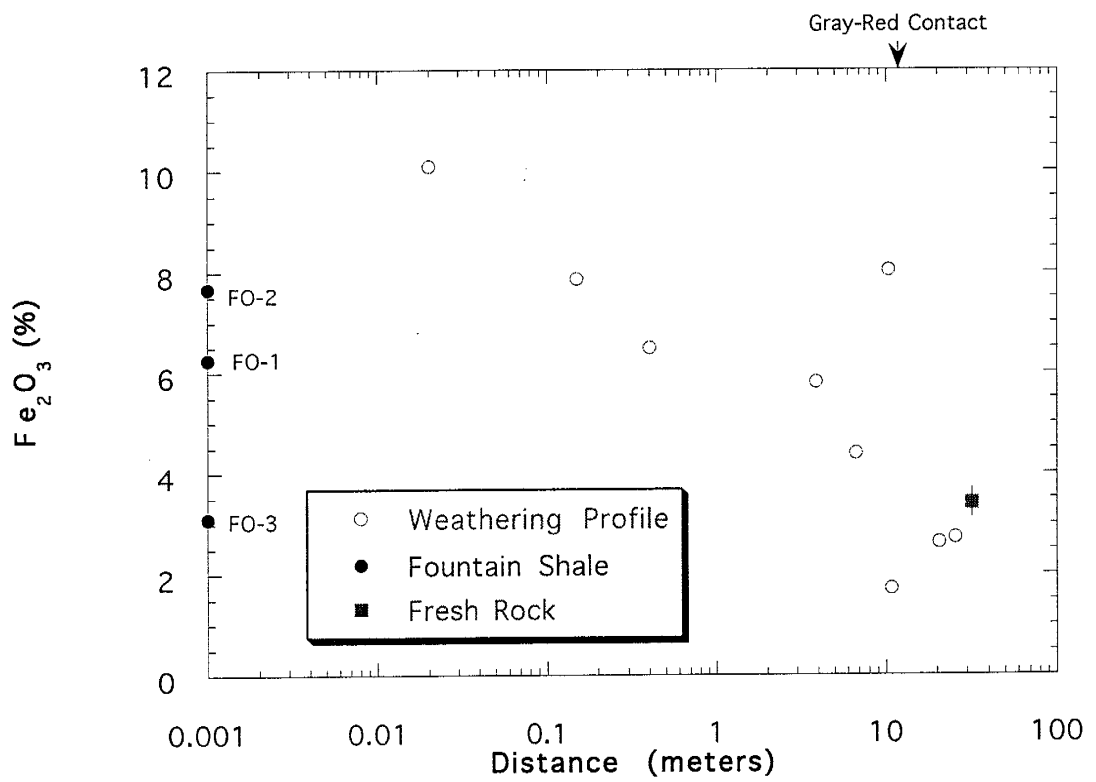


Figure A-2. Plot of Fe<sub>2</sub>O<sub>3</sub> versus distance from the Fountain Formation sediments along the Boulder granodiorite paleoweathering profile. Other information given in Figure 3.

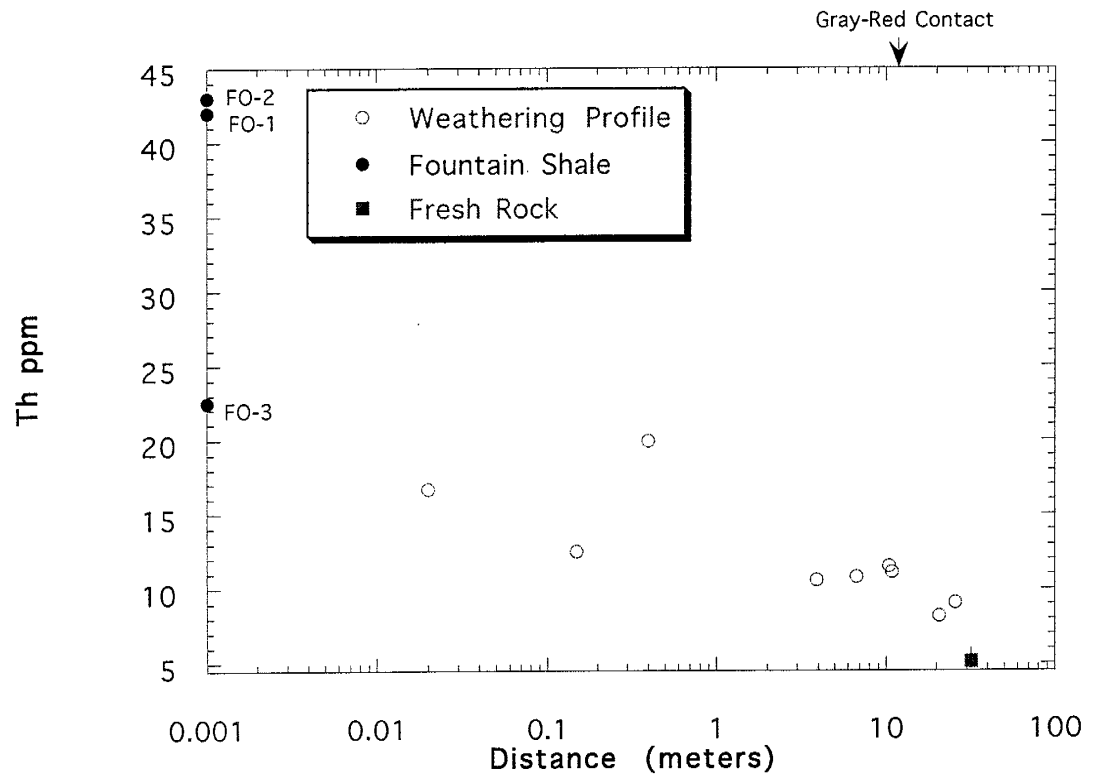


Figure A-3. Plot of Th versus distance from the Fountain Formation sediments along the Boulder granodiorite paleoweathering profile. Other information given in Figure 3.



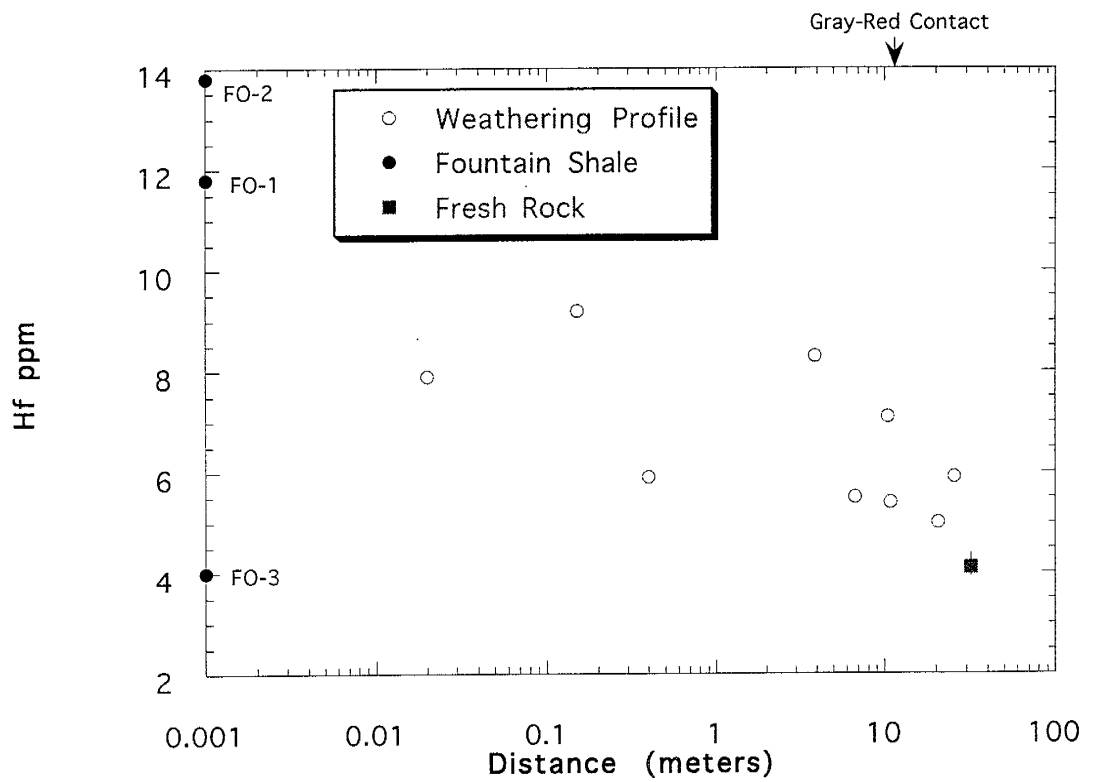


Figure A-4. Plot of Hf versus distance from the Fountain Formation sediments along the Boulder granodiorite paleoweathering profile. Other information given in Figure 3.

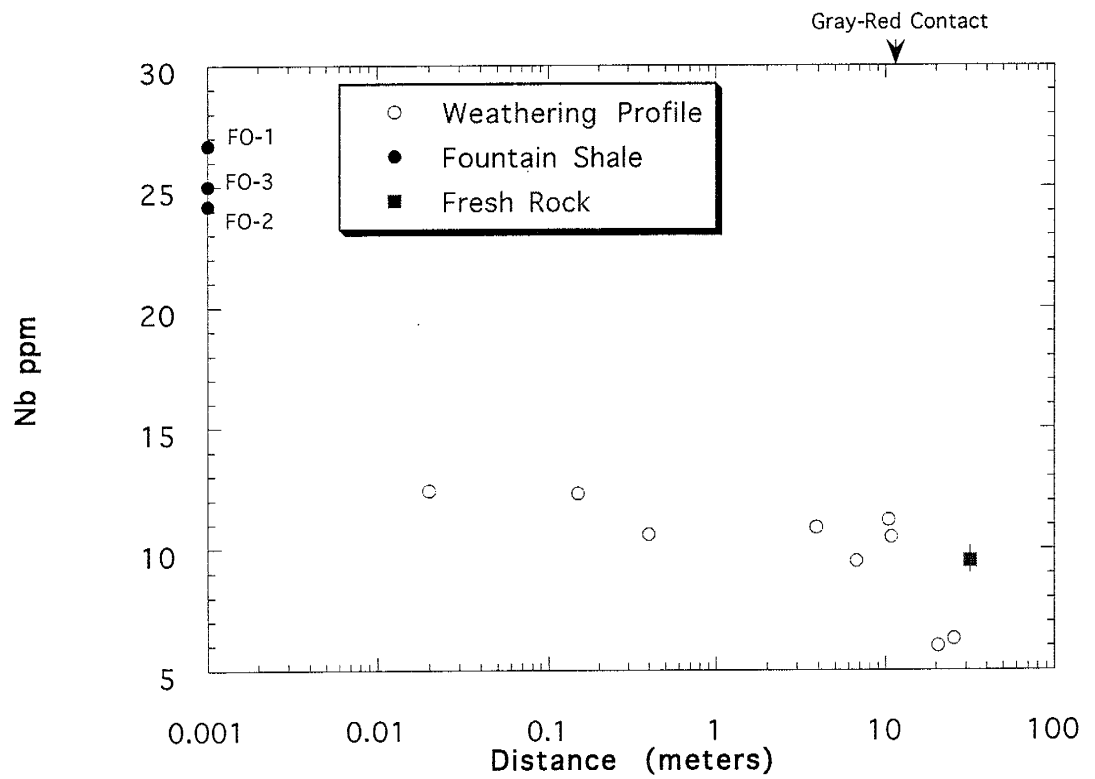


Figure A-5. Plot of Nb versus distance from the Fountain Formation sediments along the Boulder granodiorite paleoweathering profile. Other information given in Figure 3.

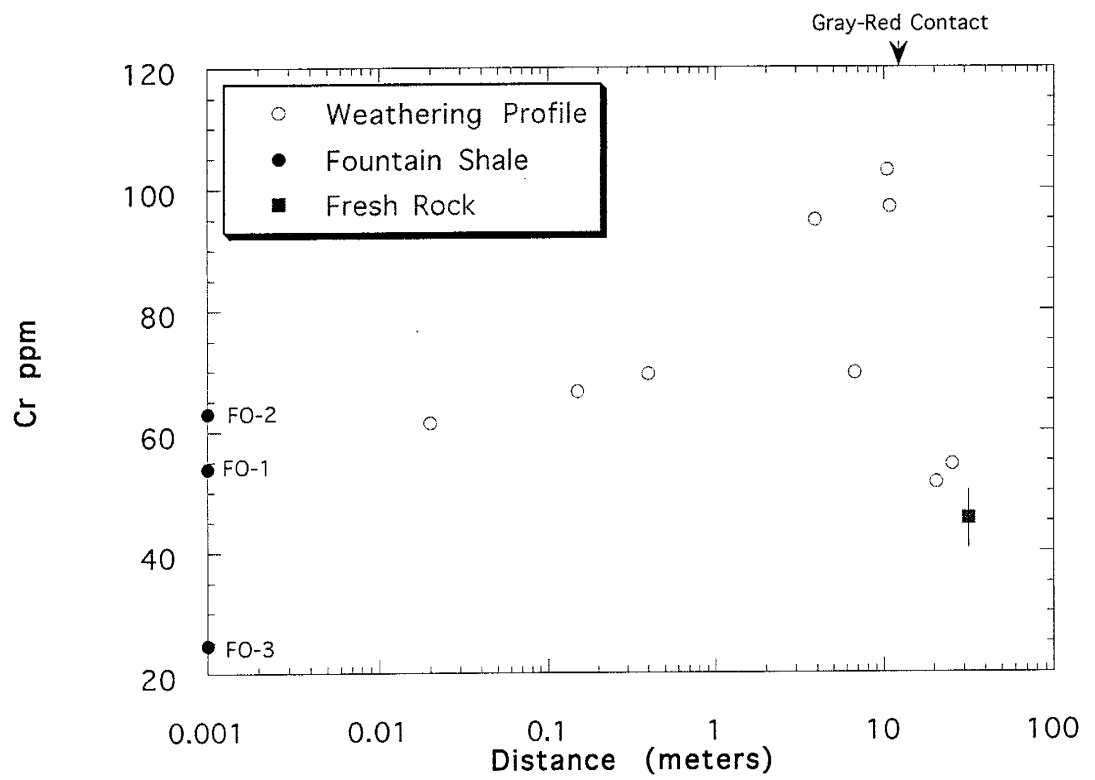


Figure A-6. Plot of Cr versus distance from the Fountain Formation sediments along the Boulder granodiorite paleoweathering profile. Other information given in Figure 3.

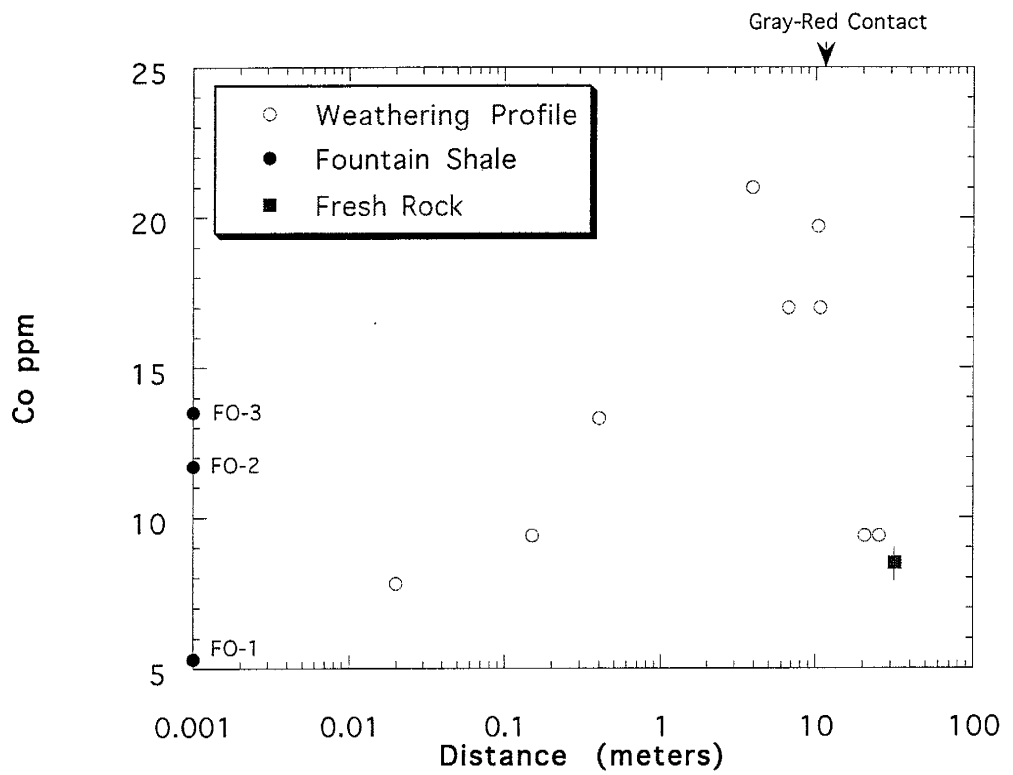


Figure A-7. Plot of Co versus distance from the Fountain Formation sediments along the Boulder granodiorite paleoweathering profile. Other information given in Figure 3.

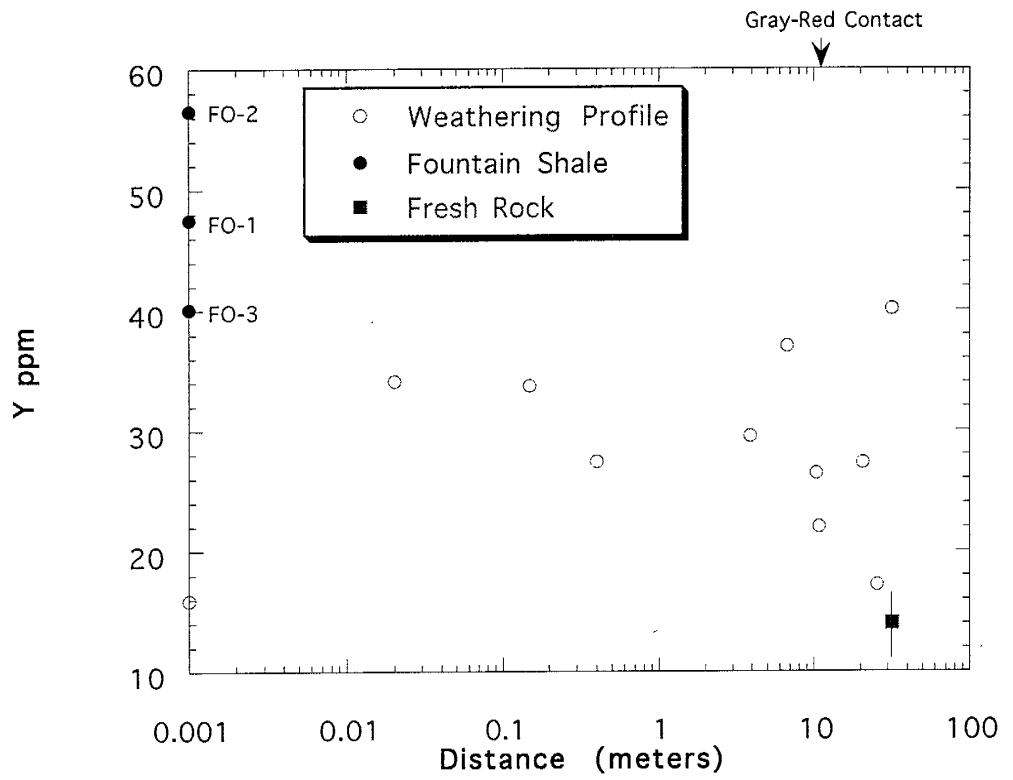


Figure A-8. Plot of Y versus distance from the Fountain Formation sediments along the Boulder granodiorite paleoweathering profile. Other information given in Figure 3.

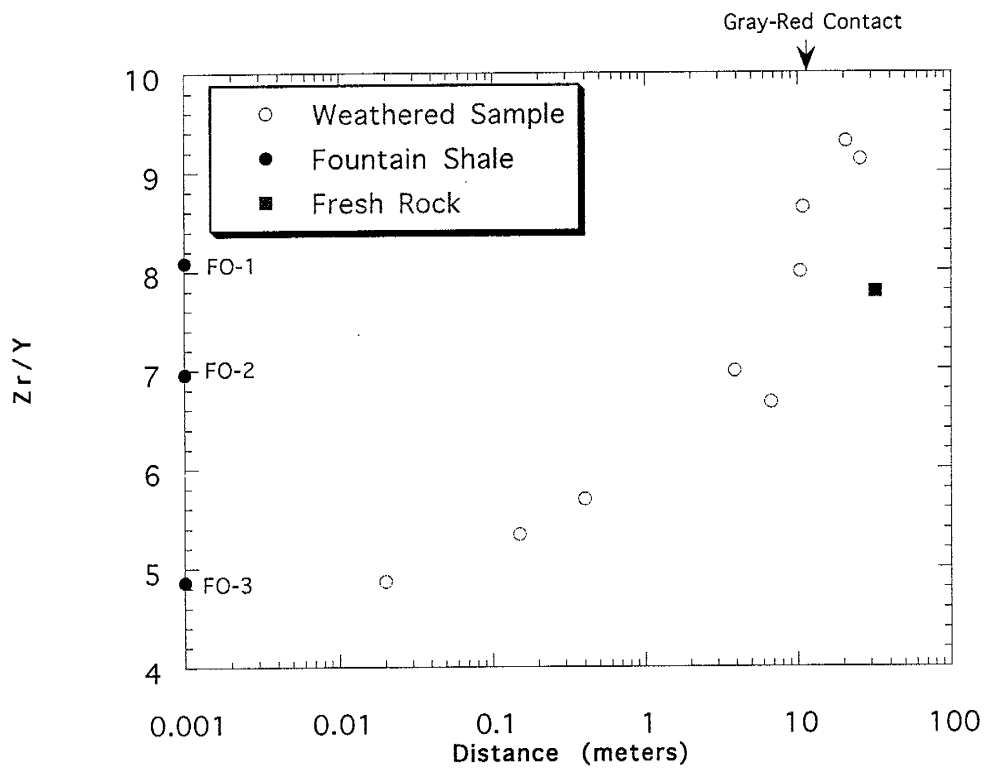


Figure A-9. Plot of Zr/Y versus distance from the Fountain Formation sediments along the Boulder granodiorite paleoweathering profile. Other information given in Figure 3.

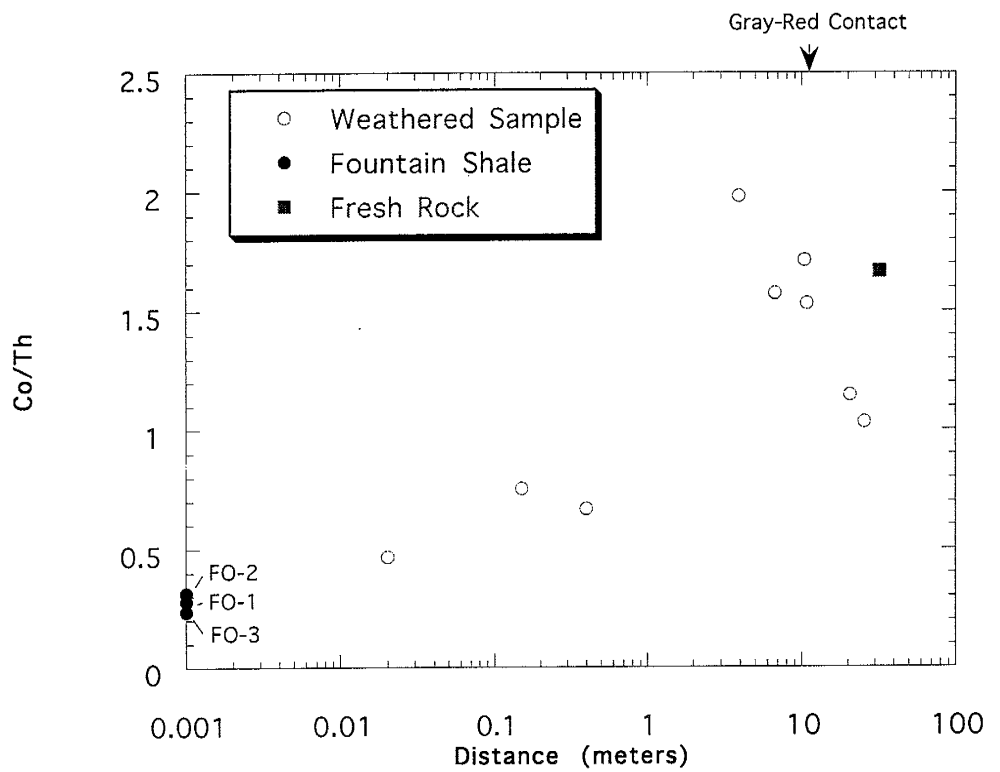


Figure A-10. Plot of Co/Th versus distance from the Fountain Formation sediments along the Boulder granodiorite paleoweathering profile. Other information given in Figure 3.

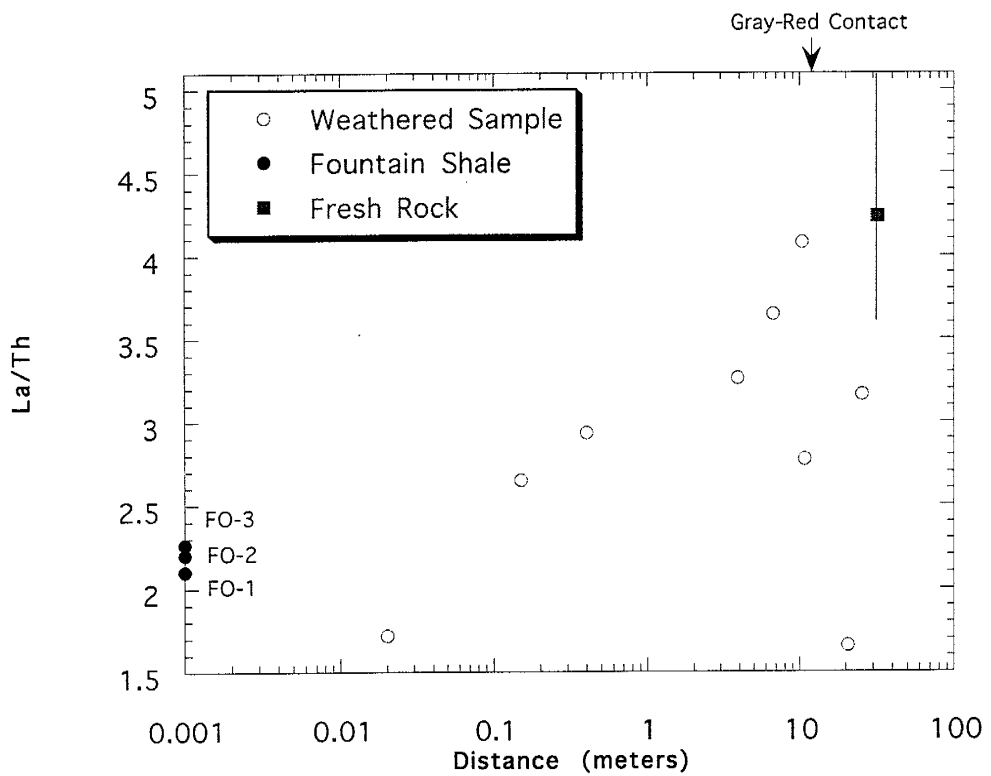


Figure A-11. Plot of La/Th versus distance from the Fountain Formation sediments along the Boulder granodiorite paleoweathering profile. Other information given in Figure 3.



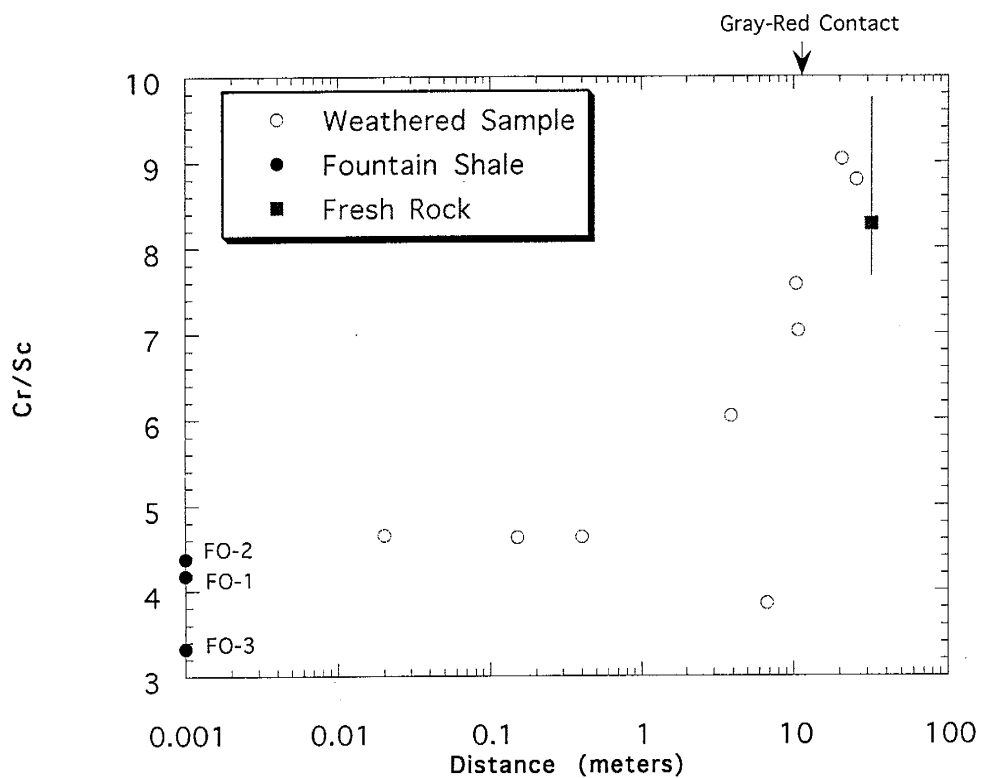


Figure A-12. Plot of Cr/Sc versus distance from the Fountain Formation sediments along the Boulder granodiorite paleoweathering profile. Other information given in Figure 3.

Appendix B  
Precision and Accuracy determined for INAA and XRF

Table B-1. Precision and accuracy for INAA determined from AN-G.

	AN-G a	AN-G b	AN-G c	x	s	C.V.	AN-G accepted	Percent Accuracy
Sc	9.83	10.02	9.95	9.93	.08	.79	10	.70
Cr	45.2	46.00	45.2	45.5	.379	.83	50	9.00
Co	24.06	24.02	24.06	24.05	.02	.08	25	3.80
Cs	.06	.10	.08	.08	.02	20.40	.06	33
Ba	36	31	51	39.30	8.50	22.00	34	15.6
Hf	.63	.37	.38	.46	.12	26.6	.38	21.1
Ta	.22	.17	.16	.18	.03	13.9	.20	10
Th	.05	.09	.14	.09	.04	39.8	.04	125
La	2.23	2.37	2.32	2.3	.06	2.51	2.0	15.5
Ce	4.70	4.86	4.7	4.8	.08	1.59	4.70	1.05
Nd	2	1.9	2.0	1.97	.05	2.38	2.4	17.9
Sm	.73	.79	.78	.77	.03	3.28	.70	10
Eu	.37	.37	.38	.37	.01	1.78	.37	0
Tb	.22	.20	.21	.21	.01	5.10	.20	4.5
Yb	.81	.83	.80	.81	.01	1.54	.85	4.2
Lu	.13	.11	.12	.12	.01	7.45	.12	1.7

x - Mean value of AN-G this study.

s - One standard deviation of x.

C.V. - Coefficient of variation =  $(s/x) \times 100$ .

Accepted values of AN-G from Govindaraju (1989).

Percent accuracy =  $[(\text{absolute value } (x - \text{accepted})) / \text{accepted}] \times 100$ .

Table B-2. Accuracy for INAA determined from G-2.

	G-2 a	G-2 b	G-2 c	x	G-2 accepted	Percent Accuracy
Sc	3.48	3.59	3.33	3.47	3.5	.86
Cr	7.0	8.10	7.0	7.4	8.7	14.94
Co	4.56	4.58	4.39	4.51	4.6	1.96
Cs	1.32	1.34	1.36	1.34	1.34	0
Ba	1719	1766	1666	1717	1882	8.8
Hf	8.06	8.10	7.87	8.01	7.9	1.39
Ta	.81	.76	.84	.80	.88	8.86
Th	22.15	22.25	22.46	22.30	24.7	9.7
U	1.83	1.91	1.76	1.83	2.07	11.59
La	86.6	86.1	85.6	86.1	89	3.26
Ce	154	153.4	157.5	154.9	160	3.19
Nd	54.7	48.2	55.6	52.8	55	5.04
Sm	7.13	7.11	6.81	7.02	7.2	2.5
Eu	1.28	1.27	1.27	1.27	1.4	0
Tb	.47	.42	.48	.46	.48	5.0
Yb	.86	.76	.74	.79	.80	1.5
Lu	.097	.091	.091	.093	.11	15.46

Accepted values from Govindaraju (1989).

Percent accuracy = [(absolute value (x- accepted)) / accepted] X 100.

Table B-3. Accuracy for INAA determined by BCR-1

	BCR-1 a	BCR-1 b	x	Accepted Value	Percent Accuracy
Sc	31.3	30.9	31.1	33	5.8
Cr	12.5	11.4	11.95	15	20.3
Co	35.8	35.4	35.6	36	1.11
Cs	.98	.92	.95	----	----
Ba	620	652	636	675	5.8
Hf	5.0	4.94	4.97	4.9	1.43
Ta	.74	.72	.729	.79	7.72
Th	5.59	5.64	5.62	6.0	6.76
U	1.49	1.55	1.52	1.7	10.6
La	24.57	24.97	24.8	25	.80
Ce	50.4	49.1	49.8	53	6.04
Nd	23.8	22.2	23.0	29	20.7
Sm	6.60	6.52	6.56	6.6	.61
Eu	1.88	1.87	1.88	1.94	3.09
Tb	1.00	1.02	1.01	1	1.0
Yb	3.25	3.22	3.24	3.36	3.57
Lu	.45	.44	.45	.50	10.0

Accepted values from Govindaraju (1989).

Percent accuracy = [(absolute value (x- accepted)) / accepted] X 100.

Table B-4. Precision for INAA and XRF determined from sample WG-3 (weathered granodiorite).

INAA	WG-3 D917	WG-3 D920	WG-3 D064	x	s	C.V.
Fe <sub>2</sub> O <sub>3</sub> T	5.59	5.95	5.94	5.83	.17	2.86
Sc	14.96	15.50	15.62	15.36	.29	1.87
Cr	69.5	76.7	74.4	75.3	3.5	4.65
Co	13.28	13.97	14.10	13.78	.36	2.61
Rb	275	283	273	277	4.32	1.56
Cs	46.9	50.0	49.2	48.7	1.31	2.69
Ba	526	728	552	602	89.7	14.9
Hf	5.90	6.46	6.65	6.34	.32	5.02
Ta	.87	.78	.802	.819	.04	4.52
Th	19.90	20.20	20.29	20.13	.17	.83
U	4.05	4.78	4.95	4.59	.39	8.49
La	58.4	57	58.7	58	1.16	2.0
Ce	117.4	118.4	118.7	118.2	.76	.64
Nd	60	55.5	65	60.2	2.48	4.12
Sm	11.06	11.0	11.02	11.03	.03	.23
Eu	1.81	1.77	1.79	1.79	.02	.95
Tb	1.00	1.01	1.01	1.01	.01	.57
Yb	2.15	2.18	2.28	2.20	.15	6.63
Lu	.312	.314	.317	.314	.002	.67

Table B-4 continued.

INAA	WG-3 D917	WG-3 D920	WG-3 D064	x	s	C.V.
SiO <sub>2</sub>	59.5	60.5	60.0	60	.13	.21
TiO <sub>2</sub>	.77	.81	.79	.79	.02	2.59
Al <sub>2</sub> O <sub>3</sub>	18.86	19.19	19.03	19.03	.17	.87
Fe <sub>2</sub> O <sub>3</sub> T	6.49	6.6	6.55	6.55	.50	7.63
MnO	.06	.07	.07	.07	.01	.08
MgO	1.11	1.05	1.08	1.08	.03	.03
CaO	.73	.78	.76	.76	.03	3.54
Na <sub>2</sub> O	.24	.19	.22	.22	.02	10.83
K <sub>2</sub> O	6.5	6.67	6.59	6.59	.09	.01
P <sub>2</sub> O <sub>5</sub>	.40	.43	.41	.41	.01	3.15

x - Mean value of WG-3.

D917 - Samples irradiated at Texas A&M 1991.

D920 - Samples irradiated at Texas A&M 1992.

D064 - Samples irradiated at University of Missouri 1992.

s - One standard deviation of the mean.

C.V. - Coefficient of Variation = (s/x) X 100.

Table B-5. Precision for INAA determined from sample WG-9 (weathered granodiorite).

INAA	WG-9 D917	WG-9 D064	x	s	C.V.
Fe <sub>2</sub> O <sub>3</sub> T	2.95	2.52	2.74	.22	7.85
Sc	6.18	6.06	6.12	.06	.98
Cr	54.5	44.3	49.4	5.1	10.32
Co	9.38	8.36	8.87	.51	5.75
Rb	176	183	179.5	3.5	1.95
Cs	27.9	25.27	26.6	1.32	4.96
Ba	1018	1284	1151	133	11.6
Hf	5.85	5.89	5.87	.02	.34
Ta	.38	.75	.57	.18	32.6
Th	9.12	23.45	16.29	7.2	44.2
U	1.75	2.23	1.99	.24	12.06
La	28.81	28.27	28.54	.27	.95
Ce	46.9	48.4	47.65	.75	1.57
Nd	22.3	22.5	22.4	.10	.45
Sm	4.54	4.36	4.45	.09	2.02
Eu	1.07	1.02	1.05	.03	2.39
Tb	.50	.46	.48	.02	4.20
Yb	1.43	1.43	1.43	0	0
Lu	.22	.21	.22	.001	.33

X - Mean value of WG-9

D917 - Samples irradiated at Texas A&M 1991.

D064 - Samples irradiated at University of Missouri 1992.

s - One standard deviation of the mean.

C.V. - Coefficient of variation = (s/x) X 100.

Table B-6. Precision for XRF determined from sample WG-6.

XRF	WG-6		x	s	C.V.
	a	b			
Rb	274.83	272.5	273.65	1.15	.42
Sr	244.9	241.9	243.4	1.50	.62
Y	27.5	27.06	27.28	.22	.81
Zr	217.4	218.12	217.76	.40	.19
Nb	10.98	11.31	11.15	.17	1.48

x - Mean value of WG-6.

s - One standard deviation of the mean.

C.V. - Coefficient of variation =  $(s/x) \times 100$ .



Appendix C  
 Chemical Analyses of Boulder Granodiorite Weathering Profile and Fountain  
 Formation Shales

Table C-1. Chemical Analyses of parent and weathered granodiorite.

	Parent	WG-9	WG-8	WG-7	WG-6	WG-5	WG-4	WG-3	WG-2	WG-1
SiO <sub>2</sub>	69.7	66.47	70.78	71.31	59.71	63.97	61.48	59.48	58.53	56.63
TiO <sub>2</sub>	.34	.37	.34	.35	.74	.55	.67	.77	.77	.77
Al <sub>2</sub> O <sub>3</sub>	14.55	13.78	12.87	14.15	17.69	16.5	17.50	18.86	20.14	20.40
Fe <sub>2</sub> O <sub>3</sub> T	3.4	2.72	3.01	1.48	7.15	3.80	5.82	5.59	6.39	10.21
MnO		.08	.06	.08	.08	.12	.09	.06	.08	.06
MgO	1.44	1.99	1.49	.98	2.42	2.49	2.41	1.11	1.55	1.25
CaO	2.64	1.58	.85	.80	.82	.77	.85	.73	.63	.49
Na <sub>2</sub> O	2.94	.97	.74	.28	.23	.23	.36	.24	.16	.21
K <sub>2</sub> O	4.09	5.29	5.60	6.80	5.99	6.99	5.89	6.50	6.90	7.18
P <sub>2</sub> O <sub>5</sub>	.18	.15	.13	.24	.41	.35	.35	.40	.28	.14
LOI		6.00	4.19	3.50	5.96	4.33	4.96	4.92	5.39	4.80
Total		99.4	99.7	100.2	101.2	100.8	100.3	99.57	100.8	102.1

Table C-1 continued.

	Parent	WG-9	WG-8	WG-7	WG-6	WG-5	WG-4	WG-3	WG-2	WG-1
Rb	174	176	180	191	273	255	274	276	284	261
Ba	780	1223	1240	1376	554	1104	620	653	615	619
Sr	529	320	316	411	243	368	208	1045	901	545
Th	5.1	9.1	8.2	11.1	11.5	10.8	10.6	19.9	12.5	16.7
U	-----	2.2	2.1	2.1	3.4	2.7	4.6	4.1	4.6	4.3
Sc	5.5	6.2	5.7	13.8	13.6	18.1	15.7	15	14.4	13.2
Cr	45.5	54.5	51.5	97	103	69.6	94.8	69.5	66.6	61.4
Co	8.50	9.40	9.40	19.70	17.00	17.00	21.00	13.30	9.40	7.80
Y	14	15.9	17.2	22	27.3	26.4	29.5	27.4	33.7	34.1
Zr	109	145	160	190	218	176	206	156	180	166
Nb	9.5	6.3	6.0	10.5	11.2	9.5	10.9	10.6	12.3	12.4
Hf	4.1	5.9	5.0	5.4	7.1	5.5	8.3	5.9	9.2	7.9
Ta	.63	.38	.37	.88	.81	.79	.77	.87	.96	1.2
La	21.6	28.8	13.6	30.8	46.9	39.4	34.6	58.4	33.1	28.7
Ce	43.4	54.3	26.4	62.1	88.7	81.4	68.2	117.4	67.4	58.7
Sm	3.19	4.54	2.59	6.93	8.45	7.89	7.46	11.1	8.04	8.27
Eu	1.04	1.07	.69	1.07	1.48	1.38	1.26	1.81	1.81	1.54
Tb	.38	.49	.33	.65	.84	.83	.93	1.0	1.2	.96
Yb	1.0	1.43	1.16	2.1	2.47	2.17	3.19	2.25	2.70	1.95
Lu	.16	.22	.18	.32	.38	.34	.46	.31	.39	.28
Eu/Eu*	1.12	.83	.89	.57	.63	.62	.57	.61	.72	.64
La/Yb n	13.09	12.21	7.11	8.89	11.51	11.00	6.57	15.73	7.43	8.92
CIA	58.36	58.36	60.14	61.21	70.55	66.01	69.51	70.62	71.03	70.16

Table C-2. Chemical Analyses of Fountain Formation shales

	FO-1	FO-2	FO-3
SiO <sub>2</sub>	58.59	59.52	66.77
TiO <sub>2</sub>	.70	.75	.60
Al <sub>2</sub> O <sub>3</sub>	19.65	20.66	18.79
Fe <sub>2</sub> O <sub>3</sub> T	6.26	7.67	1.61
MnO	.06	.05	.05
MgO	1.01	1.26	.96
CaO	.66	.41	.35
Na <sub>2</sub> O	.32	.28	.36
K <sub>2</sub> O	6.48	7.32	7.74
P <sub>2</sub> O <sub>5</sub>	.09	.14	.14
LOI	6.05	5.21	3.89
Total	99.87	103.3	101.23

Table C-2 continued.

	FO-1	FO-2	FO-3
Rb	396	411	388
Ba	553	532	671
Sr	298	403	380
Th	42	43	22.5
U	4.1	4.2	2.1
Sc	12.9	14.4	7.4
Cr	53.9	63.00	2.15
Co	11.70	13.50	5.30
Y	47.5	56.5	40.10
Zr	384.00	393.00	195.00
Nb	26.70	24.20	25.00
Hf	11.80	13.80	4.00
Ta	1.80	2.60	1.10
La	88.30	94.60	50.90
Ce	177.40	194.00	107.50
Sm	12.30	15.70	7.36
Eu	1.42	1.82	.94
Tb	1.20	1.66	.78
Yb	3.33	4.47	2.30
Lu	.47	.66	.32
Eu/Eu*	.42	.41	.45
La/Yb n	16.07	12.83	13.41
CIA	69.74	68.79	67.00

Appendix D  
Mass Balance Data for Parent Granodiorite

Table D-1. Rare earth element concentrations for minerals separated from parent granodiorite (CR1-1).

	Apatite	Allanite	Zircon	Clay	Biotite	K-feldspar	Sphene	Plagioc
La	2590	250000	167	190	38.5	.5	6000	.4
Ce	1954	100000	114	130	23.2	.4	5800	.35
Nd	1221	25000	80	90	16	.15	4600	.1
Sm	729.3	7000	61	55	9.72	.05	4000	.07
Eu	650	2000	27.5	35	5.22	1	2200	2
Tb	382.9	750	127.7	25	4.6	.02	2200	.02
Yb	257.5	100	1580	15	2.87	.02	1500	.02
Lu	261.8	80	1865	12	3.03	.02	1300	.02

Allanite and Zircon data from Gromet and Silver (1983).

## Appendix E

### Sampling, Sample Preparation, and Analytical Techniques

A total of 10 weathered granodiorite and 3 shale samples were collected for chemical analysis (see Figure 1 for sample locations). Samples were taken away from dikes and any mineralized zones present along the profile in order to avoid there possible effects on the chemical compositions. Approximately - kg of material were collected for chemical analyses to ensure a representative grain population. Approximately - kg of one incipiently weathered sample and the parent rock were collected for mineral separate work. With exception of the unweathered granodiorite, samples were unconsolidated enough to scrape off the outcrop with a geologic pick into zip lock bags. Consolidated portions of the parent rock and weathered samples were taken for density measurements. Thin sections were made from the parent, weathered rock and shale samples. At New Mexico Tech the samples were powdered to a size of 200 mesh. For Instrumental Neutron Activation Analysis the weathered samples and shales were milled using a rotary grinder with ceramic plates to the size of a fine-grained sand. The parent rock was first past through an electric chipmunk jaw crusher and then milled following the same process. For press pellet and fusion disk work, samples were ground in the TEMA mill and then powdered by hand in an agate mortar and pestle.

Thin sections were made form 9 weathered samples, two samples of the parent rock and 2 of the shale samples. Because of the unconsolidated nature of the weathered rock, samples were mounted with epoxy and then cut into thin sections. The parent granodiorite, shales, and one weathered sample were consolidated pieces of rock and made into standard thin sections. Modal analyses were performed using standard point counting techniques.

Mineral separates were performed on one incipiently weathered sample and the parent rock. Samples were crushed in an electric chipmunk jar crusher and then were ground with the rotary disk grinder using ceramic plates. Samples were separated into 40, 60, 80, 100, and 120 mesh fractions using the ROTAP sieve shaker. The 100-120 size fraction (.125-.149 mm) retained the least amount of grain aggregates and was chosen for heavy liquid separation. Plagioclase and potassium feldspar were separated using lithium metatungstate. Biotite was separated using paper shaking techniques. Methalyne iodide was used to separate the heavy mineral fraction which consisted of

zircon, allanite, apatite, and sphene. Sphene and apatite were separated further using methalyne iodide and hand picking under the binocular microscope. Zircon and allanite separates were not obtained due to their small grain size.

Density measurements were made for each of the weathered samples and the parent rock. Samples were weighed, coated in a clear nail polish to prevent deterioration upon wetting, and then re weighed. Using a graduated cylinder, water displacement values were measured for each sample and 10 values for each rock were recorded. Samples were dried between measurements. An average of these values was used to calculate the final density of each sample.

### Analytical Techniques

By Instrumental Neutron Activation Analysis the abundances of La, Ce, Nd, Sm, Eu, Tb, Yb, Lu, Hf, Ta, Sc, Co, Cr, Ba, Th, and U were determined using methods outlined by Jacobs et al. (1977) and Gibson and Jagan (1977). Whole rock samples were irradiated at Texas A&M University, College Station, Texas . The mineral separates and duplicate whole rock samples for precision and accuracy measurements were irradiated in a second run at the University of Missouri at Columbia. Samples analyzed at the Texas A&M reactor were weighed out into 300 mg increments and heat sealed in polyethylene vials. For irradiation at the University of Missouri reactor, 100 mg of each sample was heat sealed in silica vials. A long and short count were performed on the samples in each run at New Mexico Tech, 7 and 40 days after irradiation. Samples were mounted on two-coaxial Ge detectors and the gamma ray emissions were counted. The data reduction was performed on a VAX computer using the program TEABAGS (Trace Element Analysis By Automated Gamma-ray Spectrometry) (Lindstrom and Korotev, 1982). The fly ash NIST-SRM-1633a was used as a calibrating standard and run in triplicate. The other rock standards used were AN-G (anorthosite), BCR-1 (basalt), and G-2 (granite) and were analyzed as unknowns (check standards) to determine the precision and accuracy of each run. Samples WG-3 and WG-9 were analyzed multiply to determine the precision of the INAA method.

The abundances of the major elements and trace elements Rb, Sr, Y, Zr, and Nb were determined at New Mexico Tech by X-ray fluorescence (XRF) using an automated 3064 XRF spectrometer. A PDP-11 computer equipped with in-house software at the New Mexico Bureau of Mines was used to perform the data reduction. The major element abundances were determined using a fusion disc method described

by Norrish and Hutton (1969). To create fusion discs, approximately 0.5 g of sample is mixed with 2.7 g of a glass formed from lithium tetraborate, lithium carbonate, and lanthanum oxide, spectroflux-11, along with several beads of an oxidant,  $\text{NH}_4\text{NO}_3$ . The mixture was melted over an open flame in a platinum crucible, poured into a mold, cooled, and subsequently analyzed. The trace element abundances were determined using a press pellet method described by Norrish and Chappel (1977). Approximately 7 g of powdered sample mixed with 7 drops of a polyvinyl alcohol binder and a bakelite backing was pressed with up to 20 tons of pressure for 1 minute. The disks were released from pressure and analyzed. In tables B-1 through B-6 the precision and accuracy for the INAA and XRF data obtained in this study are given.

Table E-1. REE Normalizing Values

La	0.33
Ce	0.88
Nd	0.60
Sm	0.181
Eu	0.069
Gd	0.249
Tb	0.047
Yb	0.200
Lu	0.034

Chondrite values from Haskin et al. (1968).



## REFERENCES

- Banfield, J.F. and Eggleton, R.A. (1989) Apatite replacement and rare earth mobilization, fractionation, and fixation during weathering. *Clays and Clay Minerals* 37, 113-127.
- Brimhall, G.H. and Dietrich, W.E. (1987) Constitutive mass balance relations between chemical composition, volume, density, porosity, and strain in metasomatic hydrochemical systems: results on weathering and pedogenesis. *Geochim. Cosmochim. Acta* 51, 567-587.
- Condie, K.C. (1991) Another look at rare earth elements in shales. *Geochim. Cosmochim. Acta* 55, 2527-2531.
- Crichton, J.G. and Kondie, K.C. (1993) Trace elements as source indicators in cratonic sediments: a case study from the early Proterozoic Libby Creek Group. *Jour.Geol.* 101, 319-332.
- Crichton, J.G. (1992) Geochemistry and provenance of the early Proterozoic Libby Creek Group, Medicine Bow Mountains, Southeastern Wyoming. *Master's Thesis, N.M.I.M.T., Socorro, New Mexico.* 95 p.
- Cullers, R.L. (1988) Mineralogical and chemical changes of soil and stream sediment formed by intense weathering of the Danburg granite, Georgia, U.S.A. *Lithos* 21, 301-314.
- Cullers, R.L., Barrett, T., Carlson, R., and Robinson, B. (1987) Rare earth element and mineralogic changes in Holocene soil and stream sediment: a case study in the wet mountains, Colorado, U.S.A. *Chem. Geol.* 63, 275-297.
- Cullers, R.L., Chaudhuri, S., Arnold, B., Lee, M., and Wolf, Jr., C.W. (1975) Rare earth distributions in clay minerals and in the clay-sized fractions of the lower Permian Havensville and Eskridge shales of Kansas and Oklahoma. *Geochim. Cosmochim. Acta* 39, 1691-1703.

- Duddy, I.R. (1980) Redistribution and fractionation of rare earth and other elements in a weathering profile. *Chem. Geol.* 30, 363-381.
- Elderfield, H. and Sholkovitz, E.R. (1987) *Rare earth elements in the pore waters of reducing nearshore sediments*. *Earth and Planetary Science Letters* 82, 280-288.
- Fritz (1988) A comparative study of gabbro and granite weathering. *Chem. Geol.* 68, 275-290.
- Gable, D.J. (1980) The Boulder Creek Batholith, Front Range, Colorado. *U.S. Geol. Survey Prof. Paper 1101*, 87 p.
- Gibson, I.L. and Jagam, P. 1980. Instrumental neutron activation analysis of rocks and minerals, in *Mineral. Assoc. Canada Short Course in Neutron Activation Analysis in the Geosciences* (ed. G.K. Muecke) p. 109-131.
- Grant, J.A. (1986) The isocon diagram - a simple solution to the Gresens' equation for metasomatic alteration. *Econ. Geol.* 81, 1876-1982.
- Gresens, R.L. (1967) Composition-volume relationships of metasomatism. *Chem. Geol.* 2, 47-55.
- Gromet, L.P. and Silver, L.T. (1983) Rare earth element distributions among minerals in a granodiorite and their petrogenic implications. *Geochim. Chosmochim. Acta* 47, 925-939.
- Harriss, R.C. and Adams, J.A.S. (1966) Geochemical and mineralogical studies on the weathering of granitic rocks. *Amer. J. Science* 264, 146-173.
- Haskin, L.A., Haskin, M.A., Frey, F.A., and Wilderman, T.R., 1968. Relative and absolute terrestrial abundances of the REE, in *Origin and Distribution of the Elements*. Pergamon, New York. p.889-912.

- Henderson, P. (ed.) *Rare Earth Element Geochemistry*. Elsevier Science Publishing Company, Inc., New York. 510 p.
- Jacobs, J.W., Korotev, R.L., Blanchard, D.P., and Haskin, L.A., 1977. A well-tested procedure for instrumental neutron activation analysis of silicate rocks and minerals. *Jour. Radianal. Chem.*, v. 40, p. 93-114.
- Johnsson, M.J., Stallard, R.F. and Meade, R.H. (1988) First cycle quartz arenites in the Orinoco River Basin, Venezuela and Columbia. *Jour. Geol.* 96, 263-277.
- Lindstrom, D.J. and Korotev, R.L., 1982. TEABAGS: computer programs for instrumental neutron activation analysis. *Radianalyt. Chem.*, v.70, p.439-458.
- McLennan, S.M. (1989) Rare earth elements in sedimentary rocks: influence of provenance and sedimentary processes: in *Geochemistry and Mineralogy of Rare Earth Elements, Reviews in Mineralogy*, Vol. 21 169-200.
- McLennan, S.M. and Taylor, S.R. (1991) Sedimentary rocks and crustal evolution: tectonic setting and secular trends, *Jour. Geol.* 99, 1-21.
- Nesbitt, H.W. (1979) Mobility and fractionation of rare earth elements during weathering of a granodiorite. *Nature* 279, 206-210.
- Nesbitt, H.W., Markovics, G. and Price, R.C. (1980) Chemical processes affecting alkalis and alkaline earths during continental weathering. *Geochim. Cosmochim. Acta* 44, 1659-1666.
- Nesbitt, H.W. and Young, G.M. (1989) Formation and diagenesis of weathering profiles. *Jour. Geol.* 97, 129-147.
- Norrish, K. and Chappel, B.W., 1977. X-ray fluorescence and spectrometry, in *Physical Methods in Determinative Mineralogy* (ed. J. Zussman), p. 235-237 and 257-262. Academic Press, New York.

- Norrish, K. and Hutton, J.T., 1969. An accurate X-ray spectrographic method for the analysis of a wide range of geologic samples. *Geochim. Cosmochim. Acta*, v.33, p.431-453.
- Pettijohn, F.J., Potter, P.E., and Sievir, R. (1973) *Sand and Sandstone*. Springer-Verlag, New York, 618 p.
- Pliler, R. and Adams, J.A.S. (1962) The distribution of thorium and uranium in a Pennsylvanian weathering profile. *Geochim. Cosmochim. Acta* 26, 1137-1146.
- Ronov, A.B., Balashov, Y.A. and Migdisov, A.A. (1967) Geochemistry of the rare earths in the sedimentary cycle. *Geochim. Int.* 4(1), 1-17.
- Sawka, W.N. (1988) REE and trace element variation in accessory minerals and hornblende from the strongly zoned McMurry Meadows pluton. *California. Trans. Royal Soc. Edinburgh, Earth Sciences* 79, 157-168.
- Schieber, J. (1988) Redistribution of rare-earth elements during diagenesis of carbonate rocks from the mid-Proterozoic Newland Formation, Montana, U.S.A. *Chem. Geol.* 69, 111-126.
- Sholkovitz, E.R., Piegras, D.J., Jacobson, S.B. (1989) The pore water chemistry of rare earth elements in Buzzards Bay sediments. *Geochim. et Chosmochim. Acta.* 58, 2847-2856
- Suttner, L.J., Basu, A. and Mack, G.H. (1981) Climate and origin of quartz arenites. *Jour. Sediment. Petrol.* 51, 1235-1246.
- Taylor and McLennan, S.M. (1985) *The Continental Crust: Its Composition and Evolution*. Blackwell, London, 312 p.
- Wahlstrom, E.E. (1948) Pre-Fountain and recent weathering on Flagstaff Mountain near Boulder, Colorado. *Geol. Soc. America Bull.* 59, 1173-1190.

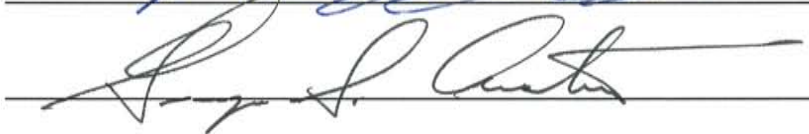
Wedepohl, K.H. (ed) (1978) *Handbook of Geochemistry*. Springer-Verlag, New York.

This thesis is accepted on behalf of the faculty  
of the Institute by the following committee:

  
\_\_\_\_\_

Adviser

  
\_\_\_\_\_

  
\_\_\_\_\_

\_\_\_\_\_

\_\_\_\_\_

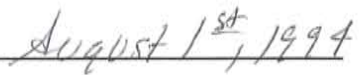
\_\_\_\_\_

Date

I release this document to New Mexico Institute of Mining  
and Technology.

  
\_\_\_\_\_

Students Signature

  
\_\_\_\_\_

Date